



## **Individual Engineering Project Thesis**

**Developing and Testing an Ultra-Wide Band Based Distance Measurement  
Device and Golf Club Selection System.**

**Matthew Hudson**

**21029866**

**ENG61010-2024-SUG1-2024-SUG2**

**Individual Engineering Project**

**BEng(Hons) Electrical and Electronic Engineering**

**Supervisor: Dr A Griffiths**

**02/05/2025**

## **Abstract**

Accurate distance measurement is a crucial factor in enhancing performance and strategic decision making in golf. Existing technologies such as GPS and laser rangefinders, while widely adopted, are often limited by environmental conditions, terrain complexity and precision constraints. This project presents the design and development of a dual unit, portable distance measurement system based on Ultra-Wideband (UWB) technology, capable of providing real time, centimetre level accuracy in varied outdoor conditions.

The system consists of two components: a static flagstick-mounted unit and a handheld receiver. Using Time of Flight (ToF) UWB ranging and barometric altitude sensing, it calculates three dimensional distances between the user and the target. A personalised club recommendation feature, based on stored shot performance data is also integrated to assist with equipment selection. Both units are built around ESP32 microcontrollers, incorporating low power design considerations such as solar charging and wake up communication protocols.

Field testing under a variety of environmental conditions demonstrated that the system achieved average errors within  $\pm 10$  cm in line of sight scenarios and maintained functionality under moderate none line of sight obstructions. These results confirm the feasibility of UWB based distance systems for sports applications and provide a foundation for further development and potential commercial integration.

## **Acknowledgement**

I would like to express my sincere gratitude to everyone who has supported me throughout this project and during my academic journey.

First and foremost, I extend my deepest thanks to Dr. A. Griffiths, my project supervisor, for their invaluable guidance, technical insight and consistent support throughout the development of this work.

I would also like to express appreciation to Emily Raeburn, whose dedicated and patient approach to teaching mathematics gave me the confidence and foundation to continue with my studies. Without her encouragement and belief in my potential, this journey may not have been possible.

To my wife, Emma, thank you for your constant support, encouragement, and the countless ways you helped me stay focused, your belief in me has pushed me to go further than I thought I could. To my children, Liam, Jack and Grace, thank you for your understanding, patience, and the sacrifices you've made while I pursued this path. Your love and support have meant everything to me.

Finally, I am grateful to the wider academic staff and technical teams at the University of Staffordshire who aided throughout the project.

This project represents more than technical achievement it stands as a reflection of the encouragement, sacrifice and belief of those around me.

## Table of Contents

Abstract .....	ii
Acknowledgement .....	iii
Table of Contents .....	iv
List of Figures .....	vii
List of Tables .....	ix
Abbreviations .....	x
1 Introduction .....	1
1.1 Aims .....	1
1.2 Objectives .....	1
2 Literature Review .....	2
2.1 Existing Technologies and Limitations .....	2
2.1.1 GPS Systems .....	2
2.1.2 Laser Range Finders .....	2
2.1.3 Summary of Limitations .....	2
2.1.4 The Need for a New Solution .....	3
2.1.5 Summary of Existing Technologies .....	3
2.2 Ultra-Wideband (UWB) Technology .....	4
2.2.1 Historical Development .....	4
2.2.2 Defining Characteristics .....	5
2.2.3 Standards and Regulatory Framework .....	5
2.2.4 Advantages of UWB .....	6
2.2.5 Limitations and Challenges .....	6
2.2.6 Summary of UWB Technology .....	6
2.3 UWB Distance Measurement Techniques .....	7
2.3.1 UWB Based Methods .....	7
2.3.2 Alternate Methods .....	8
2.3.3 Comparison of Techniques .....	9
2.3.4 Sources of Error .....	10
2.3.5 Ranging Algorithms .....	11
2.3.6 Energy Efficiency .....	12
2.3.7 Summary of UWB Distance Measuring Techniques .....	12
2.4 Related Technologies .....	13
2.4.1 Comparisons with Other Technologies .....	13
2.4.2 Integration and Compatibility .....	14
2.4.3 Unique Case: Laser Rangefinders .....	14
2.4.4 Summary of Related Technologies .....	14
2.5 Applications and Case Studies .....	15
2.5.1 Healthcare Applications .....	15
2.5.2 Smart Logistics and Warehouses .....	15
2.5.3 Consumer Electronics .....	16
2.5.4 Strengths and Challenges .....	16
2.5.5 Summary of Applications and Case Studies .....	16
2.6 Emerging Trends and Challenges .....	17
2.6.1 Future Applications .....	17
2.6.2 Challenges in Adoption .....	18
2.6.3 Future Research Directions .....	18

2.7	Summary of Literature Review .....	19
3	Methodology .....	20
3.1	Hardware Design.....	21
3.1.1	Proof of Concept Process.....	24
3.1.2	Power Systems .....	26
3.1.3	Processing and Communications .....	30
3.1.4	PCB Design and Manufacture .....	34
3.1.5	Finished Build.....	39
3.1.6	Summary of Hardware Design.....	43
3.2	Software Development .....	44
3.2.1	System Loops and Sensor Integration.....	46
3.2.2	User Interface Controls .....	49
3.2.3	Algorithm for Club Selection via SD Card.....	53
3.2.4	Communication and Positioning System .....	56
3.2.5	Signal Filtering.....	57
3.2.6	LoRa - RF Communication.....	58
3.2.7	UWB Distance Measurement .....	59
3.2.8	Wake Up Mechanism.....	61
3.2.9	Summary of Software Development.....	62
3.3	System Testing During Development .....	63
3.3.1	Power Testing .....	63
3.3.2	Altitude Sensor Testing.....	65
3.3.3	LoRa and UWB Maximum Distance Testing .....	67
3.3.4	Proof of Concept Testing .....	69
3.3.5	Summary of System Testing .....	71
3.4	Mathematical Methods .....	72
3.4.1	Distance Calculations.....	73
3.4.2	Summary of Mathematical Methods.....	75
3.5	Summary of Methodology .....	76
4	Experimental Setup.....	77
4.1	Test Equipment .....	77
4.1.1	Primary Devices .....	77
4.1.2	Measurement Tools.....	78
4.2	Test Environments.....	79
4.2.1	Test Locations .....	79
4.2.2	Environmental Conditions .....	79
4.2.3	Use of Terrain Features.....	80
4.3	Procedure.....	80
4.3.1	Data Collection .....	80
4.3.2	Test Scenarios .....	81
4.3.3	Result Processing .....	82
4.4	Summary of Experimental Setup .....	83
5	Results.....	84
5.1	Line of Sight Test Results (Flat) .....	85
5.1.1	Clear Weather Results.....	86
5.1.2	Overcast Sky Results .....	88
5.2	Negative Elevation Results (Downhill to Target) .....	90
5.2.1	Clear Weather Results.....	91
5.2.2	Adverse Weather Results .....	93

5.3	Positive Elevation Results (Uphill to Target) .....	95
5.3.1	Clear weather Results .....	96
5.3.2	Adverse Weather Results.....	98
5.4	Obstructed Line of Sight Test Results .....	100
5.4.1	Wall Obstruction.....	102
5.4.2	Natural Vegetation Obstruction (Trees and Shrubs).....	104
6	Discussions .....	106
6.1	Accuracy Across Test Conditions .....	107
6.2	Analysis of Error Sources .....	109
6.3	Impact of Elevation .....	110
6.4	Environmental Factors .....	111
6.5	Obstruction Performance.....	113
6.6	System Limitations.....	115
6.6.1	Dependency on Clear Line of Sight.....	115
6.6.2	Barometric Sensor Drift and Environmental Pressure Variation.....	115
6.7	Summary of Discussions.....	116
7	Conclusion .....	117
8	Recommendations.....	119
9	References.....	122
10	Appendices.....	126
10.1	Hardware Selection .....	126
10.1.1	Microcontroller .....	127
10.1.2	Ultra-wide Band (UWB) Module .....	128
10.1.3	Altitude Measurement.....	129
10.1.4	Communication Module .....	131
10.1.5	Data Storage.....	132
10.1.6	User Interface Components.....	133
10.1.7	Battery Selection.....	134
10.1.8	Enclosure Selection.....	135
10.2	Programming Codes.....	137
10.2.1	LoRa Distance Test Codes.....	137
10.2.2	Final Product Codes .....	139
10.3	MATLAB Codes .....	148
10.3.1	Distance Calculations (Haversine).....	148
10.4	Bill Of Materials.....	151
10.4.1	Handheld Device.....	151
10.4.2	Static Device .....	152
10.5	Photographs .....	153
10.5.1	Proof of Concept Veroboard .....	153
10.5.2	Proof of Concept Testing .....	154
10.5.3	Hardware Building.....	156
10.6	Datasheets.....	163
10.6.1	Flagstick Enclosure .....	163
10.6.2	Handheld Enclosure .....	164

## List of Figures

Figure 2.1 UWB spectrum comparison .....	4
Figure 2.2 Visualisation of ToF.....	7
Figure 2.3 Time Difference of Arrival positioning.....	8
Figure 2.4 Symmetric double sided two way ranging. ....	11
Figure 3.1 UWB Communication between Handheld Device and Flagstick Unit .....	20
Figure 3.2 Flowchart for System Operation .....	20
Figure 3.3 Proposed Static Device Flag Stick .....	22
Figure 3.4 Proposed Handheld Device .....	23
Figure 3.5 Veroboard Prototype Assembly for Proof of Concept .....	24
Figure 3.6 Veroboard Prototype Wiring Schematic .....	25
Figure 3.7 Static Unit Solar Power System Flow Diagram .....	26
Figure 3.8 Static Unit -Solar and Battery Charging Schematic .....	26
Figure 3.9 Handheld Unit Power Flow Diagram .....	27
Figure 3.10 Handheld Unit - Battery Charging Schematic .....	27
Figure 3.11 Power Regulation and Filtering Schematic .....	29
Figure 3.12 ESP32 pinout diagram.....	30
Figure 3.13 Static Unit Schematic Diagram .....	31
Figure 3.14 Handheld Unit Schematic Diagram.....	31
Figure 3.15 Flow Diagram for PCB Design and Manufacture Process .....	34
Figure 3.16 Static Unit - PCB Design Layout .....	35
Figure 3.17 Static Unit - 3D Design Layout .....	35
Figure 3.18 Handheld Unit - PCB Design Layout.....	36
Figure 3.19 Handheld Unit - 3D Design Layout.....	36
Figure 3.20 Manufactured PCB's.....	37
Figure 3.21 Finished Handheld Device (Front) .....	39
Figure 3.22 Finished Handheld Device (Front, showing USB Port) .....	40
Figure 3.23 Finished Handheld Device (Top, Showing On/Off Switch) .....	40
Figure 3.24 Static Unit (Side) .....	41
Figure 3.25 Static Unit (Top, Showing Solar Panel) .....	41
Figure 3.26 Static Unit (Full Flag View) .....	42
Figure 3.27 System Communication and Processing Flow Chart .....	45
Figure 3.28 System Loop for Sensor Reading/Updating/Display Management.....	46
Figure 3.29 Membrane Push Buttons.....	49
Figure 3.30 Handheld Device User Interface Navigation.....	51
Figure 3.31 - USB Power Monitoring Device .....	63
Figure 3.32 Altitude Test Rig (0-5m) .....	65
Figure 3.33 Comparison of Altitude Test .....	66
Figure 3.34 Maximum Range Testing .....	67
Figure 3.35 MATLAB Data Command Inputs .....	74
Figure 4.1 GPS Status Application Screenshot.....	78
Figure 5.1 LoS Measurement points .....	85
Figure 5.2 Line of Sight (Clear Weather, Graph) .....	87
Figure 5.3 Line of Sight (Overcast Weather, Graph).....	89
Figure 5.4 Measurement points (Negative Elevation) .....	90
Figure 5.5 Negative Elevation Accuracy (Clear Weather) Graph .....	92
Figure 5.6 Negative Elevation Accuracy (Overcast Weather) Graph.....	94

Figure 5.7 Measurement points (Positive Elevation).....	95
Figure 5.8 Positive Elevation Accuracy (Clear Weather) Graph.....	97
Figure 5.9 Positive Elevation Accuracy (Overcast Weather) Graph .....	99
Figure 5.10 Measurement points ( Wall Obstruction) .....	100
Figure 5.11 Measurement points (Vegetation Obstruction) .....	101
Figure 5.12 Obstructed Line of Sight (Wall) Graph .....	102
Figure 5.13 Obstructed Line of Sight (Vegetation) Graph .....	105
Figure 8.1Golf Simulator .....	120
Figure 10.1 ESP32-S3 WROOM microcontroller .....	127
Figure 10.2 UWB-DW3000 ultra-wideband (UWB) module.....	128
Figure 10.3 3D Distance Elevation .....	129
Figure 10.4 BMP388 Sensor.....	130
Figure 10.5 OLED Display Module.....	133
Figure 10.6 Membrane Touch Button Module .....	133
Figure 10.7 GEWISS GW44204 junction box .....	135
Figure 10.8 Dimensions for the Handheld Unit.....	136
Figure 10.9 Proof of Concept Veroboard .....	153
Figure 10.10 Proof of Concept Testing Photo 1 .....	154
Figure 10.11 Proof of Concept Testing Photo 2 .....	154
Figure 10.12Proof of Concept Testing Photo 3 .....	155
Figure 10.13 Proof of Concept Testing Photo 4 .....	155
Figure 10.14 Hardware Building Photo 1 .....	156
Figure 10.15 Hardware Building Photo 2 .....	156
Figure 10.16 Hardware Building Photo 3 .....	157
Figure 10.17 Hardware Building Photo 4 .....	157
Figure 10.18 Hardware Building Photo 5 .....	158
Figure 10.19 Hardware Building Photo 6 .....	158
Figure 10.20 Hardware Building Photo 7 .....	159
Figure 10.21 Hardware Building Photo 8 .....	159
Figure 10.22 Hardware Building Photo 9 .....	160
Figure 10.23 Hardware Building Photo 10 .....	160
Figure 10.24 Hardware Building Photo 11 .....	161
Figure 10.25 Hardware Building Photo 12 .....	161
Figure 10.26 Hardware Building Photo 13 .....	162

## List of Tables

Table 2.1 - Comparison of Distance Measurement Techniques .....	9
Table 2.2 - Performance Comparison: UWB vs GPS vs LiDAR .....	13
Table 3.1 - CSV Cells for Club Distances .....	54
Table 3.2 - Static and Handheld Unit Power Consumption.....	63
Table 3.3 - Solar Panel Output Voltages Vs Lux.....	64
Table 3.4 – Altitude Sensor Test Results.....	65
Table 3.5 Maximum Measured Distances .....	68
Table 3.6 – Proof of Concept Test Results .....	70
Table 5.1 - Summary of Test Scenarios and Environmental Conditions.....	84
Table 5.2 - Line of Sight Results (Clear Weather) .....	86
Table 5.3 - Line of Sight Results (Overcast Weather).....	88
Table 5.4 - Negative Elevation Results (Clear Weather).....	91
Table 5.5 - Negative Elevation Results (Overcast Weather) .....	93
Table 5.6 - Positive Elevation Results (Clear Weather).....	96
Table 5.7 - Positive Elevation Results (Overcast Weather).....	98
Table 5.8 - Obstructed Line of Sight (Wall) Results .....	102
Table 5.9 - Obstructed Line of Sight (Vegetation) Results .....	104
Table 6.1 - Average Error Across Test Scenarios.....	108
Table 6.2 - Impact of Elevation Difference Vs Error .....	110
Table 6.3 - Impact of Weather Conditions for Results .....	112
Table 6.4 - Distance/RSSI Results Under Wall and Vegetation Obstruction.....	114
Table 10.1 - Microcontroller Comparison .....	127
Table 10.2 - UWB Module Comparison.....	128
Table 10.3 - Handheld Device - Bill of Materials .....	151
Table 10.4 - Static Device - Bill of Materials .....	152

## Abbreviations

<b>AR</b>	Augmented Reality
<b>BLE</b>	Bluetooth Low Energy
<b>BMP</b>	Barometric Pressure Sensor
<b>CAD</b>	Computer Aided Design
<b>CIR</b>	Channel Impulse Response
<b>CRC</b>	Cyclic Redundancy Check
<b>DRC</b>	Design Rules Check
<b>DSTWR</b>	Double-Sided Two Way Ranging
<b>ERC</b>	Electrical Rules Check
<b>ESP32</b>	Espressif Systems Microcontroller 32-bit
<b>ETSI</b>	European Telecommunications Standards Institute
<b>FCC</b>	Federal Communications Commission
<b>FSK</b>	Frequency Shift Keying
<b>GPIO</b>	General Purpose Input/Output
<b>GPS</b>	Global Positioning System
<b>HC-12</b>	High Communication 12 (wireless serial module)
<b>I2C</b>	Inter-Integrated Circuit
<b>IDE</b>	Integrated Development Environment
<b>IET</b>	Institution of Engineering and Technology
<b>IoT</b>	Internet of Things
<b>LoRa</b>	Long Range (Low Power Wide Area Network)
<b>LoS</b>	Line of Sight
<b>NLoS</b>	None Line of Sight
<b>OLED</b>	Organic Light Emitting Diode
<b>PCB</b>	Printed Circuit Board
<b>PDoA</b>	Phase Difference of Arrival
<b>RF</b>	Radio Frequency
<b>RMSE</b>	Root Mean Square Error
<b>RSSI</b>	Received Signal Strength Indicator
<b>SDS-TWR</b>	Symmetrical Double Sided Two Way Ranging
<b>SPI</b>	Serial Peripheral Interface
<b>SVM</b>	Support Vector Machines
<b>ToA</b>	Time of Arrival
<b>ToF</b>	Time of Flight
<b>UART</b>	Universal Asynchronous Receiver Transmitter
<b>UWB</b>	Ultra-Wideband
<b>VHDL-AMS</b>	VHSIC Hardware Description Language – Analogue and Mixed-Signal Extensions

# **1 Introduction**

Accurate distance measurement on a golf course is crucial for improving player performance, enabling strategic club selection and enhancing overall game outcomes. Existing tools, such as GPS systems and laser rangefinders, have supported golfers for years, but they suffer from limitations in precision, adaptability, and ease of use. GPS systems typically produce errors of 1–5 metres due to atmospheric interference and multipath effects, while laser rangefinders require a direct line of sight and struggle in complex terrain.

Ultra-Wideband (UWB) technology offers a compelling alternative, delivering centimetre level accuracy, robustness against environmental noise and fast real time performance. This project explores the development of a distance measurement system that leverages UWB to meet the specific demands of golf course environments. The system also integrates a personalised golf club recommendation feature, providing players with actionable feedback based on individual performance data.

## **1.1 Aims**

The primary aim of this project is to design and develop a UWB based distance measurement system capable of delivering precise, real time distance readings with centimetre level accuracy. The system will be engineered to operate reliably regardless of obstacles or variations in terrain. A secondary aim is to integrate a personalised club recommendation feature that uses player specific shot data to improve decision making and support overall gameplay.

## **1.2 Objectives**

To achieve these aims, the project will first undertake a thorough review of UWB technology, evaluating its advantages over traditional GPS and laser based systems. It will then proceed to design and prototype the UWB based system, incorporating both hardware components such as a flagstick transmitter and a handheld receiver including software algorithms necessary for accurate distance calculation. The development will also include a power efficient wake up mechanism supported by solar charging and battery storage to ensure sustainable operation. In parallel, a data driven club selection algorithm will be created based on individual shot performance. Finally, the system will be validated through MATLAB calculation and real world field testing, with a focus on assessing accuracy, usability in diverse environmental and topographical conditions.

## **2 Literature Review**

The ability to measure distances accurately on a golf course is important for improving player performance, club selection and overall game strategy. Traditional distance measurement tools such as GPS systems and laser rangefinders, have served golfers for years but suffer from notable limitations, including precision issues and adaptability challenges. This project aims to address these limitations by developing a more accurate distance measurement system, specifically tailored for golf applications. The system uses advanced technologies, with a focus on Ultra-Wideband (UWB) technology, to provide real time and centimetre level accuracy.

### **2.1 Existing Technologies and Limitations**

#### **2.1.1 GPS Systems**

GPS systems are widely used for estimating distances on golf courses due to their convenience and global coverage. However, they are often inaccurate at shorter distances, with errors ranging from 1 to 5 metres due to multipath interference and atmospheric delays (Higgins, 1999). Also, GPS provides static measurements, making it unsuitable for environments where flagstick positions change frequently.

#### **2.1.2 Laser Range Finders**

Laser rangefinders provide greater accuracy than GPS systems, typically offering sub metre precision (Hood, 2023). However, they require a clear line of sight to the target, making them impractical in courses with obstructions such as trees or uneven terrain. Additionally, laser rangefinders lack the ability to provide personalised feedback based on past performance data, limiting their utility for advanced applications.

#### **2.1.3 Summary of Limitations**

These limitations point out the need for a more advanced solution that combines high accuracy, adaptability, and personalised features. UWB technology emerges as a strong candidate, addressing these weaknesses through its unique capabilities.

## **2.1.4 The Need for a New Solution**

To overcome the limitations of GPS and laser rangefinders, newer technologies such as Bluetooth Low Energy (BLE), Wi-Fi and UWB have been explored. UWB stands out due to its ability to deliver centimetre level accuracy, resilience to multipath interference, and real time adaptability. These qualities make UWB particularly suited for dynamic environments like golf courses, where precision and reliability are critical.

## **2.1.5 Summary of Existing Technologies**

Traditional distance measurement tools, such as GPS systems and laser rangefinders, provide useful functionality but exhibit notable limitations in terms of accuracy, adaptability, and environmental resilience. GPS suffers from metre level errors caused by atmospheric interference and terrain effects, while laser rangefinders require direct line of sight and are affected by course obstructions. These shortcomings highlight the need for a more advanced, precise, and flexible solution leading to the exploration of newer technologies such as Ultra-Wideband (UWB), discussed in the following sections.

## 2.2 Ultra-Wideband (UWB) Technology

Ultra-Wideband (UWB) technology is an innovative wireless communication method that transmits data over a wide frequency spectrum with low power radio signals. Its unique characteristics centimetre level accuracy, low power consumption, and robustness against interference have propelled it to the forefront of localisation and ranging technologies, particularly in areas such as sports, healthcare, and logistics (Kshetrimayum, 2009).

### 2.2.1 Historical Development

The origins of UWB can be traced back to the late 19th century, when early experiments with wide band signal generation laid the foundation for its modern applications. Heinrich Hertz's spark gap radios and subsequent research by Marconi demonstrated the potential of wide band signals, but narrowband systems soon dominated due to technological limitations (Win et al., 2009). Interest in UWB resurfaced in the 1990s, driven by advances in digital signal processing and the introduction of time hopping impulse radio. Regulatory milestones, such as the Federal Communications Commission's (FCC) allocation of the 3.1–10.6 GHz spectrum in 2002, catalysed further research and commercialisation (Chen, 2022).

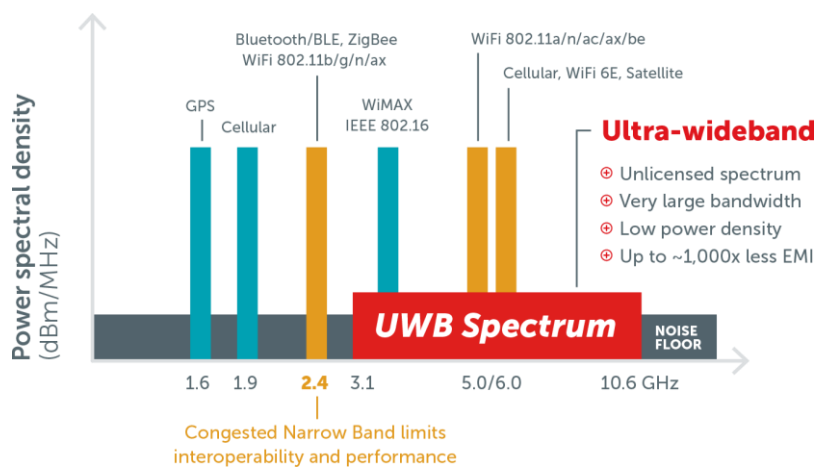


Figure 2.1 UWB spectrum comparison

(Spark Microsystems, n.d.).

## **2.2.2 Defining Characteristics**

UWB is defined as any radio signal with a bandwidth greater than 500 MHz or a fractional bandwidth exceeding 20% of its centre frequency (Kshetrimayum, 2009). Its large bandwidth allows for high temporal resolution, enabling precise distance measurements and accurate localisation. Unlike narrowband systems, which transmit over a fixed frequency, UWB signals are spread across a wide range, reducing power density, and mitigating interference with coexisting systems (Weissberger, 2022).

Key to UWB's functionality is its reliance on short pulse durations, which are transmitted as Gaussian or other waveforms. These pulses provide superior resolution in both time and frequency domains, making UWB suitable for environments where multipath interference and signal reflections would degrade accuracy in conventional systems (Zhang et al., 2020). The use of short pulses also minimises power consumption, a significant advantage for portable and IoT applications (Chen, 2022).

## **2.2.3 Standards and Regulatory Framework**

The widespread adoption of UWB has been boosted by the development of robust standards and regulatory frameworks. The IEEE 802.15.4a standard, introduced in 2007, defined UWB's physical (PHY) layer for applications requiring low power, high accuracy localisation. Subsequent updates, such as IEEE 802.15.4z, enhanced UWB's security and interoperability, addressing vulnerabilities in early implementations (Coppens et al., 2022).

In addition to IEEE standards, organisations like the FiRa Consortium and major manufacturers, including Apple, have advanced UWB's commercialisation. Apple's integration of UWB into its devices in 2022 set a benchmark for secure, high precision localisation, catalysing interest in consumer and industrial applications (Weissberger, 2022). Regulatory bodies such as the FCC and the European Telecommunications Standards Institute (ETSI) have imposed strict spectral emission masks to minimise interference with existing services ensuring UWB's compatibility in shared frequency environments.

## **2.2.4 Advantages of UWB**

UWB's strengths lie in its precision and interference resistance. Its centimetre level accuracy, achieved through Time of Flight (ToF) and Double-Sided Two-Way Ranging (DS-TWR) techniques, go beyond traditional tools like GPS and laser rangefinders (Malajner et al., 2015). UWB's low susceptibility to multipath effects and signal distortion ensures reliable performance in complex environments, such as urban areas, dense indoor settings, and golf courses.

Additionally, UWB's low power consumption and adaptability make it ideal for battery powered devices and applications requiring continuous operation. Innovations like wake up mechanisms and energy efficient hardware, such as the DW3000 series, have further enhanced UWB's appeal for portable and IoT systems (Nabki et al., 2023).

## **2.2.5 Limitations and Challenges**

Despite its advantages, UWB is not without limitations. Its shorter range compared to GPS and reliance on precise hardware calibration pose challenges in large scale deployments. Regulatory constraints, including stringent spectral emission limits, have also slowed its adoption in some markets. Furthermore, interoperability between UWB devices from different manufacturers remains a concern, with efforts by organisations like FiRa Consortium addressing these gaps (Coppens et al., 2022).

Despite these limitations, UWB's unique capabilities have enabled a wide range of real world applications across industries such as healthcare, logistics and consumer electronics. The following sections examine these applications in more detail, demonstrating UWB's versatility and impact beyond theoretical advantages.

## **2.2.6 Summary of UWB Technology**

Ultra-Wideband (UWB) technology offers significant advantages in wireless localisation, delivering centimetre level accuracy, low power consumption and resilience to interference. Its development has been supported by advances in digital signal processing, robust regulatory standards, and adoption by major technology companies. However, UWB faces limitations related to range, hardware calibration, interoperability and regulatory constraints. Understanding both the strengths and weaknesses of UWB provides essential context for evaluating its distance measurement techniques, which are explored in the next section.

## 2.3 UWB Distance Measurement Techniques

Distance measurement is central to localisation systems, with UWB offering several advanced methodologies. Key techniques include Time of Flight (ToF) and Time Difference of Arrival (TDoA), both of which leverage the unique characteristics of UWB signals to achieve high accuracy (Polonelli et al., 2022).

### 2.3.1 UWB Based Methods

- **Time of Flight (ToF)** measures the time a signal takes to travel between two points and is widely used for distance estimation in positioning systems. When implemented with Ultra-wideband (UWB) devices, ToF enables centimetre level accuracy. However, its precision can be affected by factors such as delays introduced by on-board circuits, cables, and antennas, which must be calibrated to ensure accuracy. In practice, methods like broken line approximation are applied to correct these errors and achieve reliable distance measurements (Zhang et al., 2020).

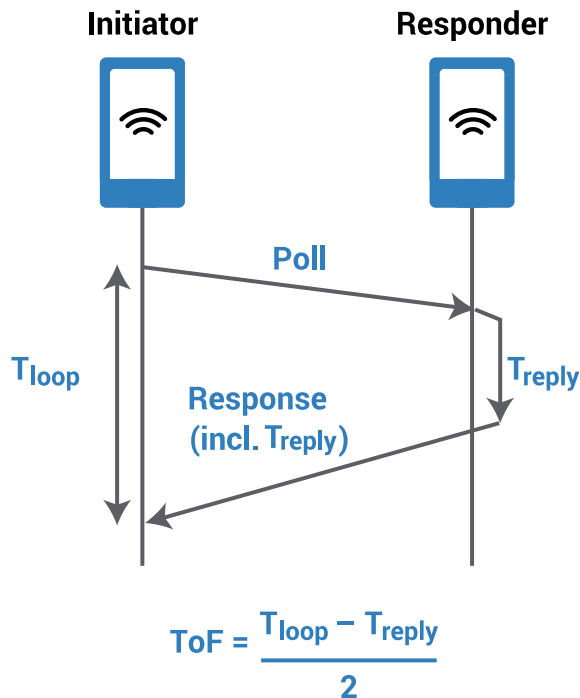


Figure 2.2 Visualisation of ToF  
(FiRa Consortium, 2024.).

- **Time Difference of Arrival (TDoA):** Improves upon ToF by utilising multiple anchors to triangulate the position, enhancing accuracy in complex environments.

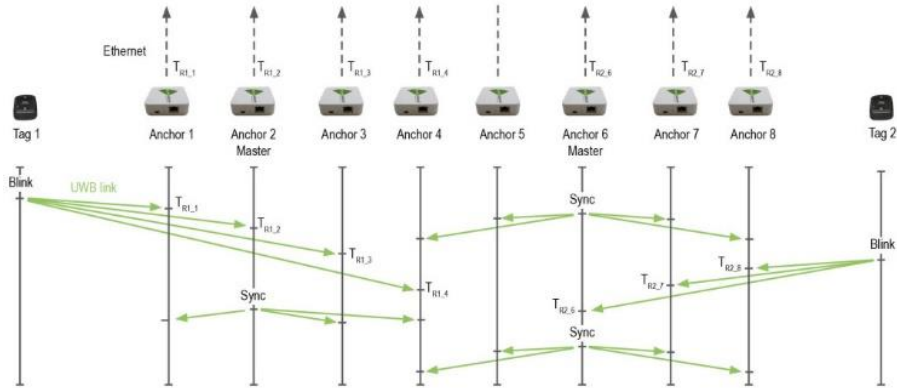


Figure 2.3 Time Difference of Arrival positioning

(Sewio, 2023.)

### 2.3.2 Alternate Methods

**Phase Based Ranging:** Phase based ranging methods, such as the Active Reflector Principle (AR-Principle), offer a cost effective alternative by using phase shifts of received signals to determine distance. This approach requires less expensive transceivers compared to UWB systems and achieves higher measurement ranges. Recent algorithms, like the Complex-Valued Distance Estimation (CDE), improve accuracy by reducing mean errors to 14.9 cm in challenging multipath scenarios (Schröder et al., 2018)

**Received Signal Strength Indicator (RSSI):** RSSI methods estimate distance by correlating signal strength with propagation loss. Although these methods are less accurate than ToF or phase based techniques, they are widely used in Bluetooth and Wi-Fi positioning systems due to their low computational requirements. Experimental evaluations indicate that RSSI is sensitive to environmental factors like signal reflections and device orientation but can be improved with filtering and machine learning techniques (Janczak et al., 2022)

**Hybrid Systems:** Combining UWB with complementary systems such as Pedestrian Dead Reckoning (PDR) mitigates the weaknesses of individual methods. PDR improves UWB accuracy in None Line of Sight (NLOS) environments by using inertial sensors to estimate movement paths. Kalman filter based fusion systems further enhance positioning performance, reducing errors by 35.5% in NLOS conditions (Kim and Pyun, 2021)

### 2.3.3 Comparison of Techniques

Table 2.1 summarises the characteristics of various distance measurement techniques, based on findings from Kim and Pyun (2021), Schröder et al. (2018), and Boussad et al. (2021).

*Table 2.1 - Comparison of Distance Measurement Techniques*

Technique	Accuracy	Cost	Advantages	Limitations
ToF/TDoA	High (<10 cm)	Moderate	High precision, robust for UWB (Kim and Pyun, 2021)	LOS-dependent, infrastructure-heavy (Kim and Pyun, 2021)
Phase Based Ranging	Moderate (15 cm)	Low	Low cost, minimal hardware (Schröder et al., 2018)	Ambiguity in multipath environments (Schröder et al., 2018)
RSSI	Low (~1 m)	Very Low	Simple, low computational load (Boussad et al., 2021)	Sensitive to environmental factors (Boussad et al., 2021)
Hybrid (UWB + PDR)	High (<20 cm)	High	Robust in NLOS, complementary fusion (Kim and Pyun, 2021)	Requires complex integration (Kim and Pyun, 2021)

Comparison of Distance Measurement Techniques (adapted from Kim and Pyun, 2021; Schröder et al., 2018; Boussad et al., 2021).

Time of Flight (ToF) and Time Difference of Arrival (TDoA) methods are ideal for this project due to their high accuracy and established use in UWB systems, which is essential for reliable distance measurement on the golf course.

Phase based ranging, while cost effective, is less suitable for this application because it struggles with accuracy in outdoor environments where signal reflections and multipath interference are common.

RSSI techniques are not viable for this system due to their poor accuracy and high susceptibility to signal fluctuations; however, reviewing them helps illustrate the precision advantage offered by UWB.

Hybrid approaches that combine UWB with pedestrian dead reckoning (PDR) or inertial sensors are promising for improving accuracy in NLOS conditions. These methods could be valuable in future iterations but are currently beyond the scope of this project due to their integration complexity.

## **2.3.4 Sources of Error**

Accurate distance measurement is critical to the performance of the proposed UWB golf system. However, all ranging techniques are susceptible to various sources of error that can degrade reliability and precision, especially in complex outdoor environments.

Key challenges include multipath interference, signal attenuation and environmental variations. For example, phase based methods are prone to ambiguity in noisy or reflective environments, which can lead to inconsistent readings. Similarly, RSSI techniques are affected by fluctuations in signal strength due to changes in device orientation, material obstructions and varying terrain conditions (Schröder et al., 2018).

Understanding these error sources is essential for selecting and implementing the most suitable UWB ranging technique. As a result, the system developed in this project prioritises Time of Flight (ToF) measurements and signal processing strategies that minimise the impact of environmental noise and multipath effects.

## 2.3.5 Ranging Algorithms

Accurate distance Ranging measurement is essential of UWB localisation. Several ranging techniques, including Time of Flight (ToF) and Time Difference of Arrival (TDoA), have been developed to leverage UWB's wide bandwidth and high resolution.

**Time of Flight (ToF):** Measures the travel time of a UWB signal between the transmitter and receiver. While ToF provides high accuracy, it can be power intensive and sensitive to clock skew in real world applications (Mazraani et al., 2017)

**Time Difference of Arrival (TDoA):** Calculates the difference in signal arrival times at multiple anchors, reducing the power requirements for tags but with potential accuracy trade-offs in environments with limited anchor coverage.

**Combined TDoA/ToF Techniques:** A unique method combines the strengths of ToF and TDoA to achieve high accuracy with reduced power consumption. Experimental results demonstrate a reduction in error to 14 cm while lowering tag power consumption by 75% (Mazraani et al., 2017)

**Ranging Protocols:** The Symmetric Double-Sided Two-Way Ranging (SDS-TWR) protocol mitigates clock drift issues and improves ranging accuracy compared to traditional TWR methods (van den Bossche et al., 2018).

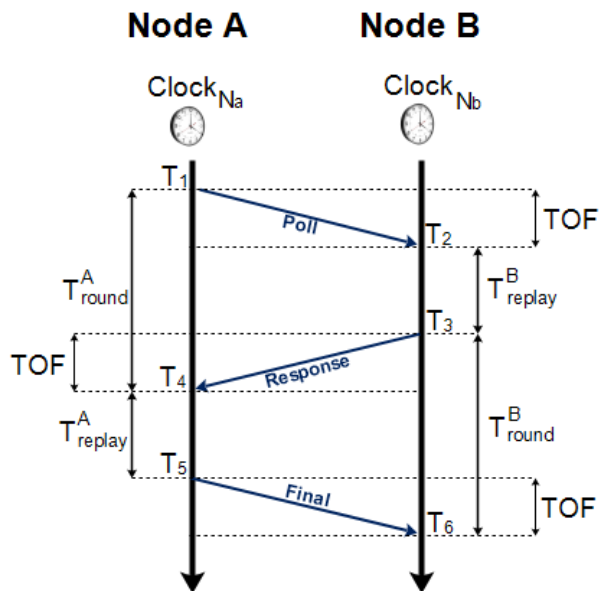


Figure 2.4 Symmetric double sided two way ranging.

(Alarifi et al., 2016)

### **2.3.6 Energy Efficiency**

Energy efficiency is a critical consideration for UWB systems, especially in IoT applications. Techniques such as combined TDoA/ToF and SDS-TWR are designed to minimise power consumption without compromising accuracy, making UWB suitable for battery powered devices in diverse environments (Mazraani et al., 2017)

### **2.3.7 Summary of UWB Distance Measuring Techniques**

This section reviewed key distance measurement techniques available for UWB systems, including Time of Flight (ToF) and Time Difference of Arrival (TDoA), along with alternate methods such as phase based ranging and Received Signal Strength Indicator (RSSI) techniques. While each method offers distinct advantages, ToF and TDoA provide the highest accuracy, making them most suitable for golf course applications where precision is critical. Challenges such as multipath interference, environmental noise, and energy efficiency were also discussed, highlighting important considerations for system design. These insights form the technical basis for selecting UWB as the preferred technology and guide the hardware and software choices detailed in the next sections.

## 2.4 Related Technologies

### 2.4.1 Comparisons with Other Technologies

UWB technology is widely regarded as a high performance solution for precise localisation and ranging. However, alternative technologies such as GPS and LiDAR present strengths and limitations that make them suitable for specific applications. Table 2.2 compares UWB with these technologies across key performance parameters.

Table 2.2 - Performance Comparison: UWB vs GPS vs LiDAR

Feature	UWB	GPS	LiDAR
Accuracy	±10 cm in NLOS (Polonelli et al., 2022)	~5 m outdoors (10 Hz GPS) (Vitanov and Nikolov, 2024)	Sub-cm in ideal conditions (Jayasuriya et al., 2020)
Energy Efficiency	Low power (IoT-suited)	High power (satellite-based)	High computational cost
NLOS Performance	Excellent	Poor (requires clear satellite view)	Limited (requires line of sight)
Cost	Moderate	Low to Moderate	High
Applications	Indoor/outdoor localisation	Outdoor navigation and tracking	Autonomous vehicles, mapping

#### Key Observations:

- UWB provides superior accuracy and NLOS performance, outperforming GPS and LiDAR in dynamic or obstructed environments (Jayasuriya et al., 2020).
- LiDAR offers unmatched precision but is limited by its reliance on clear line of sight and high costs.
- GPS, while cost effective and practical for outdoor navigation, struggles to meet the precision demands of applications requiring centimetre level accuracy (Vitanov and Nikolov, 2024).

## **2.4.2 Integration and Compatibility**

UWB's ability to integrate with existing systems further highlights its flexibility. UWB modules like the DW3000 comply with the IEEE 802.15.4z standard, ensuring interoperability across platforms and compatibility with modern IoT ecosystems.

1. **IoT Ecosystems:** UWB enables seamless integration with smart devices, such as in asset tracking and home automation applications (Coppens et al., 2022).
2. **Smartphones and Consumer Electronics:** The inclusion of UWB in Apple's U1 chip showcases its potential in consumer devices, supporting applications like AirTags for precise localisation (Coppens et al., 2022).
3. **Hybrid Systems:** UWB's ability to complement GPS or MEMS based inertial systems addresses challenges in environments with poor satellite reception or complex terrains (Jayasuriya et al., 2020).

## **2.4.3 Unique Case: Laser Rangefinders**

Laser rangefinders are another widely used localisation technology in outdoor settings, particularly in sports such as golf. According to Shotscope.com (2025) laser rangefinders excel in providing pinpoint accuracy to specific targets but require clear line of sight to function effectively. Unlike UWB, lasers struggle in NLOS environments or adverse weather conditions which limits their utility for diverse localisation applications.

## **2.4.4 Summary of Related Technologies**

Understanding UWB's technical capabilities sets the stage for exploring its real world impact. The following section examines how UWB has been successfully deployed across industries such as healthcare, logistics, and consumer electronics.

## 2.5 Applications and Case Studies

The flexibility of UWB technology has led to its adoption across different fields, ranging from healthcare to logistics and consumer electronics. This section explores real world applications and case studies that demonstrate UWB's effectiveness in addressing specific challenges.

### 2.5.1 Healthcare Applications

UWB has found significant benefit in healthcare, particularly in wireless communication and radar systems.

- **Wireless Body Area Networks (WBANs):** UWB enables on body sensors to monitor vital signs such as heart rate, glucose levels, and blood pressure with high precision. These systems operate with minimal interference and low power consumption, making them ideal for wearable health devices (Ghosh and Sahu, 2016).
- **Remote Monitoring with UWB Radar:** Non contact UWB radar is used to track physiological parameters such as respiration and heart rate in environments like ICUs and home care settings. These systems are particularly effective for neonatal care and detecting respiratory irregularities (Ghosh and Sahu, 2016).

### 2.5.2 Smart Logistics and Warehouses

The precision and reliability of UWB have made it a key enabler in smart logistics, transforming how assets and operations are managed.

- **Real Time Asset Tracking:** UWB provides 5–30 cm accuracy for tracking goods, pallets, and machinery in warehouses. This real time positioning reduces inefficiencies and improves inventory management (Elsanhoury et al., 2022)
- **Automated Guided Vehicles (AGVs):** UWB enhances AGV navigation by enabling precise localisation in complex indoor environments. Integration with IoT and AI systems further optimises route planning and collision avoidance (Elsanhoury et al., 2022)
- **Comparison with Other Technologies:** While RFID and Bluetooth are widely used for asset tracking, UWB outperforms both in terms of accuracy and range, making it indispensable for Industry 4.0 applications.

### **2.5.3 Consumer Electronics**

UWB has developed consumer devices, enabling advanced features and improved user experiences.

- **Smartphones and IoT Integration:** Modern smartphones equipped with UWB chipsets (e.g., Samsung Galaxy S21+) offer sub meter accuracy for applications such as device tracking, indoor navigation, and nearby device discovery. Tests demonstrate strong performances over distances up to 30 meters, with minor challenges outdoors (Di Pietra and Dabove, 2023).
- **Practical Use Cases:** Smartphone UWB capabilities are used in shopping centres, stadiums, and hospitals and festivals for precise navigation. Additionally, they enable seamless interaction with smart home devices, making smartphones central to IoT ecosystems.
- **Future Potential:** UWB's role in consumer devices is expanding, with potential applications in augmented reality (AR) and next generation IoT systems.

### **2.5.4 Strengths and Challenges**

#### **Strengths:**

- 1) UWB's high accuracy, robust NLoS performance, and low power consumption make it an outstanding choice for precision localisation in diverse scenarios.
- 2) Its ability to integrate with IoT systems improves its versatility.

#### **Challenges:**

- 1) Environmental factors such as multipath effects can impact accuracy, particularly in outdoor or cluttered environments (Di Pietra and Dabove, 2023).
- 2) The relatively high cost of UWB hardware remains a barrier to widespread adoption in some industries.

### **2.5.5 Summary of Applications and Case Studies**

The case studies and applications discussed highlight UWB's transformative potential across industries. From healthcare innovations to smart logistics and consumer electronics, UWB has consistently demonstrated its value in enabling precision localisation and enhancing operational efficiency. However, addressing challenges such as cost and environmental limitations will be crucial for its broader adoption in future technologies.

To fully understand UWB's future potential, it is necessary to explore emerging trends and the key challenges that must be addressed. These topics are discussed in the following section.

## **2.6 Emerging Trends and Challenges**

The use of UWB technology has accelerated in recent years, driven by its potential for high accuracy localisation and integration into diverse industries. This section explores emerging applications of UWB, and the challenges associated with its wider deployment.

### **2.6.1 Future Applications**

UWB's unique characteristics, such as below meter accuracy, low power consumption and resilience to interference, have enabled innovative applications across various fields.

#### **1) Augmented Reality (AR):**

- a) UWB supports interactive indoor environments through real time localisation. For instance, self-actuated projectors powered by UWB enable dynamic AR experiences in spaces like museums, classrooms and exhibition halls (Elsharkawy et al., 2021).
- b) The technology facilitates multiuser AR environments by tracking multiple devices simultaneously, providing scalable solutions for joint applications.

#### **2) Smart Cities and IoT:**

- a) UWB's integration into IoT systems allows real time location tracking in urban infrastructure, including smart hospitals, intelligent transportation systems and urban safety monitoring (Ulusar et al., 2020).
- b) The high accuracy of UWB, Allows Real Time Locating System (RTLS). To assist asset tracking, emergency navigation and disaster response in mission critical applications.

#### **3) Industrial Automation:**

- a) In manufacturing and logistics, UWB enables precise asset and material tracking. Low-cost systems, such as those based on the Qorvo MDEK1001 kit, demonstrate its scalability for small to medium enterprises (Volpi et al., 2023).
- b) UWB applications in robots and autonomous vehicles benefit from centimetre accuracy for efficient navigation in dynamic industrial environments, as UWB technology has been demonstrated to achieve centimetre level precision through advanced techniques such as Angle of Arrival (AoA) and Phase Difference of Arrival (PDoA), even in challenging conditions involving multipath propagation and environmental noise (Margiani et al., 2023).

#### **4) Machine Learning Integration:**

- a) Advanced algorithms, such as support vector machines (SVM) and Gaussian processes (GP), enable error mitigation and enhance localisation accuracy in complex environments (Wymeersch et al., 2012). These methods make UWB systems more reliable in mixed LOS/NLOS conditions.

## 2.6.2 Challenges in Adoption

Despite its advantages, several challenges limit UWB's widespread adoption.

- **NLOS Propagation:** None line of sight (NLOS) conditions significantly impact UWB accuracy. Techniques like machine learning based NLOS classification and mitigation have shown promise but require computational resources and extensive training data (Maranò et al., 2010).
- **Scalability:** Large scale deployments face challenges in maintaining accuracy and performance, particularly in dense urban or industrial settings where anchor density must increase (Ridolfi et al., 2021).
- **Energy Efficiency:** UWB systems are more power efficient than alternatives like Wi-Fi and Bluetooth due to their low emission levels and minimal power requirements for communication. However, large scale IoT setups, such as real time locating systems (RTLS), can still strain battery life and energy budgets because of the continuous operation required for precise synchronisation and data transmission (Minoli & Occhiogrosso, 2018).
- **Cost:** While UWB is becoming more affordable, its deployment remains costlier than technologies like RFID or Bluetooth. Balancing cost and performance are critical for small and medium enterprises (Volpi et al., 2023).
- **Regulatory Challenges:** The lack of global standardisation for UWB spectrum usage complicates international deployments. Unified standards are essential for interoperability across devices and regions (Ulusar et al., 2020).

## 2.6.3 Future Research Directions

- **Advanced Error Mitigation:** Further integration of machine learning models can address NLOS challenges and environmental interference.
- **Energy Optimisation:** Research into low power hardware and dynamic power management algorithms is necessary for large scale IoT deployments.
- **Scalable Deployments:** Developing self-calibrating anchors and hybrid localisation systems that combine UWB with other technologies like LiDAR or GPS could enhance growth.
- **Interoperability Standards:** Global efforts to standardise UWB communication protocols will ensure seamless integration across devices and industries.

## **2.7 Summary of Literature Review**

The review of existing literature highlights the limitations of traditional distance measurement tools in golf applications such as GPS systems and laser rangefinders. GPS, with its metre level accuracy and static measurements are unsuitable for the dynamic nature of golf courses where flagstick positions vary. Although GPS tools such as watches and handheld devices can offer basic club selection, their accuracy is insufficient for precise measurements, particularly at shorter distances. Laser rangefinders, though more precise are flawed by their dependency on unobstructed line of sight and their inability to adapt to environmental complexities like uneven terrain and tree coverage.

UWB technology has emerged as the optimal solution for addressing these shortcomings. UWB's centimetre level accuracy, achieved through Time of Flight (ToF) measurements, allows for reliable distance estimation even in challenging none line of sight (NLoS) conditions. By implementing two way communication between a flagstick mounted transceiver and a handheld receiver, this system ensures accurate and dynamic distance measurement. UWB's low susceptibility to multipath interference further enhances its reliability in complex outdoor environments like golf courses.

However, existing research reveals significant gaps in the application of UWB to sports, particularly golf:

1. Limited studies on implementing two way UWB communication systems specifically tailored for distance measurement in golf.
2. A lack of field validated prototypes demonstrating the feasibility of integrating UWB with personalised performance feedback systems.
3. Minimal exploration of energy efficient designs, such as solar powered wake up mechanisms, for sustainable outdoor applications.

This project addresses these gaps by developing an UWB system that combines precise distance measurement with a personalised club recommendation algorithm. By using a transceiver based two way communication system using Time of Flight (ToF) measurements, the project trials real time adaptability and centimetre level accuracy in outdoor conditions. The use of ToF enables precise and reliable distance estimation by calculating the signal travel time between the flagstick mounted transmitter and the handheld receiver. The insights gained from the literature review provide a foundation for designing, implementing and testing the proposed system, with the goal of improving golfer performance and advancing UWB's application in sports technology.

### 3 Methodology

This chapter outlines the methodology behind the development and implementation of the proposed UWB golf distance measurement and club selection system. The goal was to create a robust, low power solution capable of delivering accurate real time distance data on a golf course while also enhancing gameplay through personalised club recommendations.

The system is divided into two primary components:

1. **Flagstick Unit:** A solar powered static device mounted near or on the flagstick, equipped with a UWB transceiver and barometric sensor for altitude data.
2. **Handheld Device:** A portable user-facing unit that initiates communication, receives distance and altitude data, processes it using onboard algorithms, and displays both the 3D distance and a recommended club via an OLED interface.



Figure 3.1 UWB Communication between Handheld Device and Flagstick Unit

These two units work together using Time of Flight (ToF) ranging and wireless communication to deliver precise distance measurements, even in variable terrain and weather conditions.

The system calculates distances using Time of Flight (ToF) measurements between the flagstick mounted transmitter and the handheld receiver. Flow chart shown in Figure 3.2 shows the proposed system design process. The system then uses stored golfer shot data from an SD memory card to recommend the most suitable club for the distance measured.

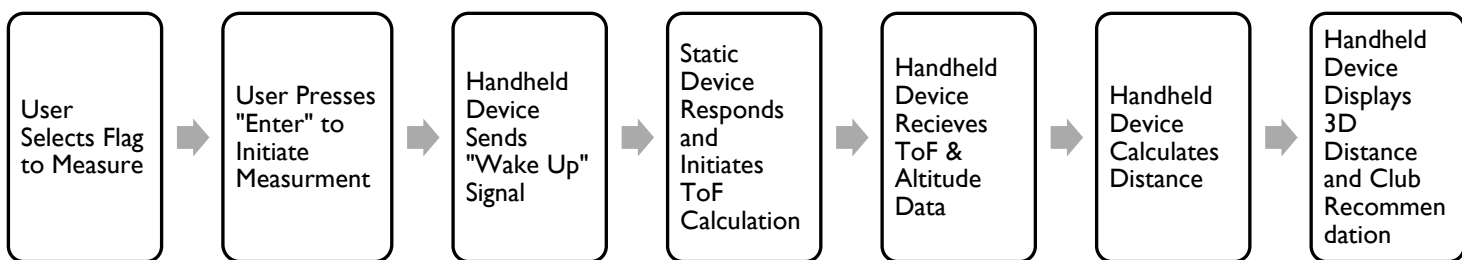


Figure 3.2 Flowchart for System Operation

### **3.1 Hardware Design**

The hardware design for the system is divided into two distinct components: the flagstick unit and the handheld device. Each unit was developed with specific functional requirements in mind, including environmental durability, power efficiency and reliable communication performance. The selection of hardware components was based on a detailed comparison with alternative technologies, considering factors such as accuracy, cost, energy efficiency and ease of integration.

A full justification and comparison of component choices can be found in Appendix 10.1 . This section outlines the design considerations, component integration, and construction process for both devices, detailing how they work together to deliver accurate distance measurements and user interaction in a golf course environment.

The final component selection reflects a balance between performance, cost and ease of integration. The ESP32-S3 platform provided a capable and flexible processing base, while the UWB modules enabled precise ranging essential to the system's core functionality. The BMP388 barometric sensors offered consistent altitude data and the LoRa (HC-12) modules ensured reliable long range communication between devices. Supplementary components such as the OLED display, microSD card and TP4056 charging module were selected for their reliability and proven performance in embedded systems. Together, these choices enabled the development of a compact and modular system ready for field testing.

## Flagstick Unit

The flagstick unit comprises several key components essential to its functionality. At its core is an ESP32 microcontroller, which manages the system's logic and communication. The unit uses a DWM3000 Ultra-Wideband (UWB) transceiver module to enable precise distance measurement between the flagstick and the handheld receiver. Power is supplied through a solar panel connected to a DC-DC converter, which enables continuous battery charging and ensures the system can operate autonomously in outdoor conditions.

The hardware was developed on a custom printed circuit board (PCB) designed in KiCad, which integrates the ESP32, the DWM3000 module, and power management circuitry into a compact and efficient layout. A key feature of the design is the implementation of a wake up mechanism, triggered by a signal from the handheld device. This allows the flagstick unit to remain in a low power sleep mode until needed, significantly extending battery life.

Figure 3.3 illustrates the proposed layout of the static flagstick device, showing the integration of solar charging, microcontroller logic and UWB communication within the physical enclosure.



Figure 3.3 Proposed Static Device Flag Stick

## Handheld Device

The handheld unit serves as the user interface and control point for the system. It features an ESP32 microcontroller paired with a DWM3000 UWB transceiver module, which handles precise two way communication with the flagstick unit. An SD card reader is integrated to store user specific shot performance data, such as average distances achieved with different clubs, enabling personalised club recommendations.

To present information in real time, the device includes an OLED screen that displays the measured distance to the flagstick as well as the recommended club for the shot. The interface also includes a set of user buttons that allow golfers to navigate between different holes or measurement modes and to initiate UWB distance measurements manually.

Again, the custom PCB was developed in KiCad, with a layout that accommodates the ESP32, DWM3000, and all peripheral components. The design includes additional input/output (I/O) headers to support future functionality and hardware expansion. The SD card reader, OLED display and user buttons were integrated into a fully functional prototype, with careful attention to power management, layout constraints and user ergonomics.

Firmware was developed to support a range of operations, including hole selection, data logging, and initiating distance measurements via a double sided two way ranging protocol. The software also enables communication with the flagstick device, handling both wake up signals and the reception of UWB measurement data.

Figure 3.4 shows the proposed layout of the handheld device, illustrating the integration of communication, display, storage, and user interaction components into a cohesive, portable unit.

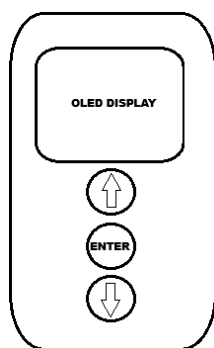


Figure 3.4 Proposed Handheld Device

### 3.1.1 Proof of Concept Process

Before committing to a full PCB design, an initial Veroboard prototype was developed to validate the core functionality and integration of the system's key components. This early-stage prototype enabled rapid testing, troubleshooting and iteration during the hardware development phase.

#### Veroboard Prototype Assembly

To support the design and functionality of the proposed UWB distance measurement system an initial Veroboard prototype was assembled (Figure 3.5). The prototype served as a proof of concept for the integration of all hardware components and allowed for rapid testing and debugging prior to creating a printed circuit board (PCB).

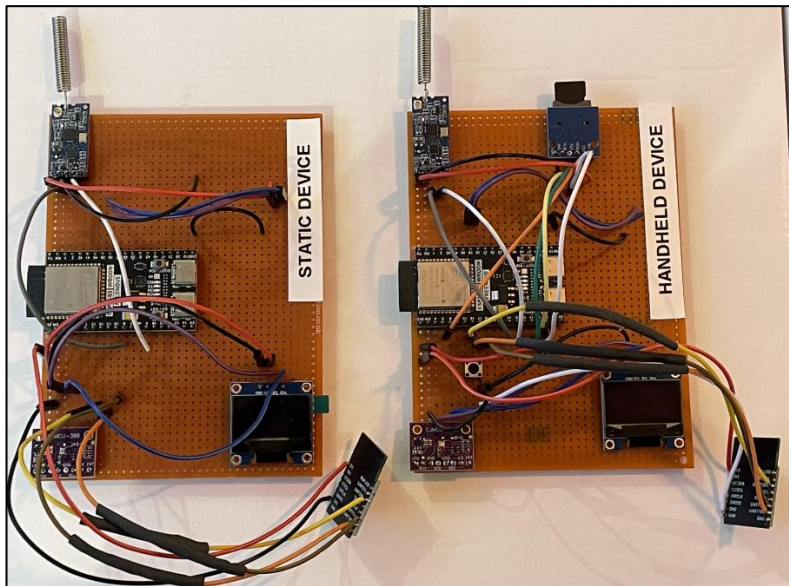


Figure 3.5 Veroboard Prototype Assembly for Proof of Concept

The main components used in the prototype included:

1. **ESP32 Microcontroller:** Served as the core processing unit, managing communication and data logging.
2. **DW3000 UWB Module:** Provided precise ranging capabilities based on single sided two way ranging (SS-TWR) using the IEEE 802.15.4z standard.
3. **Card Module:** Enabled data logging of key metrics such as RSSI, ToF, altitude and measured distances for results. The SD card function will be later utilised to store the users golf shot data for the club selection algorithm.
4. **OLED Screen:** Displayed real time output from the system.

## Wiring and Communication

The components were connected on the Veroboard using Serial Peripheral Interface (SPI) and Inter Integrated Circuit (I2C) communication protocols. SPI handled communication with the DW3000 and SD card modules, while I2C was used for the BMP388 barometric sensor. A common ground was maintained throughout the setup to ensure stable communication and prevent floating signals.

Figure 3.6 shows the wiring schematic for the Veroboard prototype and layout.

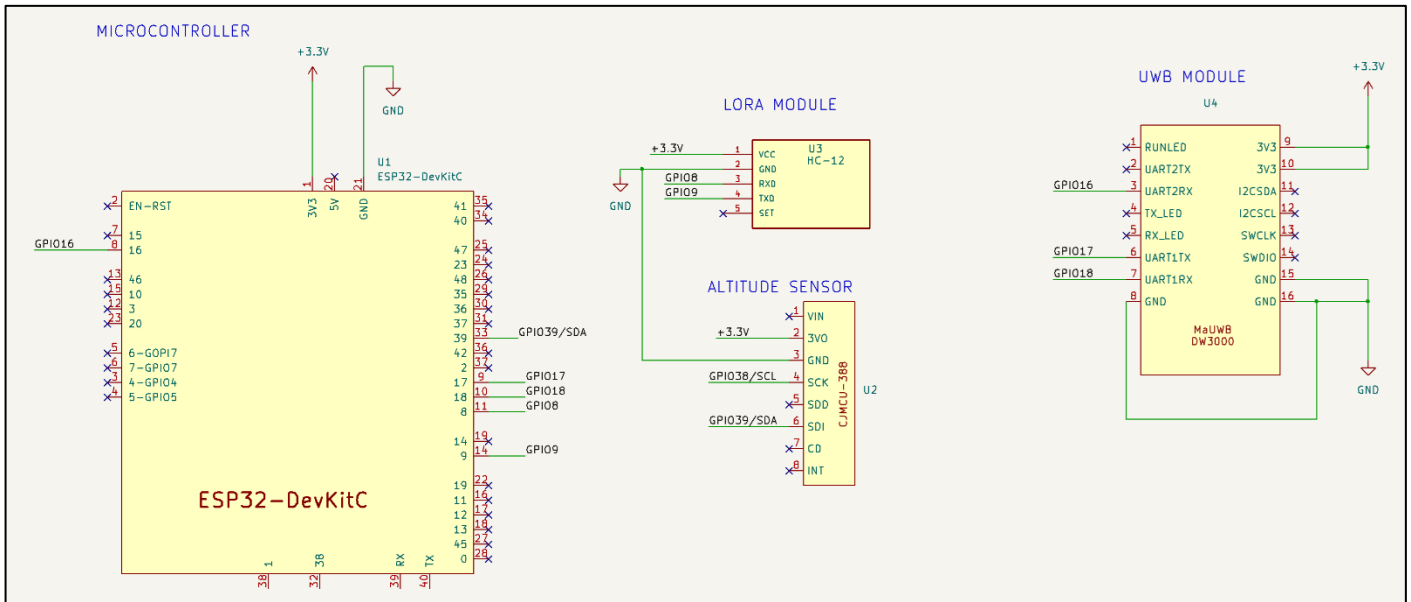


Figure 3.6 Veroboard Prototype Wiring Schematic

Power was supplied via USB battery banks connected directly to the ESP32 development board. This setup allowed the prototype to be tested in a flat sports field validating core system functionality prior to PCB design.

Photographs of the Veroboard unit during testing can be found in Appendix 10.5.2.

### 3.1.2 Power Systems

The power systems for both the static and handheld devices were designed to be modular, compact, and reliable. Each system is powered by a 3.7 V 2000 mAh lithium-polymer (LiPo) battery and uses a dedicated charging circuit to manage power delivery and battery protection. Flow diagrams and circuit schematics are provided to illustrate the full implementation.

#### Static Unit Power Input Configuration

The static unit incorporates a 5 V 230 mA solar panel system to enable autonomous, long term operation while eliminating the need for manual charging. The panel was specifically sized to match the surface area of the enclosure for efficient integration. However, field testing revealed that output voltage could drop as low as 3.69 V under overcast conditions, which is insufficient for charging the lithium-polymer battery directly.

To address this a boost converter (MT3608) was introduced to step up the variable solar output to a stable 5 V, ensuring consistent input to the TP4056 lithium-ion charge controller, which requires a minimum input of 4.4–4.5 V. The TP4056 safely manages the charging process for the 3.7 V 2000 mAh LiPo battery, using a constant-current/constant-voltage (CC/CV) charging profile. Finally, a low dropout (LDO) voltage regulator steps the battery output down to 3.3 V, delivering clean and stable power to the system's electronics.

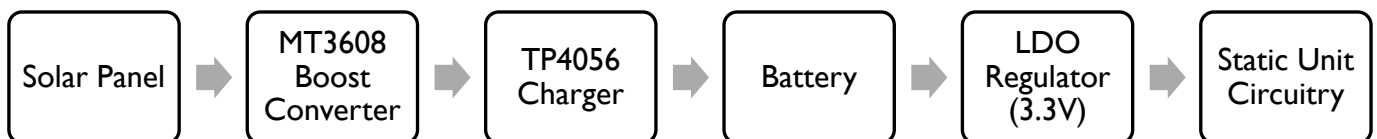


Figure 3.7 Static Unit Solar Power System Flow Diagram

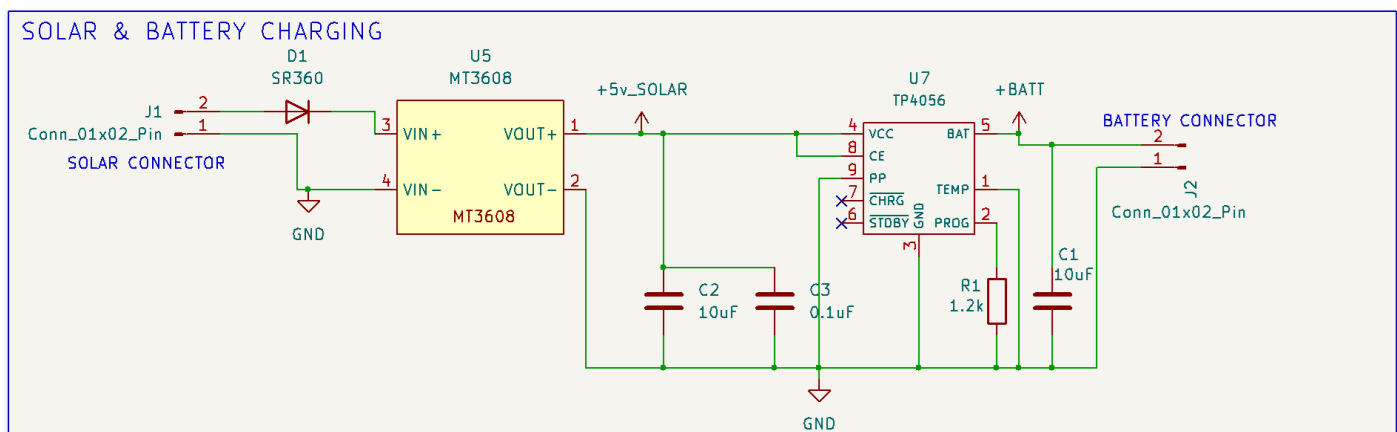


Figure 3.8 Static Unit -Solar and Battery Charging Schematic

## Handheld Unit Power Input Configuration

The handheld device is powered and charged via a 5V USB-C input. Like the static unit, the battery is charged through a TP4056 lithium-ion charge controller module, which manages charging safely using a constant current/constant voltage (CC/CV) profile. The output is then regulated to 3.3 V using a low dropout regulator (LDO). The system also includes an optional on/off switch between the battery and the LDO input, allowing the device to be safely powered down without disconnecting the battery particularly useful during programming, storage or debugging.

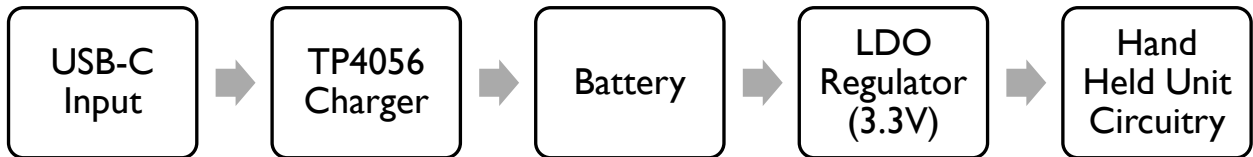


Figure 3.9 Handheld Unit Power Flow Diagram

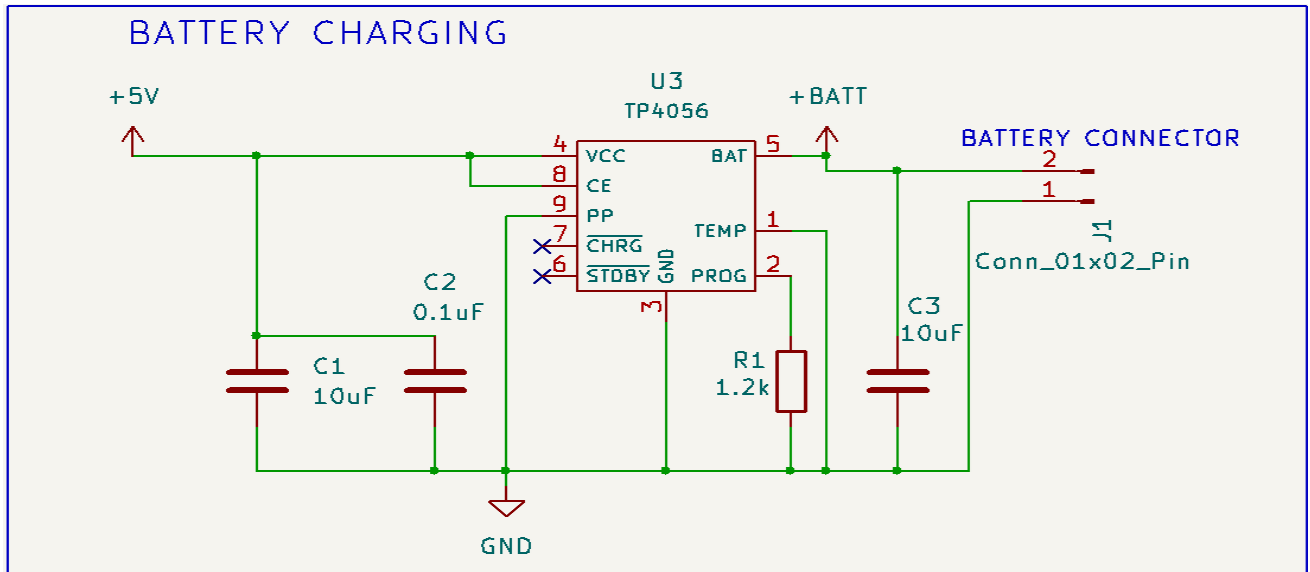


Figure 3.10 Handheld Unit - Battery Charging Schematic

## Battery and Charging Design

Both units use the same 3.7 V 2000 mAh lithium-polymer battery (model LP103554), chosen for its balance of capacity, compact form factor and compatibility with the ESP32-S3's 3.3 Volt operating requirements. The TP4056 charge controller manages the charging process and is configured for an approximate charging current of 833 mA using a 1.2 kΩ resistor connected to the PROG pin. This value was selected to ensure reasonably fast charging while staying within safe operating limits for the battery.

The formula used to determine the charge current is as follows:

*Equation 3.1 Charging Current Formula*

$$I_{CHG} = \frac{1000}{R_{PROG}}$$

Where:

- $I_{CHG}$  = Charging Current in mA
- $R_{PROG}$  = is programming resistor in kΩ

$$I_{CHG} = \frac{1000}{1.2} \approx 833mA$$

## Additional Circuit Features

To ensure stable operation, bypass capacitors were added in accordance with TP4056 datasheet recommendations. A 10 µF electrolytic capacitor (C1) and a 0.1 µF ceramic capacitor (C2) were placed on the TP4056 input side to suppress ripple and voltage spikes. A 10 µF capacitor (C3) was placed at the battery output to stabilise voltage during load changes.

The entire power subsystem was designed with flexibility in mind. The static unit benefits from solar powered autonomy while the handheld device allows convenient USB charging.

## Powering and Filtering

For voltage regulation, the SPX3819 low dropout regulator (U7/U8) was used to step down the battery voltage to a stable 3.3 Volt. The SPX3819 is suitable for low noise applications and requires minimal external components. In accordance with the datasheet, a 4.7  $\mu$ F capacitor (C4) was placed on the input, and a 10  $\mu$ F capacitor (C5) on the output, to maintain stability and filter out transients. Seen in Figure 3.11

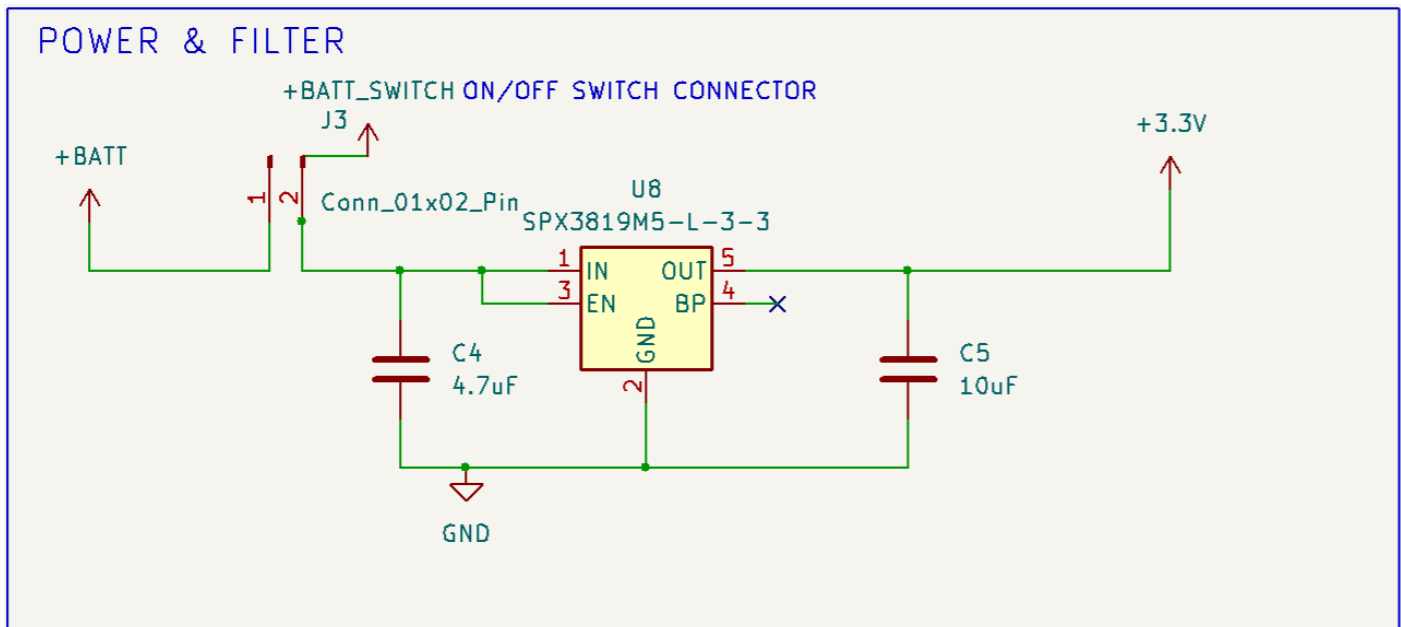


Figure 3.11 Power Regulation and Filtering Schematic

### 3.1.3 Processing and Communications

Both the handheld and static units use the Freenove ESP32-S3 WROOM DevKit, selected for its dual core performance, integrated Wi-Fi and Bluetooth (Wi-Fi disabled in this application) and its wide GPIO availability for peripheral integration as seen in the pin out diagram in Figure 3.12 below.

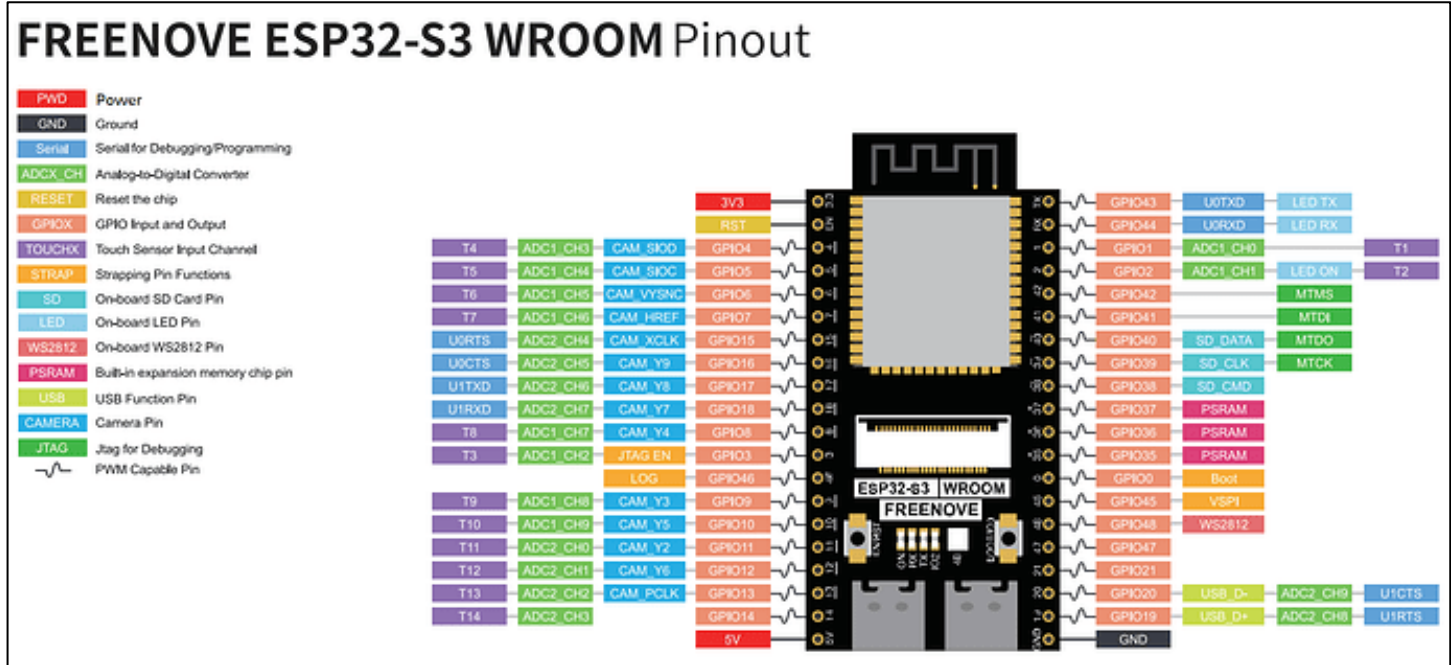


Figure 3.12 ESP32 pinout diagram

(Freenove, 2024).

The schematics for both devices were designed, tested and created using KiCad, a professional grade PCB design tool, as shown in Figure 3.13 and Figure 3.14

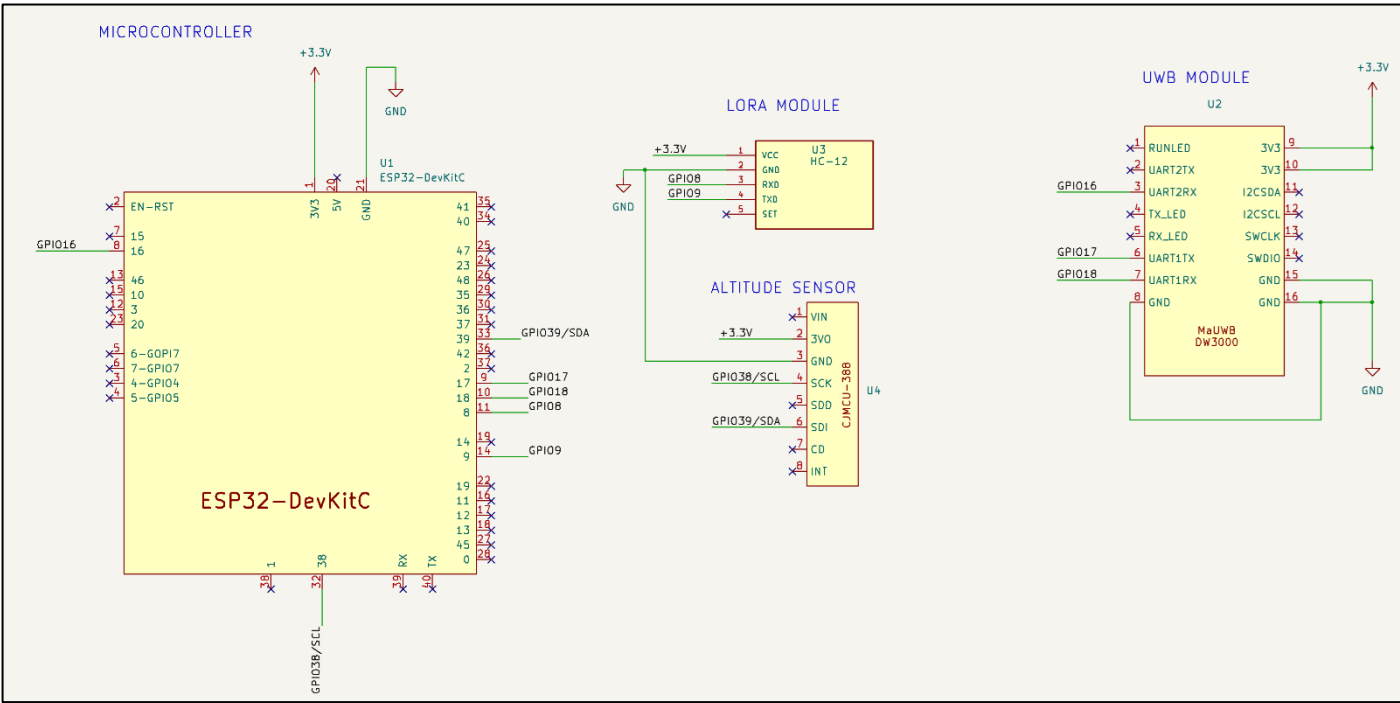


Figure 3.13 Static Unit Schematic Diagram

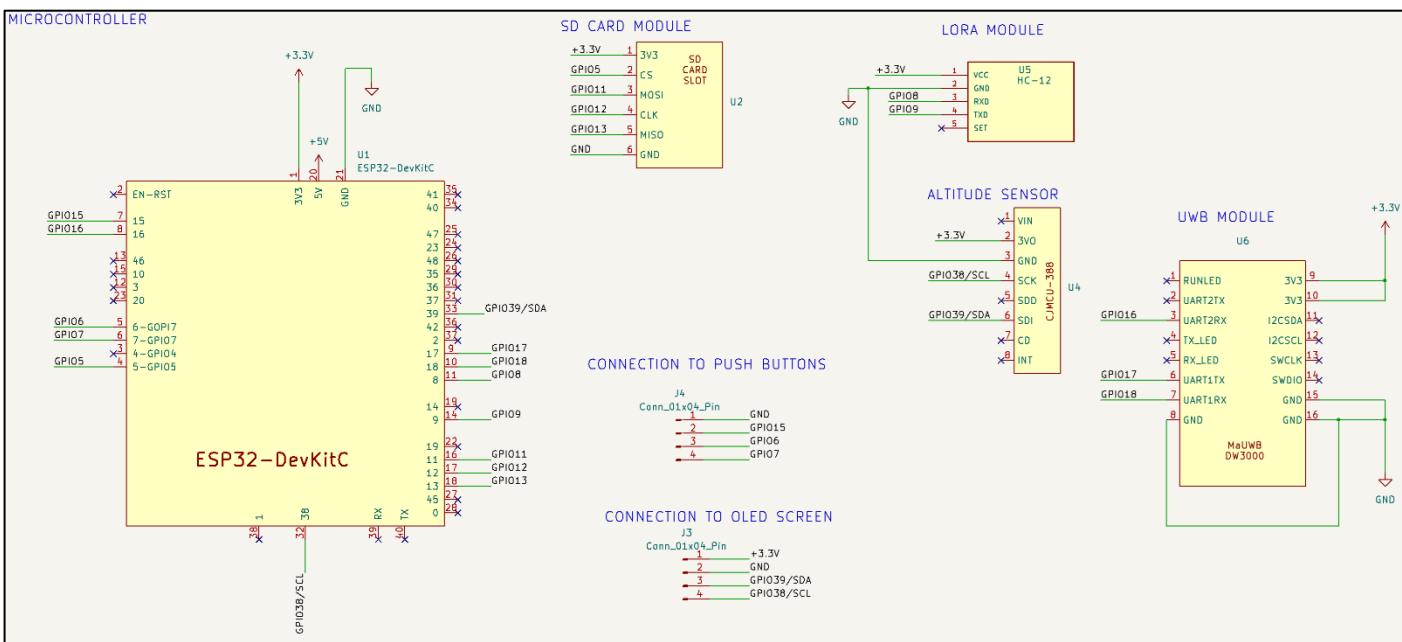


Figure 3.14 Handheld Unit Schematic Diagram

## **Microcontroller Integration**

Each ESP32-S3 board receives a regulated 3.3 V supply from the SPX3819 LDO as shown in Figure 3.11. GPIO pins were assigned based on peripheral requirements and cross referenced against the ESP32 datasheet and pinout chart in Figure 3.12 to avoid conflicts with internal functions or boot modes.

**The following peripheral modules were interfaced directly to the ESP32.**

### **UWB (Ultra-Wideband) Module – DW3000**

- Communicates via UART2 (GPIO16 for TX, GPIO17 for RX)
- Powered by 3.3 V and shares GND with the microcontroller.
- Used to measure horizontal distance between handheld and static units using time of flight ranging.

### **LoRa Module (HC-12)**

- Communicates via UART1 (GPIO8 TX, GPIO9 RX)
- 3.3 V powered.
- Transmits altitude data between units over long distances (e.g., static → handheld)

### **Altitude Sensor (BMP388)**

- Communicates via Inter Integrated Circuit (I2C) (GPIO38 = SCL, GPIO39 = SDA)
- Powered via 3.3 V
- Provides altitude data to allow 3D distance calculation.

### **OLED Display (Handheld Only)**

- Also uses I2C (shares bus with BMP388)
- Displays user interface, measurements, and calculated results.
- Connected via GPIO38 (SCL), GPIO39 (SDA)

## **SD Card Module (Handheld Only)**

The SD card module interfaces with the ESP32 via the Serial Peripheral Interface (SPI) protocol and is used to store sensor data, system logs and user club distance data in a .csv format. This allows for persistent data logging during field testing and offline access to personalised distance data during normal operation.

The SPI connections are as follows:

- **CS (Chip select):** GPIO 15- Selects the SD card during SPI communication.
- **MOSI (Master Out, Slave In):** GPIO 11 - Transfers data from the ESP32 to the SD card.
- **CLK (Clock) :** GPIO 12 - Provides the clock signal that synchronises data transfer.
- **MISO (Master In, Slave Out):** GPIO 13 – Sends the data from the SD CARD BACK TO THE ESP32

## **Push Buttons (Handheld Only)**

- Connected to GPIO6, GPIO7, and GPIO15
- Configured as digital inputs with internal pull-up resistors.
- Used to interact with the user interface on the OLED display( Up, Down and Enter Buttons).

The hardware design ensures that both devices maintain consistent operation using a shared architecture and communication structure with minor variations to accommodate the needs of the portable handheld form factor.

### 3.1.4 PCB Design and Manufacture

The printed circuit boards (PCBs) for both the handheld and static units were designed using KiCad, an open source electronic design automation (EDA) tool. The schematic designs had already been developed and verified as a proof of concepts (see Section 3.3.4), forming the basis for the PCB layout.

Designs were constrained by the internal dimensions of the chosen enclosures (as discussed in Section 10.1.8), and care was taken to position components and connectors so they would align with openings for USB, switches and sensors. Component footprints and mounting holes were selected based on datasheet specifications and KiCad's verified libraries.

To ensure signal integrity and reliability, particular attention was paid to:

- Keeping power and ground traces short and wide
- Avoiding signal trace crossover
- Grouping related modules (e.g., power, microcontroller, communication)
- Using clear silkscreen labelling for easier assembly and testing

KiCad's Electrical Rules Check (ERC) and Design Rules Check (DRC) tools were used to identify and resolve any issues prior to manufacture. Once the design passed these checks, the Gerber and drill files were exported.

Figure 3.15 below shows the process used for designing the PCB's.

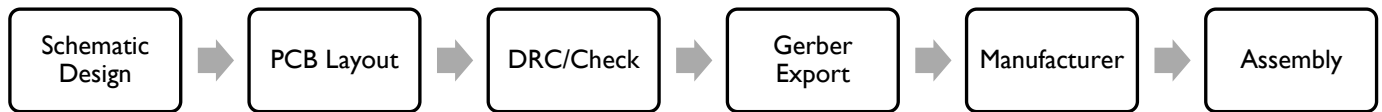


Figure 3.15 Flow Diagram for PCB Design and Manufacture Process

The circuit trace layout and 3D view for the Static unit can be seen in Figure 3.16 and Figure 3.17

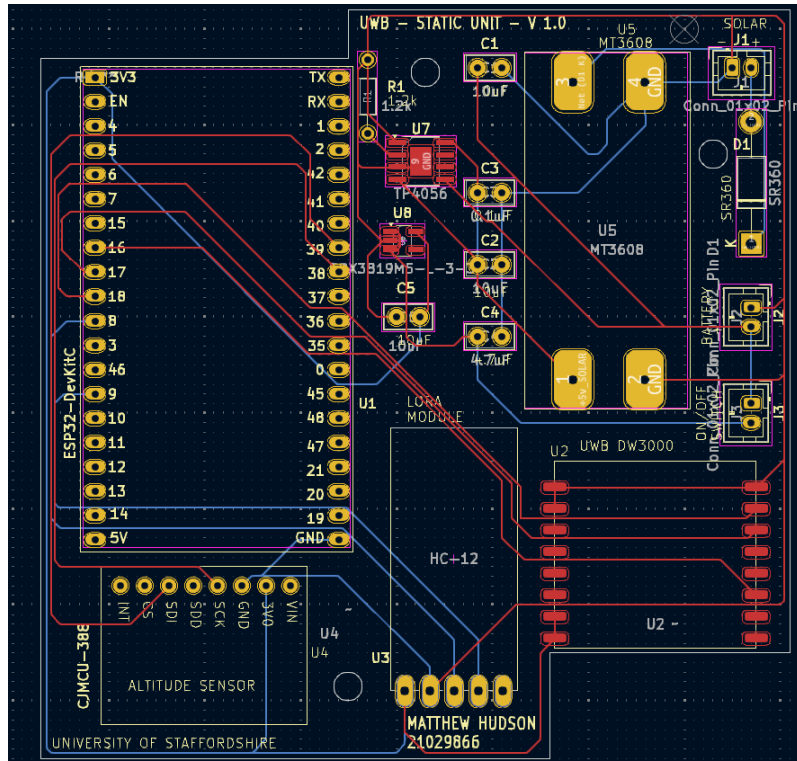


Figure 3.16 Static Unit - PCB Design Layout

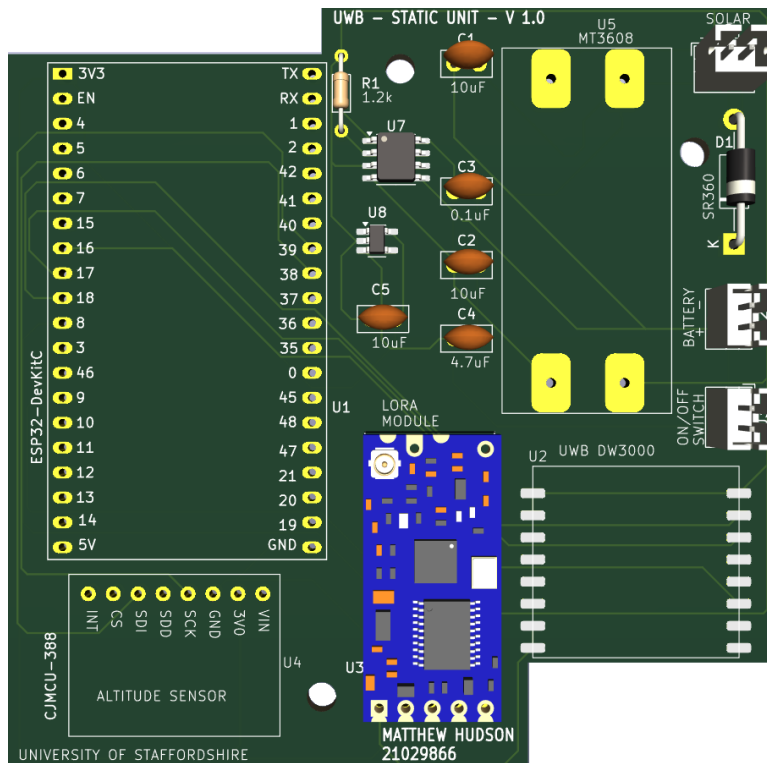


Figure 3.17 Static Unit - 3D Design Layout

The circuit trace layout and 3D view for the Handheld unit can be seen in Figure 3.18 and Figure 3.19.

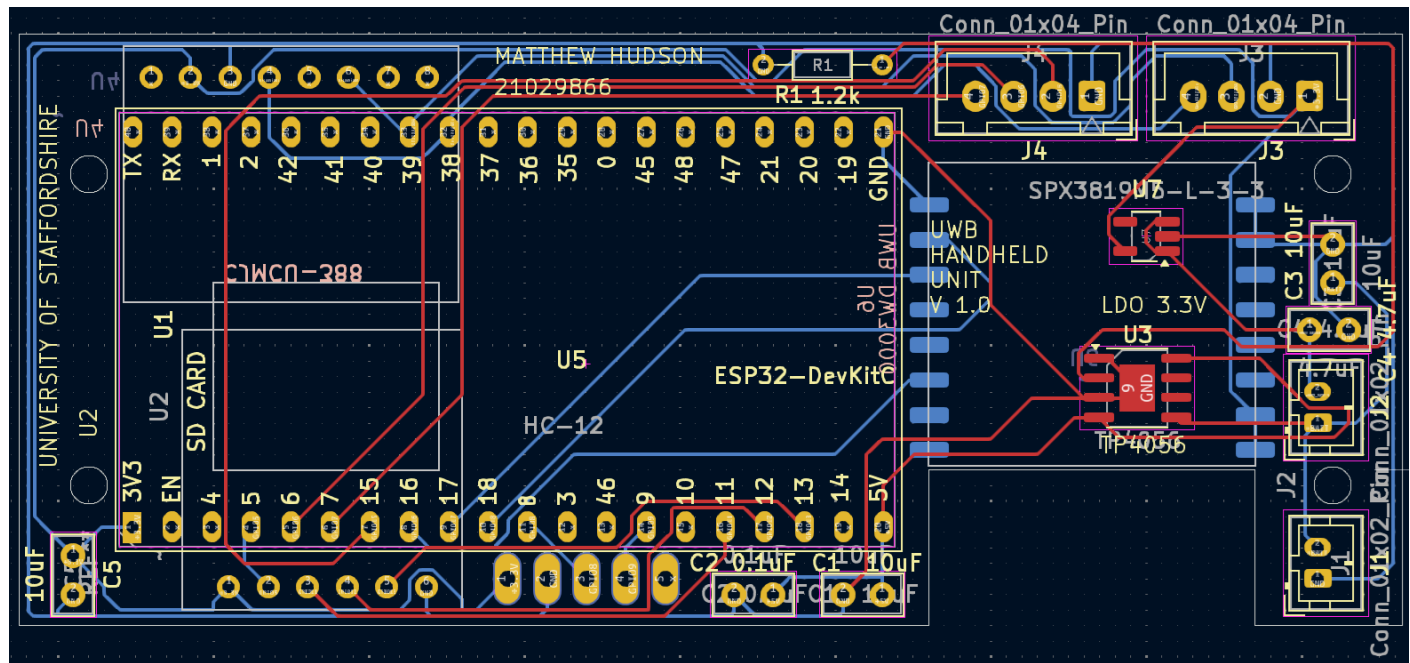


Figure 3.18 Handheld Unit - PCB Design Layout

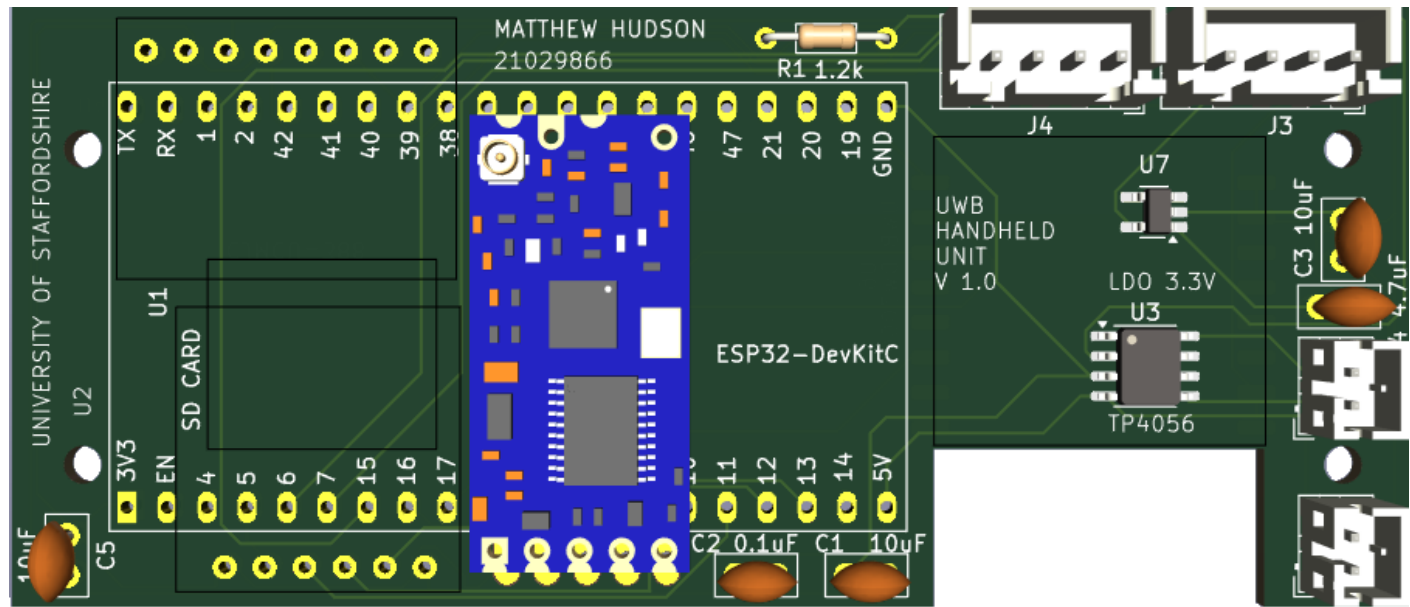


Figure 3.19 Handheld Unit - 3D Design Layout

These files were submitted to a PCB fabrication service (PCBWay.com) which provided manufacturing for both boards. The final boards included clear silkscreen labels, mounting holes and through hole or surface mount footprints to support hand assembly using standard soldering equipment. The received PCB's can be seen in Figure 3.20 below.

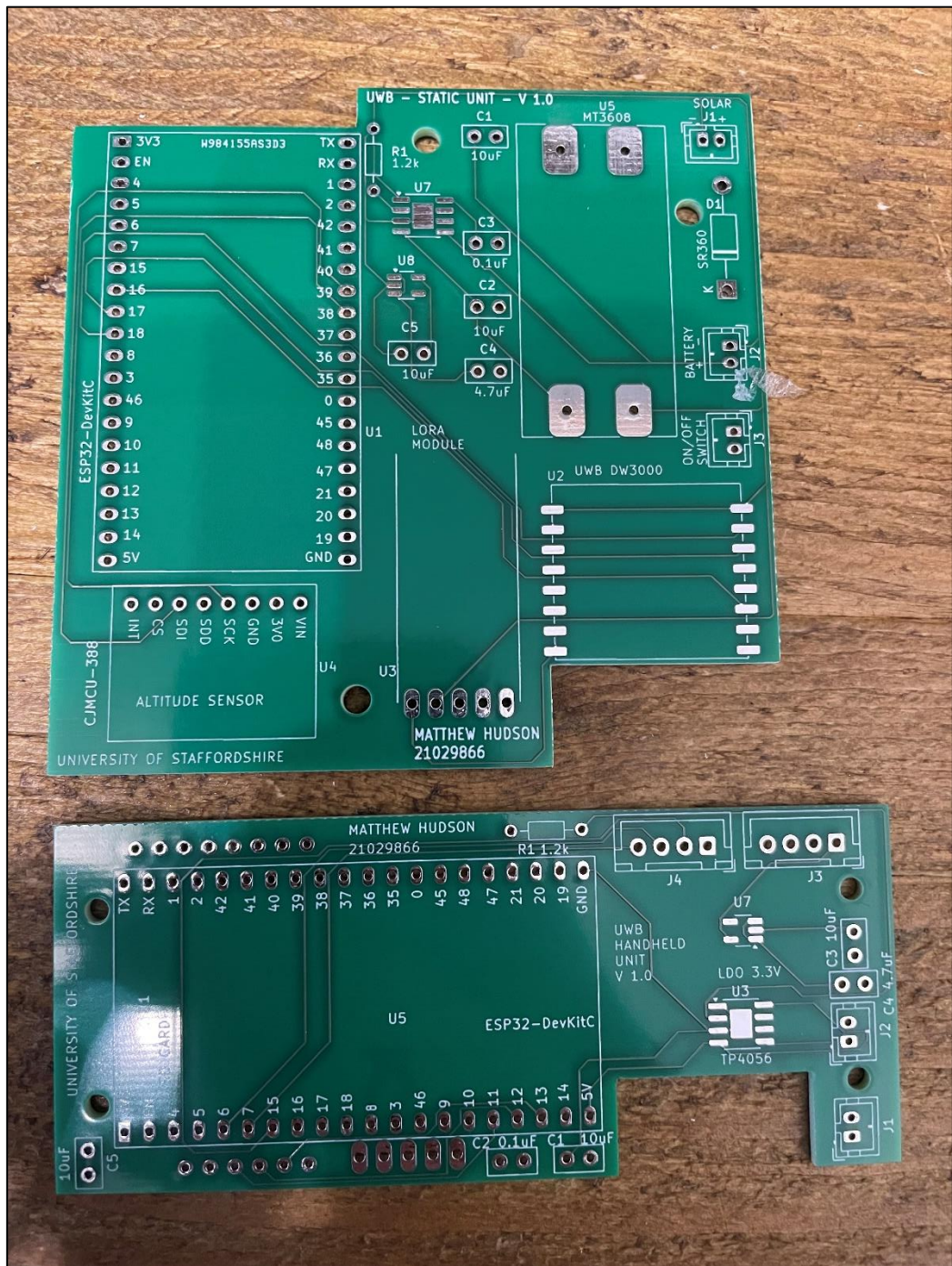


Figure 3.20 Manufactured PCB's

## Assembly

Following fabrication, both PCBs were populated manually using standard through hole and surface mount soldering techniques. The assembly process was carried out in stages to reduce the risk of damage, identify faults early and simplify debugging.

Components were soldered in logical groups according to subsystem priority:

1. **Power system:** battery connector, TP4056 charger, LDO regulator
2. **Microcontroller and basic passives:** ESP32-S3 DevKit headers, decoupling capacitors
3. **Peripheral modules:** UWB, LoRa, SD card, sensors and display
4. **Connectors and user interface components:** buttons, switches, pin headers

After each stage, the board was partially powered to verify functionality:

- Voltage regulators were checked for correct output.
- The ESP32 was flashed with test code to confirm serial comms.
- Modules were tested individually using simple sketches to confirm communication.

This progressive approach ensured issues could be isolated and resolved without risking the entire board.

A full Bill of Materials (BOM) was prepared to keep track of the components used for each PCB and can be found in Appendix 10.4.

### **3.1.5    Finished Build**

The final assembly of both the handheld unit and the static anchor unit reflects the successful integration of all electronic, mechanical, and user interface components discussed in the previous sections. The process is documented further in Appendix 10.5.3, including photographs of key stages during construction.

The fully assembled printed circuit boards (PCBs) were installed into their respective enclosures, with all subsystems tested for electrical integrity and firmware stability. Care was taken to ensure that both units were compact and weather resistant suitable for outdoor use on a golf course.

The images below show the completed handheld and static units in their final form:

#### **Handheld Unit**



*Figure 3.21 Finished Handheld Device (Front)*



Figure 3.22 Finished Handheld Device (Front, showing USB Port)



Figure 3.23 Finished Handheld Device (Top, Showing On/Off Switch)

## Static Unit



Figure 3.24 Static Unit (Side)

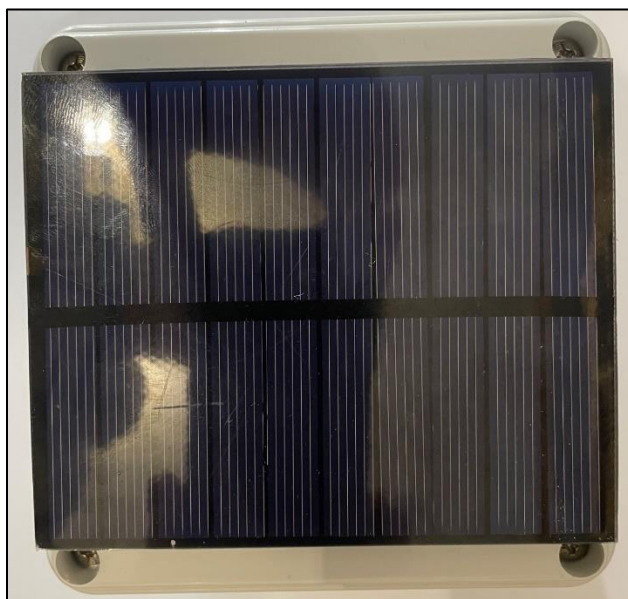


Figure 3.25 Static Unit (Top, Showing Solar Panel)



Figure 3.26 Static Unit (Full Flag View)

### **3.1.6 Summary of Hardware Design**

The hardware design process successfully brought together a range of sensors, wireless communication modules and user interface elements to meet the functional requirements of the system. The final design features two distinct devices a handheld unit and a static anchor unit each optimised for its specific role within the overall architecture.

The handheld unit integrates a 0.96" OLED display, a 3-button input interface, an ESP32 microcontroller and multiple peripheral modules including UWB, LoRa (HC-12), microSD and a BMP388 barometric sensor. The static unit, acting as a fixed reference point, includes its own ESP32, UWB module, LoRa radio and BMP388 sensor for altitude reference.

Both units are powered by rechargeable lithium-ion batteries, regulated by onboard charging and voltage conversion circuitry. Components were selected for low power consumption, high reliability and compatibility with the ESP32's I/O capabilities.

Prototyping was carried out using custom designed PCBs, assembled, and validated in logical stages. Enclosures were selected and modified to protect internal components while allowing ease of access and visibility for the user. The result is a field ready system capable of accurate 3D distance measurement through wireless communication and onboard computation.

## 3.2 Software Development

This section outlines the software development process behind the handheld and static units, detailing how sensor integration, user interaction, data communication, and decision making logic were implemented. The firmware was developed using the Arduino framework and written in C++ to run on ESP32 microcontrollers.

The software has been modularly broken down into key subsystems:

- The main system loop and event handling.
- User interface controls and menu navigation.
- Club recommendation logic using SD card data.
- Inter unit communication and positioning using UWB and LoRa.

Each subsection below describes the functionality and implementation of these components. All code listings have been excluded from the main body for clarity, the complete code for both the handheld and static units are found in Appendix 10.2.

The full working source codes provided in Appendix 10.2.2 detail the complete firmware for both the handheld and static units of the UWB system. These codes are written in C++ using the Arduino framework and are structured to handle sensor integration, communication protocols (UWB and LoRa), user interface logic and data processing. The handheld unit's code includes features for initiating distance measurements, receiving data, displaying output on the OLED screen and recommending golf clubs based on user data from the SD card. The static unit's code manages the reception of wake up signals, response with distance and altitude data, and power efficient operation using low power modes.

To upload the code to each ESP32-S3 microcontroller, the Arduino IDE was used with the appropriate board definitions installed via the Espressif Systems board manager URL. Each device was connected via USB-C to the development machine. Within the Arduino IDE, the correct COM port and board model (ESP32-S3 Dev Module) were selected, and the code was compiled and flashed using the "Upload" button. Successful uploading was confirmed via the serial monitor, where real time outputs and debugging information could be viewed for validation and troubleshooting.

This section also includes a detailed system level software architecture diagram (Figure 3.27). It captures how the handheld and static units interact through UART based communication protocols (UWB and LoRa), how peripheral components interface via SPI and I2C and how the system manages non blocking logic using millis() timers. This diagram reflects the actual implementation structure and provides a deeper view of internal processes and hardware communication flow.

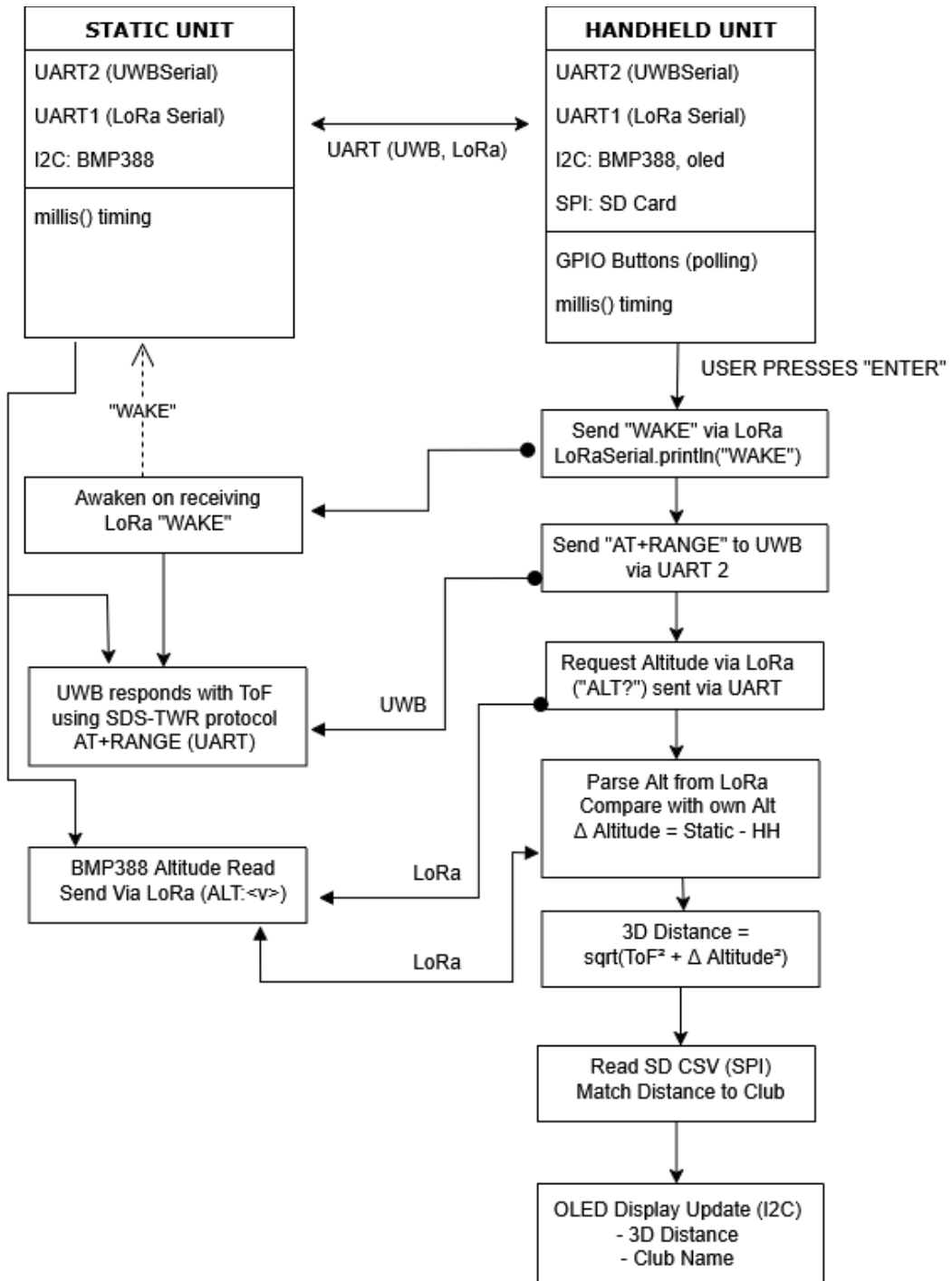


Figure 3.27 System Communication and Processing Flow Chart

### 3.2.1 System Loops and Sensor Integration

The main program logic for both the handheld and static units follows a structured loop-based execution model. The program relies on the Arduino framework's `loop()` function, which runs continuously after the `setup()` phase. This approach ensures that sensor readings, user input handling and communication tasks are performed repeatedly and in real time.

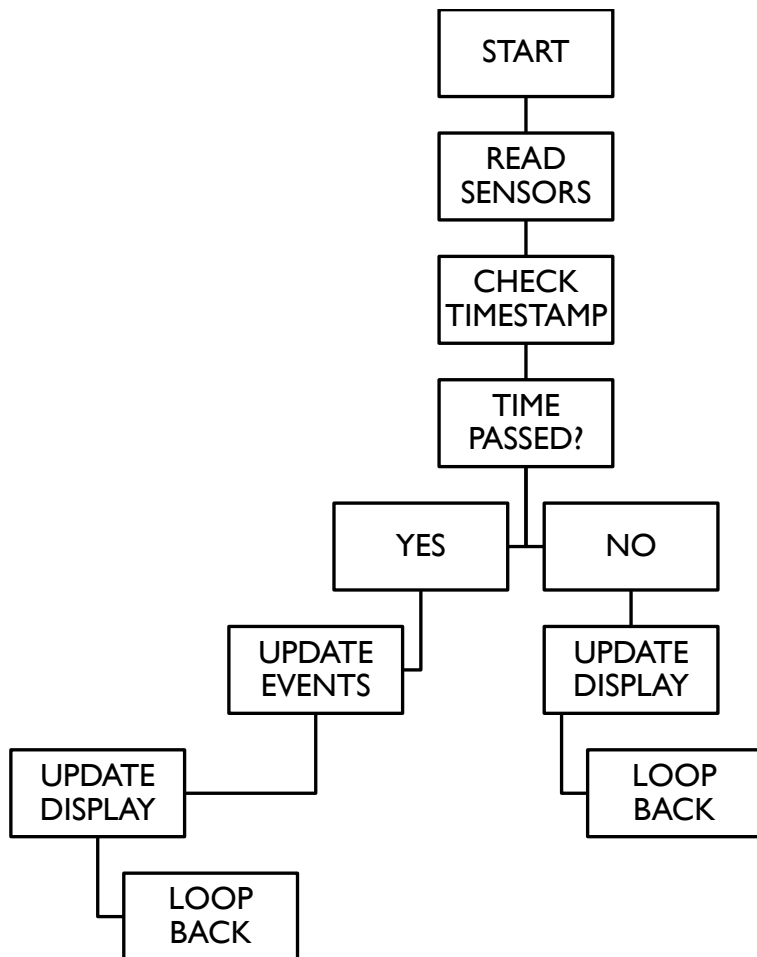


Figure 3.28 System Loop for Sensor Reading/Updating/Display Management

## Main Execution Loop

The core logic inside the loop() function operates using none blocking timing, using the millis() function to schedule events without introducing delays. This allows the system to manage multiple asynchronous tasks such as updating the display, reading buttons, or communicating over serial without interrupting the responsiveness of the user interface.

*Code 3.1*

```
unsigned long now = millis();

if (now - lastDisplayTime >= DISPLAY_INTERVAL) {
    // Update display
    lastDisplayTime = now;
}

if (dataActive && now - lastUpdateTime >= UPDATE_INTERVAL) {
    // Trigger UWB ranging
    lastUpdateTime = now;
}
```

By comparing the current time (now) with the last recorded event times (lastDisplayTime, lastUpdateTime), the system achieves predictable periodic actions without blocking delays.

## Sensor Integration (BMP388 Altimeter)

Both the handheld and static units integrate an Adafruit BMP388 barometric pressure sensor for altitude measurement. This sensor communicates over the I2C bus and provides accurate relative altitude based on atmospheric pressure.

The initialisation takes place during setup():

*Code 3.2*

```
if (!bmp.begin_I2C(0x77)) {  
    while (1); // Halt if sensor init fails  
}
```

Altitude is then read during the main loop using:

*Code 3.3*

```
if (bmp.performReading()) {  
    handheldAlt = bmp.readAltitude(SEA_LEVEL_PRESSURE);  
}
```

The local sea level pressure is predefined in the firmware taken from the Met Office website and can be calibrated for local conditions:

*Code 3.4*

```
#define SEA_LEVEL_PRESSURE 1028.0
```

This altitude reading is an input for computing the 3D distance between the handheld unit and the static anchor. The handheld's altitude is compared with the anchors to calculate the vertical component of distance, enabling a true three dimensional measurement rather than simple horizontal range.

## Data Loop Events

The system loop governs:

- **Display refresh** (every 3 seconds)
- **Sensor updates**
- **User interface responsiveness**
- **Serial communication timing**

This modular, event based loop ensures that the device remains power efficient, responsive and capable of handling time sensitive sensor and communication tasks.

### 3.2.2 User Interface Controls

The handheld device features a minimal but intuitive user interface comprising a 0.96" OLED display (Figure 10.5) and a 3 button control system seen in Figure 3.29. These buttons include:

- **Enter** (Centre button): Used for selection and activation.
- **Up** (Top button): Used to navigate upward in menu options.
- **Down** (Bottom button): Used to navigate downward in menu options.

#### Physical Layout



Figure 3.29 Membrane Push Buttons

(AliExpress, 2024)

The buttons are configured with internal input pullups on general purpose input/output (GPIO) pins 15,4 and 10 in the firmware to simplify wiring. A basic debouncing system is implemented using millis() timestamps to prevent erroneous state changes:

Code 3.5

```
#define BTN_ENTER 15
#define BTN_UP    4
#define BTN_DOWN  10
```

## Menu Navigation Logic

All interface interactions operate through a state machine defined in code via the MenuState enum:

*Code 3.6*

```
enum MenuState {  
    MENU_MAIN,  
    MENU_SETTINGS,  
    MENU_UNITS,  
    MENU_ENGINEER,  
    MENU_ACTIVE_DATA  
};
```

Depending on the active state, user input is processed accordingly. For example, the following snippet shows how the “Enter” button toggles between menus or triggers a return to the main menu when held:

*Code 3.7*

```
if (digitalRead(BTN_ENTER) == LOW) {  
    if (enterPressStart == 0) enterPressStart = now;  
    else if (!enterHoldTriggered && now - enterPressStart >= 2500) {  
        currentMenu = MENU_MAIN;  
        enterHoldTriggered = true;  
    }  
}
```

A long press of  $\geq 2.5$  seconds on the Enter button acts as a "back to home" override from any screen while short taps are used for selection.

## Display Rendering

All menus and data are drawn on the OLED screen using the Adafruit\_SSD1306 library. For example, when in “MENU\_ENGINEER” state key values are shown such as UWB distance, RSSI, and altitude:

*Code 3.8*

```
display.println("ENGINEER VIEW");  
display.print("Alt HH: "); display.println(handheldAlt, 2);  
display.print("Alt Static: "); display.println(staticAlt, 2);  
display.print("2D Dist: "); display.println(uwbDist, 2);  
display.print("RSSI: "); display.println(rssi, 1);
```

The use of monochrome screens with small fonts ensures all data is readable even in bright outdoor conditions.

## Menu Flow and Behaviour

A full breakdown of the menu system is shown in Figure 3.30. This includes all user accessible states such as:

- **Distance + Club** mode (auto exits after 15 seconds).
- **Settings Menu** for unit and engineering options.
- **Unit Selection** (meters/yards).
- **Engineer View** showing raw sensor data.

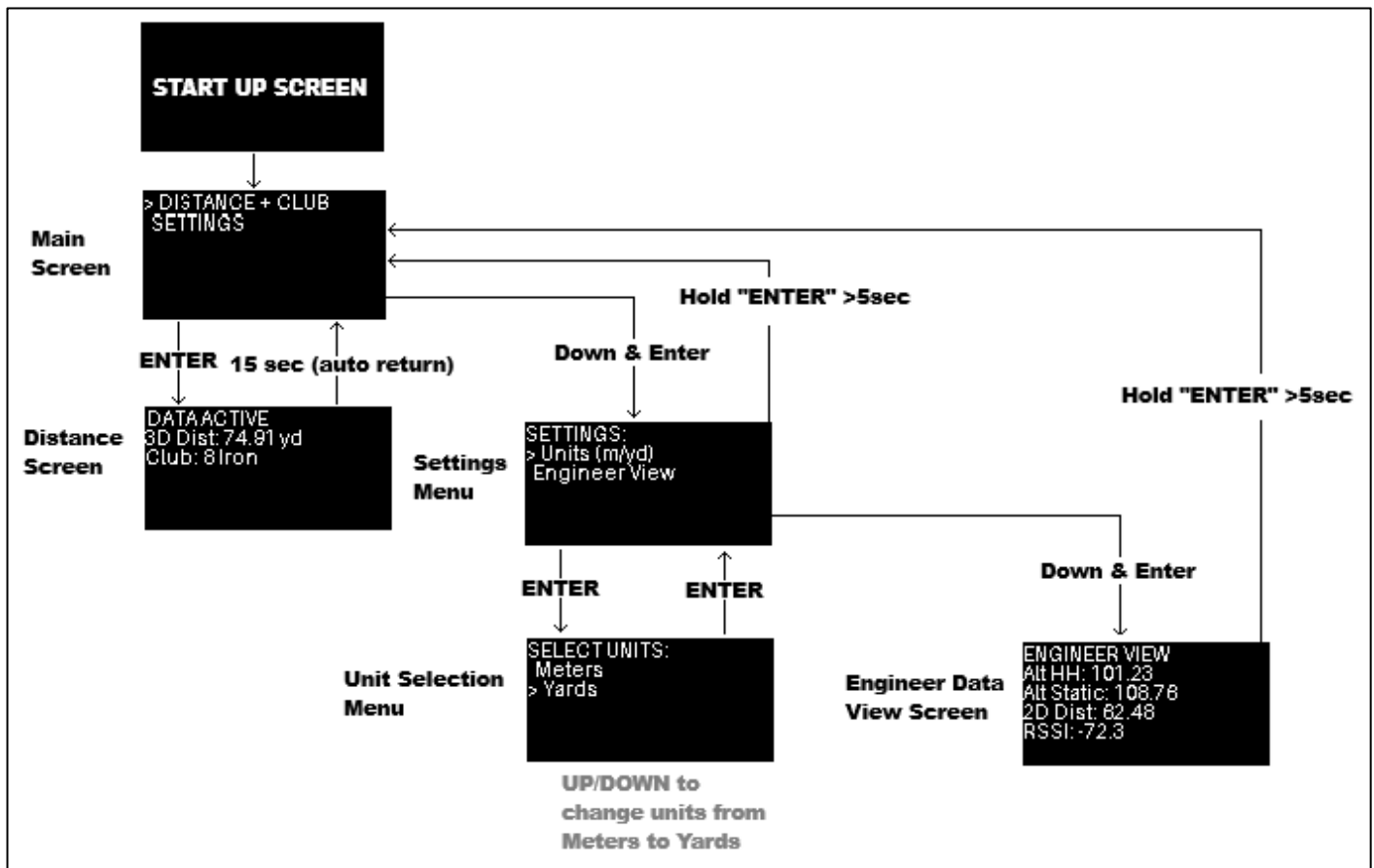


Figure 3.30 Handheld Device User Interface Navigation

The button inputs allow seamless interaction using only directional navigation and a single selection input.

## Button Input Handling

Each button is continuously monitored in the main program loop. When a button is pressed the system checks whether enough time has passed since the last press (to avoid accidental double clicks) and then performs the appropriate action based on the current menu.

Here's how the Up button is handled in code:

*Code 3.9*

```
if (digitalRead(BTN_UP) == LOW && now - lastButtonPress > BUTTON_DEBOUNCE) {  
    if (currentMenu == MENU_MAIN || currentMenu == MENU_SETTINGS) {  
        menuIndex = (menuIndex - 1 + 2) % 2;  
    } else if (currentMenu == MENU_UNITS) {  
        unitsMenuItemIndex = (unitsMenuItemIndex - 1 + 2) % 2;  
    }  
    lastButtonPress = now;  
}
```

This logic performs two key functions:

1. **Debouncing:** Ensures that only one action is registered per press, even if the button is held or pressed rapidly.
2. **Menu Navigation:** Moves the selection up within the current menu.

The line of code below uses a modulo operation to allow circular navigation. For example, if the user is at the top of the menu and presses the Up button, it wraps around to the last item creating a continuous scrolling effect:

*Code 3.10*

```
menuIndex = (menuIndex - 1 + 2) % 2;
```

## Saving Chosen Settings

User preferences, as golf is predominantly played in Yards and not Meters the user has the chance to change unit type (meters or yards), this is stored using the ESP32's non-volatile Preferences API:

*Code 3.11*

```
void saveUnitSetting(bool yards) {
    prefs.begin("settings", false);
    prefs.putBool("useYards", yards);
    prefs.end();
}

void loadUnitSetting() {
    prefs.begin("settings", true);
    useYards = prefs.getBool("useYards", false);
    unitsMenuItemIndex = useYards ? 1 : 0;
    prefs.end();
}
```

### 3.2.3 Algorithm for Club Selection via SD Card

A key feature of the device is its ability to recommend a golf club based on the measured distance to the target. This is achieved through a configurable algorithm that reads predefined distance ranges from a .csv file stored on an SD card. The logic behind this selection process is simple, efficient and user editable, allowing the user to tailor club recommendations to their individual playing style.

#### SD Card Setup and Formatting

To ensure compatibility with the ESP32 microcontroller and the SD library used in the firmware, the SD card was formatted using the FAT32 file system. This format is required for reliable read/write operations using SPI communication. Once formatted, the file clubmap.csv was placed in the root directory of the SD card.

The firmware initialises the card during startup:

*Code 3.12*

```
if (!SD.begin(SD_CS)) Serial.println("SD Card Init Failed.");
```

If the card is missing, improperly formatted, or if the file is unreadable, the system handles the error by assigning the club label as "N/A".

## CSV File Structure

The file clubmap.csv shown in Table 3.1 stores golf club names and their associated distance ranges in yards. The system assumes the data is sorted in ascending order and uses the first match found for the distance range.

Each line follows the format:

Table 3.1 - CSV Cells for Club Distances

min_distance	max_distance	club_name
0	50	Lob Wedge
50	70	Sand Wedge
70	90	Gap Wedge
90	110	Pitching Wedge
110	125	9 Iron
125	135	8 Iron
135	145	7 Iron
145	155	6 Iron
155	165	5 Iron
165	175	4 Iron
175	185	3 Iron
185	200	Hybrid
200	220	3 Wood
220	270	Driver

## Algorithm Overview

When a distance is calculated by the system (in yards or meters, depending on user settings), the firmware opens the clubmap.csv file stored on the SD card and searches for a range that the distance falls into.

Code 3.13

```
void updateClubLabel(float distance) {
    File file = SD.open("/clubmap.csv");
    if (!file) {
        clubLabel = "N/A";
        return;
    }
    clubLabel = "N/A";
    bool firstLine = true;
    while (file.available()) {
        String line = file.readStringUntil('\n');
        line.trim();
        if (firstLine) { firstLine = false; continue; }
        int c1 = line.indexOf(',');
        int c2 = line.indexOf(',', c1 + 1);
        if (c1 == -1 || c2 == -1) continue;
        float min = line.substring(0, c1).toFloat();
        float max = line.substring(c1 + 1, c2).toFloat();
        String label = line.substring(c2 + 1);
        if (distance >= min && distance < max) {
            clubLabel = label;
            break;
        }
    }
    file.close();
}
```

The system compares the current distance against each range and assigns the first matching club name to the clubLabel variable. If no range matches, the label remains as "N/A".

## Integration with Display

The selected club is displayed on the OLED screen during the Active Data screen:

Code 3.14

```
display.print("Club: ");
display.println(clubLabel);
```

This output provides the user with a real time recommendation based on measurable data, simplifying club selection during play.

### 3.2.4 Communication and Positioning System

The system relies on two separated units a handheld unit and a static unit (anchor) to accurately determine the distance between the user and a fixed point (such as the flag or a target location). This is achieved by combining data from two wireless communication protocols:

- **UWB (Ultra-Wideband)** for precise horizontal distance measurements.
- **LoRa (Long Range Radio)** for transmitting altitude data.

The handheld unit receives and processes both data streams to compute a true 3D distance which is then used for real time club recommendation.

## Overview of Dual Unit Architecture

The system architecture is split into:

- A handheld unit, carried by the user, equipped with an OLED screen, SD card, buttons, a BMP388 sensor, a UWB module, and a LoRa module.
- A static unit, placed at a fixed reference point on the top of the flag stick, containing a BMP388 sensor, UWB module and a LoRa module.

Each unit independently reads sensor data and transmits relevant information. The handheld unit is responsible for fusing the data to calculate the 3D distance.

### 3.2.5 Signal Filtering

To improve the stability and reliability of UWB distance measurements in the system, a one dimensional Kalman filter was implemented. This recursive algorithm estimates the true value of a dynamic variable by continuously updating its prediction based on prior estimates and new measurements. In this project, a custom SimpleKalmanFilter class was used to filter UWB data, initialised with predefined error parameters to balance responsiveness and noise suppression:

*Code 3.15 Kalman Parameters*

```
SimpleKalmanFilter kalmanUWB(0.5, 1, 0); // measurement error, estimate error,  
initial estimate
```

Every raw UWB distance reading, received via serial communication is processed through the filter using:

*Code 3.16 Kalman Process*

```
uwbDist = kalmanUWB.updateEstimate(rawUWB);
```

This approach reduces the effect of spurious fluctuations often present in UWB measurements, resulting in smoother and more realistic distance values used for downstream calculations, such as 3D Euclidean range determination and golf club recommendation. The use of Kalman filtering in this context is supported by Feng et al. (2020), who demonstrated that fusing UWB data with Kalman filtering significantly improves measurement stability in real time embedded systems for indoor positioning. Their work highlights how even basic forms of filtering can suppress measurement noise and improve tracking consistency in sensor based navigation systems.

### 3.2.6 LoRa - RF Communication

To enable wireless data transfer between the static and handheld units, the system uses a LoRa 433 MHz serial RF modules. These modules operate on the 433.4–473.0 MHz band and supports UART communication.

#### Purpose and Role

The LoRa modules are used to transmit altitude data from the static (anchor) unit to the handheld unit. This data is essential for calculating the vertical component of the 3D distance measurement.

Every second, the static unit sends an altitude message over its serial connection to the LoRa module:

*Code 3.17*

```
LoRaSerial.print("ALT:");
LoRaSerial.println(altitude, 2);
```

The handheld unit receives this message via its own LoRa module and parses the value to update the current static reference altitude.

#### Communication Details

- **Baud Rate:** 9600 bps (standard and reliable for embedded devices)
- **Interface:** UART (HardwareSerial(1) in the code)
- **Message Format:** Simple ASCII strings prefixed with "ALT:" to allow easy parsing.

#### Integration in the Firmware

The LoRa modules are initialised as secondary hardware serial ports on both devices:

*Code 3.18*

```
HardwareSerial LoRaSerial(1);
LoRaSerial.begin(9600, SERIAL_8N1, LORA_RX, LORA_TX);
```

The handheld continuously monitors this serial port during operation to check for new incoming data, which is used to maintain an up to date static altitude for accurate 3D positioning.

### 3.2.7 UWB Distance Measurement

The system uses Ultra-Wideband (UWB) technology to perform high precision ranging between the handheld and static units. UWB is known for its ability to measure distances by calculating the Time of Flight (ToF) between two devices, one configured as a Tag and the other as an Anchor.

The modules used in this system are based on the Qorvo DW3000 chipset and communicate using a simple AT command interface via UART.

#### Device Configuration

Each UWB module must be configured upon startup using the AT+SETCFG command. This defines the module's ID, role, communication rate, and whether range filtering is enabled.

##### *On the static unit (Anchor):*

*Code 3.19*

```
UWBSerial.println("AT+SETCFG=1,1,1,0");
```

This sets:

- ID = 1
- Role = Anchor (1)
- Baud rate = 6.8 Mbps
- Range filtering = Off

##### *On the handheld unit (Tag):*

*Code 3.20*

```
UWBSerial.println("AT+SETCFG=0,0,1,0");
```

This sets:

- ID = 0
- Role = Tag (0)
- Baud rate = 6.8 Mbps
- Range filtering = Off

(The tag is responsible for initiating the ranging process, while the anchor responds to the request)

## Ranging Procedure

The handheld unit triggers a measurement by sending:

*Code 3.21*

```
UWBSerial.println("AT+RANGE");
```

This initiates a two-way ranging process (TWR), where the time taken for a message to travel to the anchor and back is used to calculate distance. The anchor responds automatically with the calculated range, which is printed over UART in the following format:

*Code 3.22*

```
AT+RANGE=tid:0,mask:80,seq:197,range:(752,0,0,0,0,0,0,0),rss:(-70.3,0,0,0,0,0,0,0)
```

From this message:

- range:(752) → The distance to Anchor 0 is 752 cm (7.52 meters)
- rss:(-70.3) → The signal strength of the measurement

The handheld system parses this response, extracts the range, and (optionally) applies a scaling factor or correction:

*Code 3.23*

```
if (uwbDist < 75.0) {  
    uwbDist *= 1.00;  
} else {  
    uwbDist *= 1.02; // Minor correction at longer ranges  
}
```

This value becomes the horizontal component of the 3D distance calculation.

### 3.2.8 Wake Up Mechanism

To initiate the distance measurement process, the handheld unit sends a "WAKE" message to the static unit via the LoRa 433 MHz RF link. This occurs automatically when the user selects the “Distance + Club” option from the main menu, indicating that they are ready to receive a distance reading.

The message is transmitted using:

*Code 3.24*

```
LoRaSerial.println("WAKE");
```

This transmission acts as a trigger, ensuring that the static unit is aware of the request and can begin or continue sending its altitude data. While the static unit currently transmits altitude continuously, the inclusion of the wake up message lays the groundwork for more advanced power saving features in future iterations such as only enabling data transmission on demand, reducing unnecessary RF activity and extending battery life.

### **3.2.9 Summary of Software Development**

The software development process successfully brought together multiple subsystems into a responsive embedded system solution. Through a combination of real time sensor data, structured menu navigation, configurable club logic and communication between units, the system delivers accurate distance measurements and intelligent club recommendations to the user. The use of modular code, timed event loops and none blocking logic ensures that the system remains efficient and user friendly during operation.

This software layer not only drives the functionality of the device but also supports scalability and future enhancements, such as power management or extended data logging, without requiring significant structural changes.

### 3.3 System Testing During Development

Before the final prototype was assembled and evaluated, several subsystem level tests were conducted to guide design decisions and verify core functionality. These tests helped confirm the viability of the selected components, identify limitations and optimise performance for the intended use case.

#### 3.3.1 Power Testing

##### Power Consumption

Power consumption was measured by powering each device through a USB power meter shown in Figure 3.31 during active operation. This setup recorded voltage, current and power draw under real use conditions. Readings were taken while the devices were actively measuring altitude, performing UWB ranging and updating the OLED display. The Results are seen in Table 3.2.



Figure 3.31 - USB Power Monitoring Device

Table 3.2 - Static and Handheld Unit Power Consumption

Static Unit					HandHeld Unit				
Voltage (V)	Current (A)	Power (W)	mWh	mAh	Voltage (V)	Current (A)	Power (W)	mWh	mAh
5.001	0.191	0.94	445	89	5.008	0.088	412	930	186

Using the current draw from Table 3.2, the theoretical runtimes for the batteries were calculated using the battery information from the datasheet as follows:

*Equation 3.2 - Battery Run Time*

$$\text{Runtime} = \frac{\text{Battery Capacity}(mAh)}{\text{Current Draw } (mA)}$$

### Static Unit:

$$\frac{2000}{191} \approx 10.5 \text{ hours}$$

### Handheld Unit:

$$\frac{2000}{88} \approx 22.7 \text{ hours}$$

These calculations assume continuous peak operation without low power modes. In practice, runtime is expected to be extended by sleep functions and idle periods.

### Solar Panel Testing

Additionally, a solar panel voltage test was conducted using a digital voltmeter and handheld lux meter. Readings were taken at consistent orientation and times of day under varying weather conditions, with lux levels recorded to quantify lighting conditions.

*Table 3.3 - Solar Panel Output Voltages Vs Lux*

Test Condition	Lux (lx)	Solar Panel Voltage (V)
Full Sunlight	94,763	5.107
Bright Overcast	58,963	4.85
Dull Overcast	18,567	3.69
Indoors	350	1.02

These results highlight the solar panel's performance limitations under low light. Dull overcast conditions resulted in voltages below the minimum required by the TP4056 charging circuit. This confirmed the necessity of integrating a boost converter to maintain system functionality across all weather conditions.

The data gathered was used to validate power estimates and confirm the need for a boost converter in the solar charging setup.

### 3.3.2 Altitude Sensor Testing

To verify the accuracy of the BMP388 altitude sensor, measurements were taken at different heights from ground level, as shown in Figure 3.32. The device was incrementally raised from 0 meters to 5 meters, and the altitude readings were recorded against GPS device proved measurements.

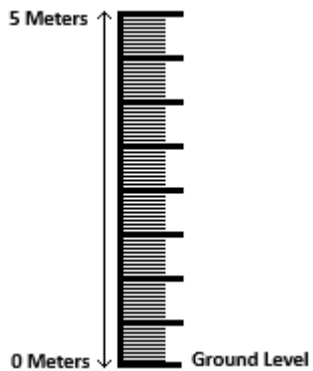


Figure 3.32 Altitude Test Rig (0-5m)

To validate the accuracy of the BMP388 altitude sensor, measurements were taken at various heights and compared against GPS derived expected altitude values. The recorded values are presented in Table 3.4, and a graphical representation is shown in Figure 3.33.

Table 3.4 – Altitude Sensor Test Results

<u>Distance (m)</u>	<u>GPS Status Expected Altitude (m)</u>	<u>BMP388 Altitude (m)</u>	<u>Error</u>	<u>Error Percentage</u>
0	187.2	187.62	0.42	0.22%
1	188.2	188.55	0.35	0.19%
2	189.2	189.59	0.39	0.21%
3	190.2	190.65	0.45	0.24%
4	191.2	191.55	0.35	0.18%
5	192.2	192.5	0.3	0.16%

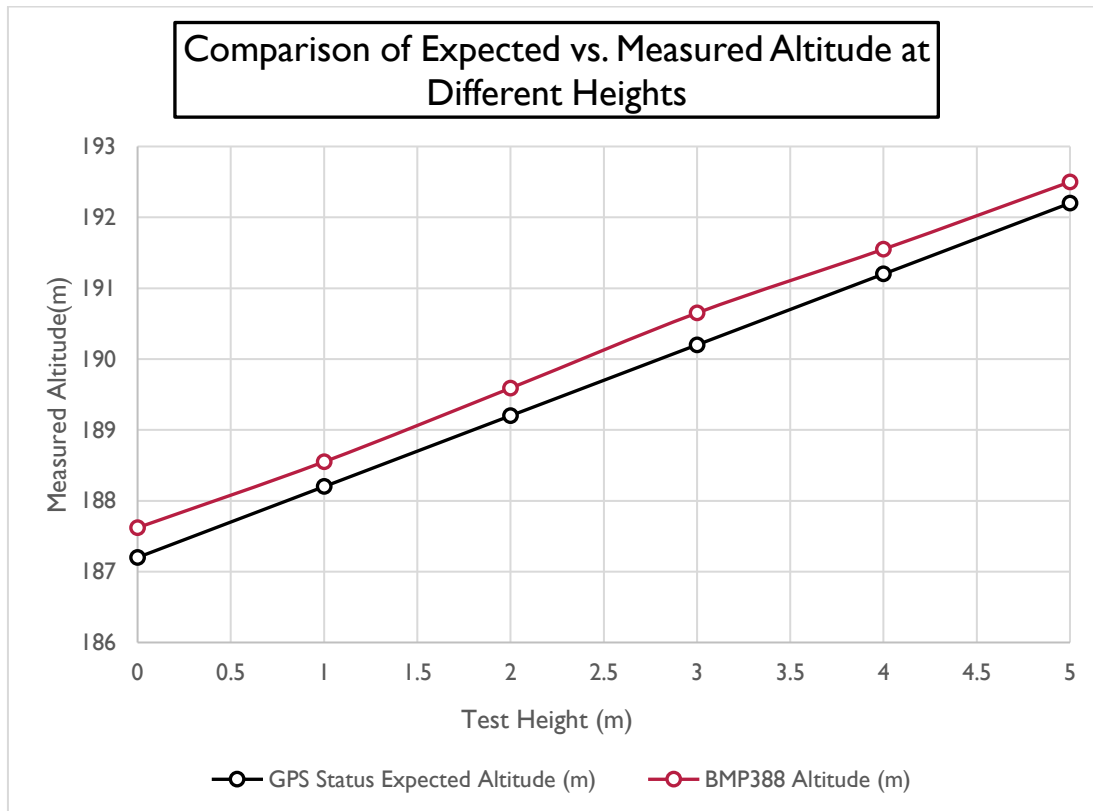


Figure 3.33 Comparison of Altitude Test

As seen in the results the BMP388 altitude values are consistently slightly higher than the GPS derived expected values. However, this offset is systematic and remains relatively constant across different heights, indicating that the sensor is providing stable and repeatable measurements.

Since both the static unit and the handheld unit will use the same BMP388 sensors, this consistent offset will not introduce significant errors in final measurements. Any deviation will be automatically accounted for when calculating relative distances between the two units.

The absolute altitude error at each measurement point is minimal, with an average error percentage of just 0.20%. This confirms that the BMP388 sensor is highly reliable for relative altitude measurements, making it suitable for the intended application.

### 3.3.3 LoRa and UWB Maximum Distance Testing

To evaluate the effective communication range of the system's wireless modules, dedicated open-field tests were conducted to characterise both the LoRa (HC-12) and UWB (DWM3000) performance under ideal conditions. These tests were carried out in an unobstructed environment across a large lake shown in Figure 3.34, providing a clear line of sight between devices to simulate best case operating scenarios.

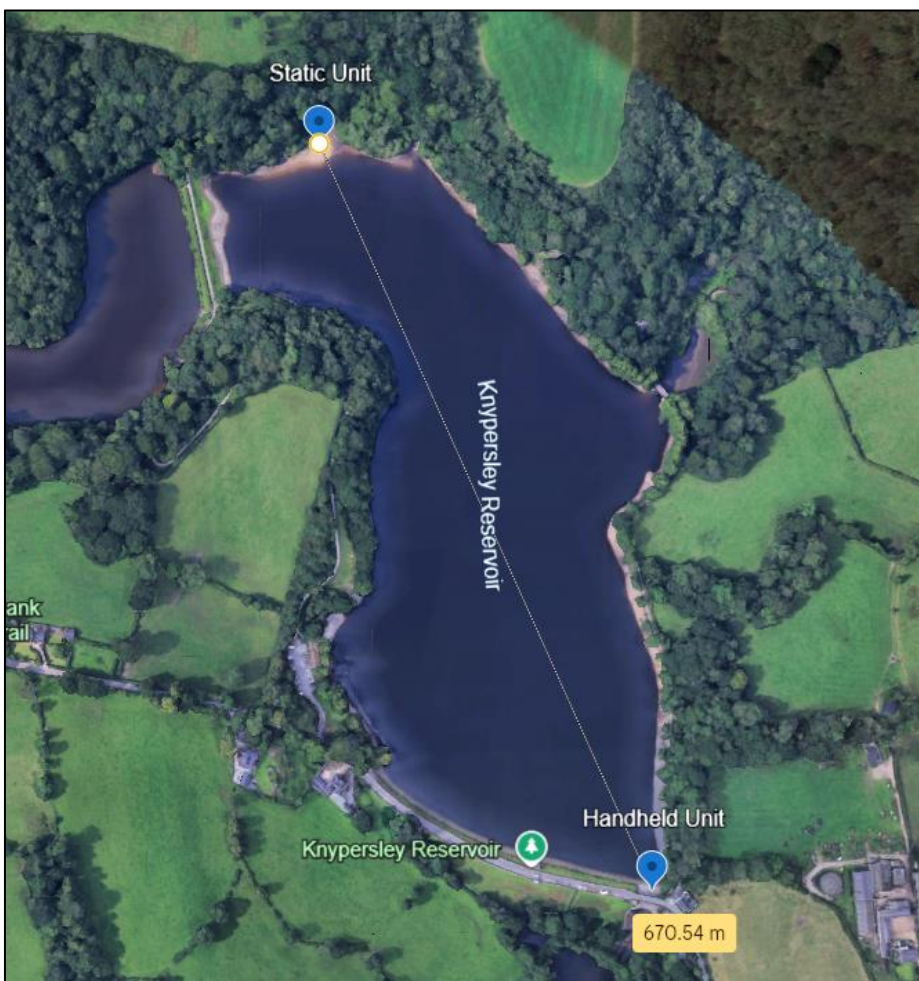


Figure 3.34 Maximum Range Testing

(Google Earth, 2025).

For the LoRa (HC-12) module, a basic test script was flashed to both devices (Seen in Appendix 10.2.1) where the static unit transmitted a recurring "PING" message every second. The handheld device monitored incoming messages and illuminated an onboard LED to visually indicate real time link status. The handheld unit was gradually moved away from the static unit, with range measurements taken at regular intervals until the communication link showed degradation or was lost. The results can be in Table 3.5.

*Table 3.5 Maximum Measured Distances*

Device	Maximum Distance (m)
LoRa	670
UWB	393

The LoRa module demonstrated a stable one way communication range of up to **670 meters**, consistent with the manufacturer's datasheet under ideal conditions. This validated its suitability for low data rate transmissions such as periodic altitude updates within the intended golf course environment.

In addition to LoRa testing, the UWB (DWM3000) module's effective range was also evaluated. A similar methodology was employed, where the handheld device initiated ranging sessions with the static unit at increasing distances. Successful two way ranging was indicated by successful distance readouts without transmission errors. The UWB system maintained stable, accurate distance measurements up to a maximum distance of **393 meters**, beyond which communication reliability began to degrade.

This result is considered fully acceptable for the intended golf application, as the average amateur golfer's maximum driving distance rarely exceeds 300 meters. Therefore, the system's UWB performance sufficiently covers the operational requirements for all practical shot scenarios encountered on a golf course.

### **3.3.4 Proof of Concept Testing**

To validate the full functionality of the system shown in Section 3.1, before final PCB production and enclosure integration, a comprehensive proof of concept test was carried out using fully soldered Veroboard prototypes of both the handheld and static units. This test served as the first full demonstration of the system's end to end capabilities from user interaction and menu control, through to wireless communication, distance measurement, and OLED feedback.

The test was conducted in an open outdoor space using a calibrated measuring wheel to mark 5 meter intervals, ranging from 5 m to 100 m away from the static anchor. At each marked location, the handheld unit was positioned, allowed to stabilise, and the displayed 3D distance was recorded. The static unit remained stationary during the test and transmitted altitude data over 433 MHz RF using the LoRa (HC-12) module. UWB modules on both units handled horizontal distance measurement in real time.

Photographs of this test can be seen in Appendix 10.5.2.

## Measured Results

The results are summarised in Table 3.6. Each row includes the actual measured distance, the corresponding value reported by the device, the received signal strength (RSSI), and the absolute error between actual and measured values.

Table 3.6 – Proof of Concept Test Results

Actual (m)	Measured (m)	RSSI	Error
5.00	5.16	-81.74	-0.16
10.00	10.14	-81.74	-0.14
15.00	14.99	-83.96	0.01
20.00	19.86	-80.79	0.14
25.00	24.87	-81.13	0.13
30.00	29.82	-81.32	0.18
35.00	34.83	-83.74	0.17
40.00	39.54	-82.89	0.46
45.00	44.42	-82.2	0.58
50.00	49.49	-82.89	0.51
55.00	54.39	-83.47	0.61
60.00	59.2	-90.3	0.80
65.00	64.4	-90.3	0.60
70.00	69.5	-90.3	0.50
75.00	74.38	-88.92	0.62
80.00	78.79	-91.74	1.21
85.00	83.29	-121.7	1.71
90.00	85.41	-90.3	4.59
95.00	92.53	-90.08	2.47
100.00	96.81	-121.7	3.19

Results indicated highly consistent readings up to approximately 80 m, with most errors remaining within  $\pm 1.5$  m. Beyond this range, the system began to underestimate distance more significantly, with maximum error reaching **4.59 m** at 90 m, and 3.19 m at 100 m. This behaviour is likely due to decreased signal to noise ratio, multipath reflections or limitations in UWB timing precision at longer distances.

## Firmware Compensation

To account for this consistent underestimation at longer ranges, a small compensation factor was added to the firmware. The adjustment increases measured UWB distances by 2% beyond a threshold of 75 m:

*Code 3.25 - Error Correction*

```
if (uwbDist < 75.0) {  
    uwbDist *= 1.00;  
} else {  
    uwbDist *= 1.02;  
}
```

This simple correction helped to improve long distance accuracy while preserving precision at shorter ranges. The adjustment was validated in further testing and retained in the final version of the system.

This proof of concept test demonstrated that all subsystems including UWB ranging, altitude correction, wireless communication, and display were working cohesively. It provided the confidence required to move forward with final PCB design and enclosure integration.

### 3.3.5 Summary of System Testing

A series of targeted development tests were conducted to validate the core subsystems of the prototype, including power stability, altitude sensing accuracy, wireless communication range and basic system integration. Results confirmed that the selected components and initial design choices met the functional requirements for the handheld and static devices. These findings provided critical feedback for refining the final hardware and software configurations, ensuring a robust foundation for full system integration and field testing described in the following sections.

### 3.4 Mathematical Methods

This section outlines the mathematical methods used to generate reference distances during the testing phase. These calculations served as a baseline to evaluate the accuracy of the system's real time 3D distance outputs.

Two main techniques were applied:

1. **GPS based ground distance:** calculated using the Haversine formula to estimate horizontal separation between two GPS points.
2. **Altitude adjusted 3D distance:** derived by combining the Haversine calculated horizontal distance with barometric altitude differences, producing a full line of sight measurement.

Both methods were implemented in MATLAB and used to create direct comparisons with the distances reported by the UWB device. This allowed for accurate, repeatable validation across varied terrain. Full scripts are included in Appendix 10.3.

### 3.4.1 Distance Calculations

To determine the distances between measurement points, a combination of GPS based Haversine calculations and altitude adjustments were used. The Haversine formula was applied to compute the horizontal ground distance, while the altitude difference was incorporated to derive the 3D line of sight distance using the Pythagorean theorem.

#### Haversine Formula for Horizontal Distance

The Haversine formula calculates the great circle distance between two points on a sphere based on their latitude and longitude:

*Equation 3.3 - Haversine Formula*

$$a = \sin^2\left(\frac{\Delta\phi}{2}\right) + \cos(\phi_1) * \cos(\phi_2) * \sin^2\left(\frac{\Delta\lambda}{2}\right)$$

$$c = 2 * \text{atan}(\sqrt{a}, \sqrt{1-a})$$

$$d = R * c$$

Where:

- $\phi_1, \phi_2$  = latitude of point 1 and point 2 in radians
- $\lambda_1, \lambda_2$  = longitude of point 1 and point 2 in radians
- $\Delta\phi = \phi_2 - \phi_1$
- $\Delta\lambda = \lambda_2 - \lambda_1$
- $R = 6371$  km (Earth's approximate radius)
- $d$  is the great circle distance (horizontal distance on the Earth's surface)

The calculated horizontal distance was then used alongside the altitude difference to compute the true 3D distance using the Pythagorean theorem:

*Equation 3.4 - 3D Distance Equation*

$$D_{3D} = \sqrt{d^2 + (\Delta h)^2}$$

Where:

- $D_{3D}$  = Line of sight (3D) distance
- $d$  = 2D distance
- $\Delta h$  = Altitude difference between the two points

To simplify the process and ensure consistent and accurate calculations a custom MATLAB script was developed to perform the distance calculations described above. The script, detailed in Appendix 10.3, enables the automated comparison between GPS and the UWB device measured data.

Figure 3.35 outlines the process commands used in MATLAB to calculate horizontal and 3D distances between a static point and multiple measurement points. The script takes user inputs, applies the Haversine formula for 2D ground distance, combines it with barometric altitude differences, and outputs comparison tables and visual plots for analysis.



Figure 3.35 MATLAB Data Command Inputs

The script begins by prompting the input of the static reference point's GPS coordinates (latitude, longitude, and altitude). Following this to enter the measurement point data for each of the mobile test positions (M<sub>1</sub> to M<sub>n</sub>) including the latitude, longitude, altitude, and the corresponding 3D distance measured by the UWB Device.

For each measurement point, the script first applies the Haversine formula to calculate the horizontal distance from the static point. This value is then combined with the vertical altitude difference using the Pythagorean theorem, resulting in a computed GPS based 3D line of sight distance.

Once all points are processed, the script generates a comparison table displaying each point's GPS calculated 3D distance alongside the 3D distance reported by the device including the difference in errors.

To visually interpret the results, a graph is plotted to illustrate the relationship and differences between the two distance sets.

This automated approach not only increases computational efficiency and repeatability but also supports clear validation of the device's performance under real world conditions.

### **3.4.2 Summary of Mathematical Methods**

This section outlined the mathematical principles underpinning the distance measurement system, including two dimensional ranging via UWB Time of Flight (ToF) calculations and three dimensional distance adjustments using barometric altitude data. By combining horizontal distance measurements with vertical displacement corrections through the Pythagorean theorem, the system achieves precise real world positioning necessary for golf course environments. These calculations form a critical link between raw sensor data and the actionable outputs of the system, directly influencing its performance in field testing.

### **3.5 Summary of Methodology**

This chapter detailed the complete methodology undertaken in the development of a UWB golf distance and club recommendation system. The design was broken into two core hardware units: a handheld device for user interaction and processing and a static flagstick mounted unit for ranging and environmental sensing. A modular approach was used throughout to ensure maintainability and testability.

Key hardware components were selected based on performance, power efficiency and communication capabilities. The ESP32 microcontroller was central to both units, chosen for its dual core processing, low power modes, and versatile I/O. Ultra-wideband (UWB) technology was employed for precise distance measurement using a time of flight protocol while LoRa was used for low power, long range data exchange between devices.

Software was developed using the Arduino framework in C++, with a none blocking loop structure to ensure responsive interaction and efficient timing control. The firmware was divided into functional subsystems, including UI navigation, SD card storage for club logic, UWB ranging, LoRa messaging and altitude sensing. A detailed system architecture diagram was included to illustrate real time software flow and communication paths.

Hardware design progressed from initial Veroboard prototypes through to custom PCB development and enclosure design. Power systems were tested and optimised, incorporating solar charging, LiPo batteries, and voltage regulation to support long term autonomous use. Each subsystem underwent iterative bench and field testing to ensure performance and reliability.

Finally mathematical models were developed to calculate reference distances using GPS coordinates and altitude readings. These were used as a baseline to validate the UWB distance measurements during field testing. A MATLAB script was created to automate this process and output comparison graphs.

With the design and development complete, the following chapter presents the testing results, performance evaluation, and comparison between the system's measurements and reference values.

## 4 Experimental Setup

This chapter describes the experimental setup used to evaluate the accuracy and performance of the final system. The aim of testing was to assess the system's ability to measure and display real time 3D distances between the handheld and static units under realistic conditions. Ground truth distances were calculated separately using GPS coordinates and barometric altitude data, as described in Chapter 3.

Testing was conducted outdoors to replicate conditions like those in which the system is intended to operate, such as on a golf course.

### 4.1 Test Equipment

The experimental evaluation was carried out using the final, fully assembled versions of both the handheld and static units, as developed, and described in Section 3.1.5. Each device contained all functional subsystems, enclosed and powered via battery for untethered outdoor use.

The following equipment and tools were used during testing:

#### 4.1.1 Primary Devices

##### Handheld Unit

- ESP32-S3 microcontroller
- 0.96" OLED display
- BMP388 barometric sensor
- LoRa (HC-12 433 MHz RF) module
- UWB module
- SD card for club mapping
- 3-button user interface
- Internal 18650 lithium-ion battery

##### Static Unit

- ESP32-S3 microcontroller
- BMP388 barometric sensor
- LoRa (HC-12 RF) module
- UWB module (configured as anchor)
- Internal rechargeable battery

## 4.1.2 Measurement Tools

- **Smartphone with GPS App:** GPS coordinates were logged using a high accuracy mobile GPS application to calculate reference horizontal distances via the Haversine formula.( See Figure 4.1 below)
- **MATLAB (Post Processing):** Used for reference distance calculation, error analysis and result visualisation ( Described in Section 3.4.1).
- **Notepad:** To log results from the handheld unit.
- **Temperature/Humidity Device:** To log conditions of each test.

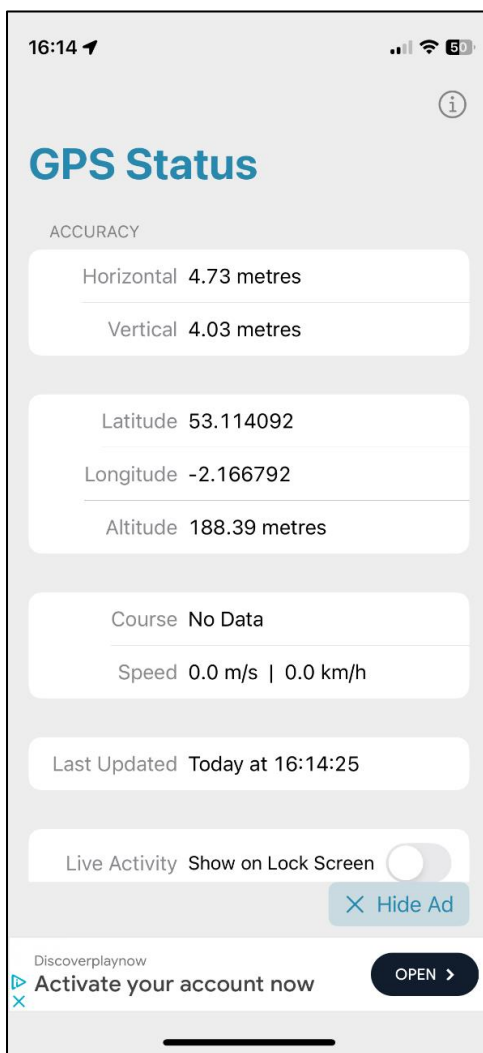


Figure 4.1 GPS Status Application Screenshot

## 4.2 Test Environments

The experimental evaluation of the system was conducted in open outdoor environments chosen to replicate real world use cases, such as golf courses, sports fields or rural landscapes. These locations allowed for flexible placement of the static and handheld units over extended distances and provided varied terrain and conditions for thorough testing.

### 4.2.1 Test Locations

Unlike the controlled, interval based proof of concept test this phase of testing used natural reference points and notable landmarks (e.g., trees, posts, path boundaries) to define positions. Testing was carried out at multiple outdoor sites, including open sports fields and a local golf course to ensure realistic use case conditions were represented.

To ensure the repeatability and accuracy of elevation testing scenarios, permission was obtained from a local golf course to conduct measurements on site. Temporary, environmentally safe grass paint was used to discreetly mark the specific measurement points on the course terrain. This approach allowed for repeated testing under varying weather conditions (clear, overcast or adverse) while maintaining consistent reference positions across different test sessions. The use of fixed points minimised positional errors and ensured fair comparison of distance measurements across different environmental scenarios.

At each test point, the GPS coordinates including latitude, longitude, and altitude were recorded using a smartphone GPS tool. These coordinates were later used in post processing to calculate reference distances using the Haversine formula and altitude adjustments.

### 4.2.2 Environmental Conditions

Tests were performed under a range of real world weather conditions to assess the system's performance stability in changing environments:

- **Sunny conditions:** clear skies, bright sunlight, low humidity
- **Overcast/dull conditions:** cloud cover, higher humidity, diffused lighting.

Environmental variables were recorded at the start of each session using a mobile weather app:

- **Temperature:** 12 °C to 21 °C
- **Humidity:** 55% to 85%

These parameters were logged alongside test results to monitor any potential correlation with measurement accuracy, particularly for the barometric sensors or UWB signal quality.

#### **4.2.3 Use of Terrain Features**

In addition to open field testing, some measurements were taken with partial or full obstructions (e.g., trees, mounds, or walls) placed between the handheld and static units. This allowed the system to be evaluated under none line of sight (NLOS) conditions, reflecting realistic use cases where natural obstructions might interfere with wireless performance.

### **4.3 Procedure**

The goal of testing was to evaluate the system's accuracy in real world conditions by comparing its measured 3D distance to calculated reference values based on GPS and barometric altitude data. A structured approach was followed to ensure repeatability, coverage of various scenarios and analysis of the results.

#### **4.3.1 Data Collection**

At each test point, the following steps were carried out:

1. The handheld unit was moved to a specific landmark or position, chosen for clear physical separation from the static unit.
2. The GPS coordinates (latitude, longitude and altitude) of the handheld location were recorded using a smartphone app GPS logger.
3. The displayed distance on the OLED screen of the handheld unit was manually recorded once readings had stabilised.
4. Ambient environmental conditions (temperature, humidity, sky conditions) were logged using a mobile weather app.
5. Notes were made regarding terrain, signal loss, or unusual device behaviour.

This process was repeated across multiple locations and in varying terrain and weather conditions resulting in a diverse dataset for evaluation.

### **4.3.2 Test Scenarios**

To assess the system's performance under realistic conditions, three key test scenarios were designed. Each was tailored to a specific use case and measurements were recorded across multiple points to evaluate consistency, range accuracy and communication reliability. For each scenario, GPS coordinates and altitude were logged alongside the system's displayed distance reading.

#### **Line of Sight (LOS) Testing**

This baseline test was designed to assess the system's core accuracy under ideal conditions. The handheld unit was moved to 11 different locations (M1–M11) along an open, grass field, maintaining clear line of sight to the static anchor unit throughout.

At each point:

- The GPS coordinates (latitude, longitude, and altitude) were recorded.
- The device's displayed 3D distance was logged once readings stabilised.
- Environmental conditions (temperature, humidity, sky condition) were noted.

This test provided the cleanest dataset for comparison with calculated reference values and was used as the benchmark for system performance.

#### **Elevation Change Testing**

To evaluate the system's altitude compensation capability, tests were conducted on sloped terrain. The static unit remained at a fixed elevation, while the handheld unit was moved to locations that were noticeably higher or lower in vertical position.

At each location:

- GPS altitude and coordinates were recorded to estimate relative height.
- The 3D distance output on the handheld was logged and compared to reference values.
- Observations were made regarding stability of barometric readings under changing elevation.

This test allowed the accuracy of the barometric sensors and the 3D distance formula to be validated under none level terrain conditions.

## **Obstructed No Line of Sight (NLOS) Testing**

This scenario aimed to replicate real world use cases where walls, trees or other natural features block direct visibility between devices. The static unit remained in a fixed location, while the handheld unit was positioned behind a:

- Wall
- Natural Vegetations (Trees, shrubs)

These positions were selected to test the resilience of UWB and LoRa signal transmission under none line of sight (NLOS) conditions. Distance measurements were again recorded and compared to reference values to assess whether obstructions had a noticeable impact on accuracy or stability.

### **4.3.3 Result Processing**

All collected data was compiled and post processed using a MATLAB script (Appendix 10.3), which:

- Calculated the horizontal ground distance using the Haversine formula.
- Incorporated the altitude difference between static and handheld units.
- Produced the reference 3D distance.
- Computed error values between the device's output and the calculated ground truth

This process enabled direct comparison between expected and measured results and supported quantitative evaluation of the system's performance.

## **4.4 Summary of Experimental Setup**

A structured experimental approach was developed to evaluate the performance of the distance measurement system in real world conditions. The testing setup incorporated both the fully assembled handheld and static units and was carried out across multiple outdoor locations with varied terrain and environmental conditions.

Three distinct test scenarios were designed to reflect realistic use cases:

- Clear line of sight.
- Vertical elevation changes (Positive and Negative).
- Obstructed line of sight.

Measurement points were selected based on natural landmarks and GPS coordinates were logged at each position. Device readings were recorded manually and later compared to reference values calculated using the Haversine formula and altitude differences.

Environmental data such as temperature and humidity were also logged to examine potential influences on sensor behaviour and signal stability. Supporting tools including GPS logging applications, measuring wheels and MATLAB scripts were used to increase result accuracy and enable detailed analysis in the following chapter.

This comprehensive setup ensured that the system was evaluated in a variety of realistic, practical scenarios, providing a strong foundation for analysing the device's true performance in Section 5.

## 5 Results

This chapter presents the experimental results obtained during field testing of the developed handheld distance measurement system. A series of trials were conducted under controlled and natural outdoor conditions to evaluate system performance in terms of 3D distance accuracy, robustness under varying environmental influences, and reliability in both line of sight (LOS) and no line of sight (NLOS) scenarios.

Testing environments included flat terrain, negative and positive elevation changes, and physical obstructions such as concrete walls and vegetation. Each distance test scenario was tested under differing weather conditions (e.g., clear, overcast, rainy) to assess how factors such as humidity and temperature affected UWB signal propagation and barometric altitude correction.

At each measurement point, the system's UWB derived distance readings were recorded and compared against GPS based 3D reference distances, calculated using the Haversine formula with integrated vertical correction.

An overview of the test environments and their associated conditions is provided in Table 5.1, which summarises key parameters across all trials.

*Table 5.1 - Summary of Test Scenarios and Environmental Conditions*

Test Scenario	Terrain Type	Weather	Temp (°C)	Humidity (%)	Elevation Profile	Obstruction
Flat LOS – Clear	Flat	Clear	14	45	None	None
Flat LOS – Overcast	Flat	Overcast	4	80	None	None
Negative Elevation – Clear	Downhill (– 15.75 m)	Clear	17	50	Static below handheld	None
Negative Elevation – Rain	Downhill (– 15.75 m)	Rain	7	89	Static below handheld	None
Positive Elevation – Clear	Uphill (+26.61 m)	Clear	17	50	Static above handheld	None
Positive Elevation – Rain	Uphill (+26.61 m)	Rain	7	89	Static above handheld	None
Obstructed – Wall	Flat	Clear	11	20	None	2.2 m solid wall
Obstructed – Vegetation	Flat	Clear	11	20	None	Light tree coverage

## 5.1 Line of Sight Test Results (Flat)

This section presents the performance of the system when tested in flat terrain with an unobstructed, direct line of sight between the handheld and static units. The trial was repeated under both clear and overcast weather conditions to assess the effect of atmospheric variation on distance accuracy.

The arrangement of the measurement points used during this test is illustrated in Figure 5.1. The image, produced using Google Earth, shows the approximate positions of points M1 through M11 within the test area. The layout demonstrates the consistent distance intervals and the uninterrupted line-of-sight maintained between the handheld and static units during the trial.

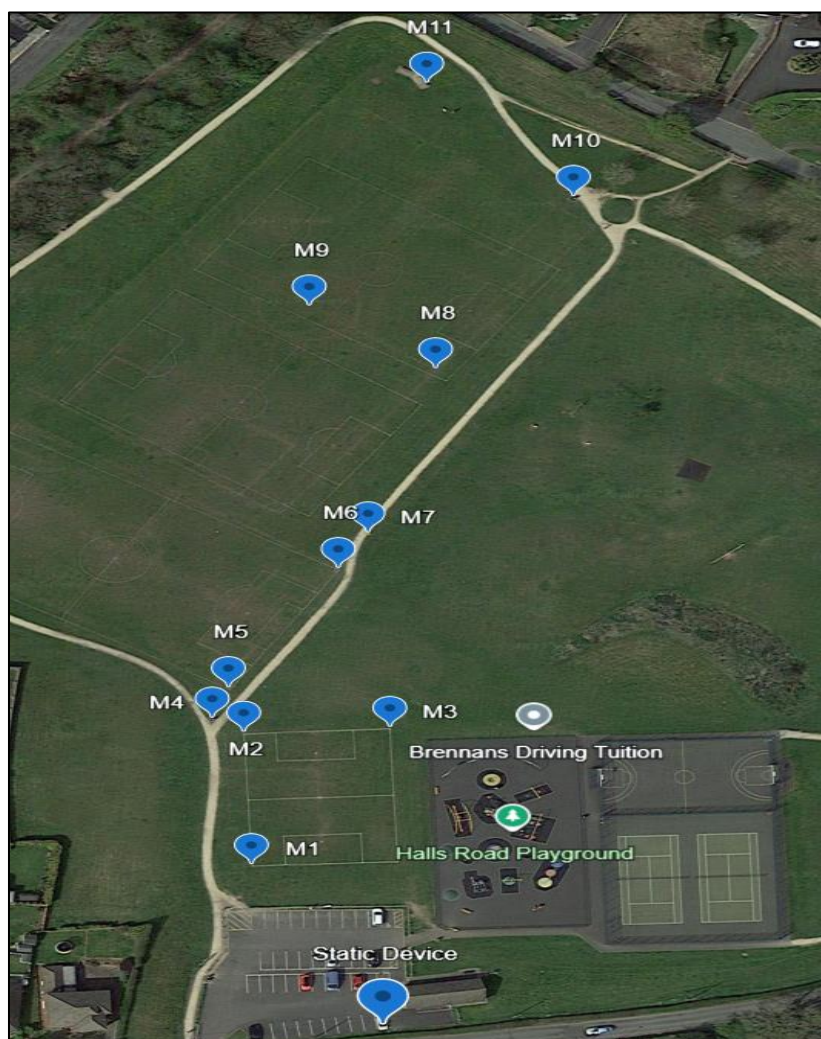


Figure 5.1 LoS Measurement points  
(Google Earth, 2025)

### 5.1.1 Clear Weather Results

The first test scenario was conducted under clear sky conditions with a temperature of 14 °C and 45% relative humidity. This represented the system's optimal operating environment, with direct line of sight between the handheld and static units and minimal atmospheric interference.

Eleven measurement points (M1–M11) were tested, with the GPS coordinates and altitude recorded at each location to calculate a reference 3D distance using the Haversine formula combined with altitude adjustment. The UWB device's internal 3D distance calculation was recorded from the OLED display and compared directly to the reference values.

The individual results for each measurement point are summarised in Table 5.2

*Table 5.2 - Line of Sight Results (Clear Weather)*

Point	UWB Distance (m)	GPS 3D Distance (m)	Error (m)
M1	14.2	14.09	0.110
M2	49.22	49.238	0.018
M3	53.78	53.677	0.103
M4	54.13	53.966	0.164
M5	61.59	61.591	0.001
M6	93.77	93.447	0.323
M7	104.01	103.69	0.317
M8	149.65	149.38	0.269
M9	163.79	163.69	0.095
M10	200.93	200.46	0.469
M11	225.12	225.11	0.006

The measured and reference distances are visualised in Figure 5.2, which plots the device reported UWB values against the ground truth GPS 3D distances across all eleven points.

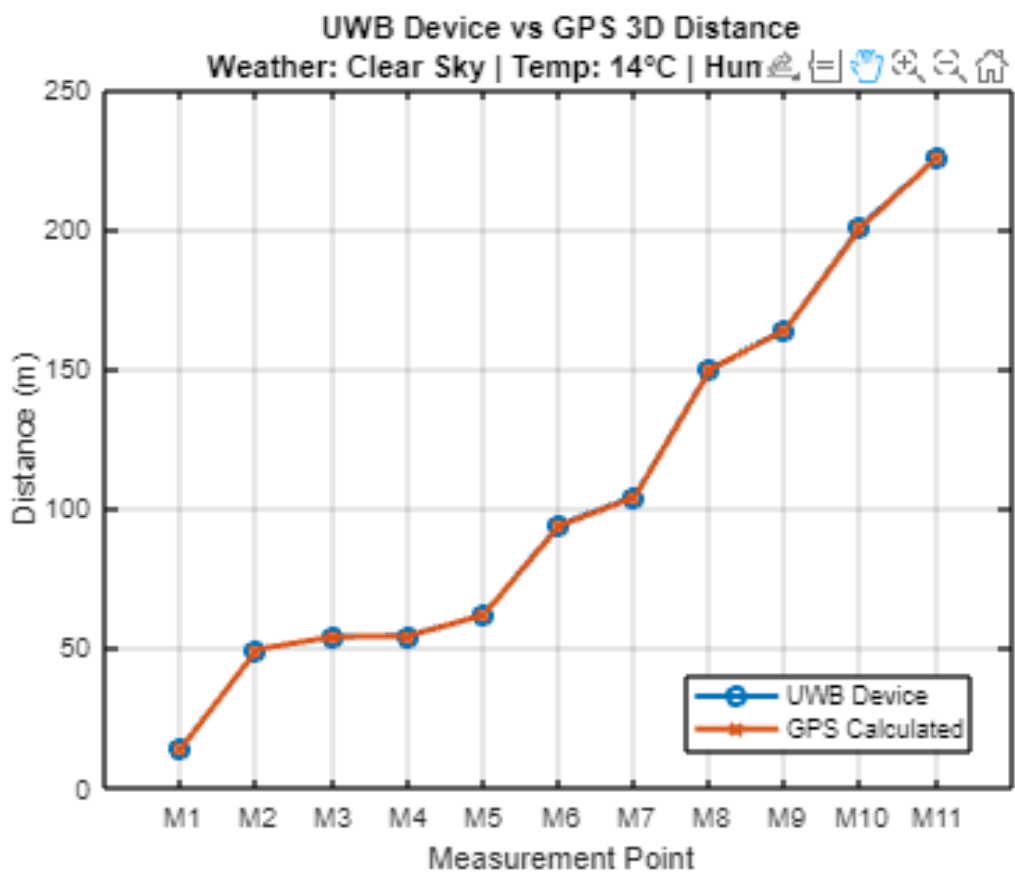


Figure 5.2 Line of Sight (Clear Weather, Graph)

## Analysis

The results show excellent agreement between the UWB measured distance and the reference 3D distance, with an average absolute error of 0.18 m across all points. This validates the accuracy of the UWB distance measurement and barometric altitude integration under ideal conditions.

Notably, even at longer distances (above 200 m), the error remained below 0.5 m, demonstrating consistent performance throughout the entire range. No communication interruptions or signal degradation were observed during the trial.

These results confirm that under line of sight conditions and favourable weather the system is capable of highly accurate 3D distance measurement suitable for the intended use case.

## 5.1.2 Overcast Sky Results

A second line of sight test was carried out under overcast weather conditions with an ambient temperature of 4 °C and 80% relative humidity. The goal was to evaluate the consistency of the system under colder, more humid conditions that may influence barometric pressure readings and signal propagation.

As with the previous trial, the handheld unit was moved to the same eleven test points (M1–M11) with full visibility to the static device. At each point, GPS coordinates were logged, and 3D reference distances were calculated for comparison.

The full numerical results for each point are summarised in Table 5.3.

Table 5.3 - Line of Sight Results (Overcast Weather)

Point	UWB Distance (m)	GPS 3D Distance (m)	Error (m)
M1	14.03	14.09	0.060
M2	49.03	49.24	0.208
M3	53.45	53.68	0.227
M4	54.15	53.97	0.184
M5	61.67	61.59	0.079
M6	93.65	93.45	0.203
M7	104.12	103.69	0.427
M8	149.5	149.38	0.119
M9	163.99	163.69	0.295
M10	201.11	200.46	0.649
M11	225.07	225.11	0.044

The measured and reference distances are visualised in Figure 5.3, which plots the device reported UWB values against the ground truth GPS 3D distances across all eleven points.

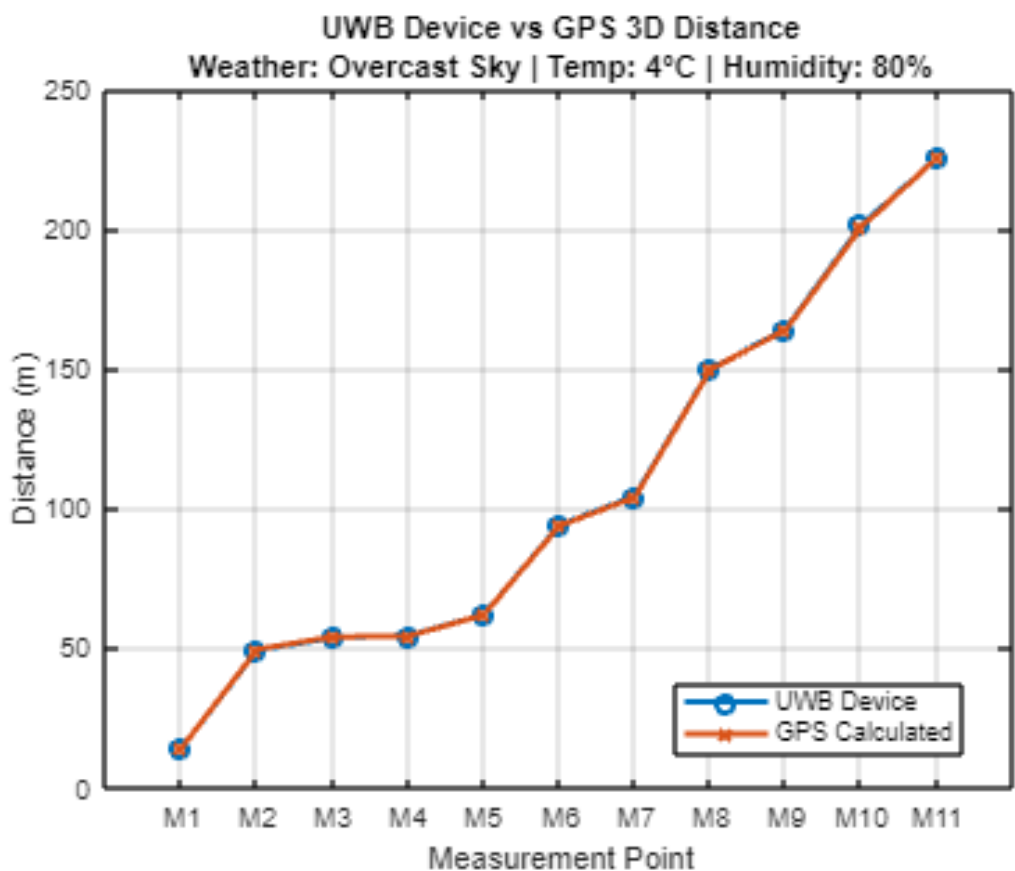


Figure 5.3 Line of Sight (Overcast Weather, Graph)

## Analysis

The UWB system maintained high accuracy across all points in overcast conditions, with an average absolute error of approximately 0.24 m. This is slightly higher than the result under clear conditions (0.18 m), suggesting a modest impact from increased humidity and lower temperature, particularly at longer distances.

Despite these environmental changes, the device demonstrated stable and reliable performance, with no signal interruptions or notable outliers. Measurement trends remained highly consistent with the calculated GPS reference values.

## 5.2 Negative Elevation Results (Downhill to Target)

This section examines the performance of the system when measuring distance with the target positioned below the user along a natural incline a negative elevation scenario. The static unit was placed at the bottom of the slope, while the handheld unit was moved progressively uphill across twelve measurement points (M1–M12).

Based on barometric readings, the static unit was located at an altitude of 158.81 m, and the highest measurement point (M12) reached 174.56 m, resulting in a total elevation difference of approximately 15.75 m. Full line of sight was maintained throughout the trial in both weather conditions.

To evaluate environmental effects on accuracy, the test was conducted in both clear weather and rainy conditions. The approximate layout of the measurement points is illustrated in Figure 5.4, which shows the test site visualised using Google Earth images.



Figure 5.4 Measurement points (Negative Elevation)

(Google Earth, 2025)

### 5.2.1 Clear Weather Results

Environmental conditions during the test included clear sky, an ambient temperature of 17 °C and 50% relative humidity. GPS coordinates and altitude were logged at each measurement point, and 3D reference distances were calculated using the Haversine formula with vertical correction. The UWB measured distances were recorded from the handheld display.

A detailed comparison of the recorded distances is presented in Table 5.4 below.

Table 5.4 - Negative Elevation Results (Clear Weather)

Point	UWB Distance (m)	GPS 3D Distance (m)	Error (m)
M1	40.9	40.84	0.060
M2	42.38	43.03	0.645
M3	62.15	61.92	0.227
M4	69.5	69.77	0.270
M5	88.78	88.68	0.099
M6	97.51	97.99	0.476
M7	111.8	111.98	0.175
M8	129.17	129.43	0.255
M9	151.65	151.94	0.288
M10	159.02	159.27	0.246
M11	179.32	179.39	0.069
M12	195.34	195.66	0.316

The measured and reference distances are visualised in Figure 5.5, which plots the device reported UWB values against the ground truth GPS 3D distances across all twelve points.

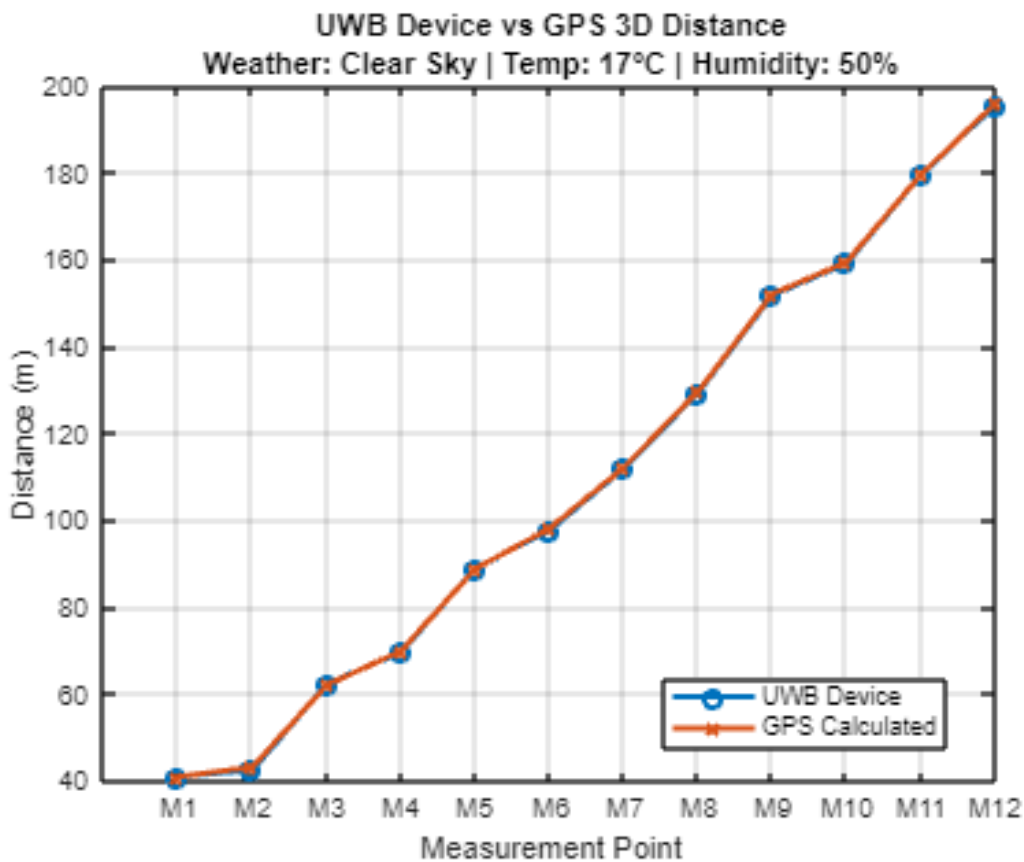


Figure 5.5 Negative Elevation Accuracy (Clear Weather) Graph

## Analysis

The system performed reliably in the presence of a consistent downhill gradient. Across all twelve measurement points, the average absolute error remained low, at approximately 0.26 m, demonstrating strong agreement between the UWB device output and the GPS derived reference values.

While slightly higher error was observed at M2 and M6, no significant deviation or pattern of drift was found. These results confirm that the altitude compensation algorithm based on the Pythagorean correction using barometric data functions effectively on sloped terrain. Additionally, the stable performance across increasing distances suggests that both UWB ranging and barometric sensors remained accurate under these conditions.

## 5.2.2 Adverse Weather Results

Environmental conditions during this trial included rainfall, with an ambient temperature of 7 °C and 89% relative humidity. As in the previous test, GPS coordinates and altitude were logged at each measurement point, and reference 3D distances were calculated using the Haversine formula with vertical correction. The UWB-measured distances were again recorded from the handheld device display.

A detailed comparison of the recorded distances is presented in Table 5.5 below.

Table 5.5 - Negative Elevation Results (Overcast Weather)

Point	UWB Distance (m)	GPS 3D Distance (m)	Error (m)
M1	40.65	40.84	0.190
M2	42.95	43.03	0.075
M3	61.9	61.92	0.023
M4	70.08	69.77	0.310
M5	88.4	88.68	0.281
M6	98.14	97.99	0.154
M7	112	111.98	0.025
M8	129.2	129.43	0.225
M9	151.7	151.94	0.238
M10	159.12	159.27	0.146
M11	179.12	179.39	0.269
M12	195.3	195.66	0.356

The measured and reference distances are visualised in Figure 5.6, which plots the device reported UWB values against the ground-truth GPS 3D distances across all twelve points.

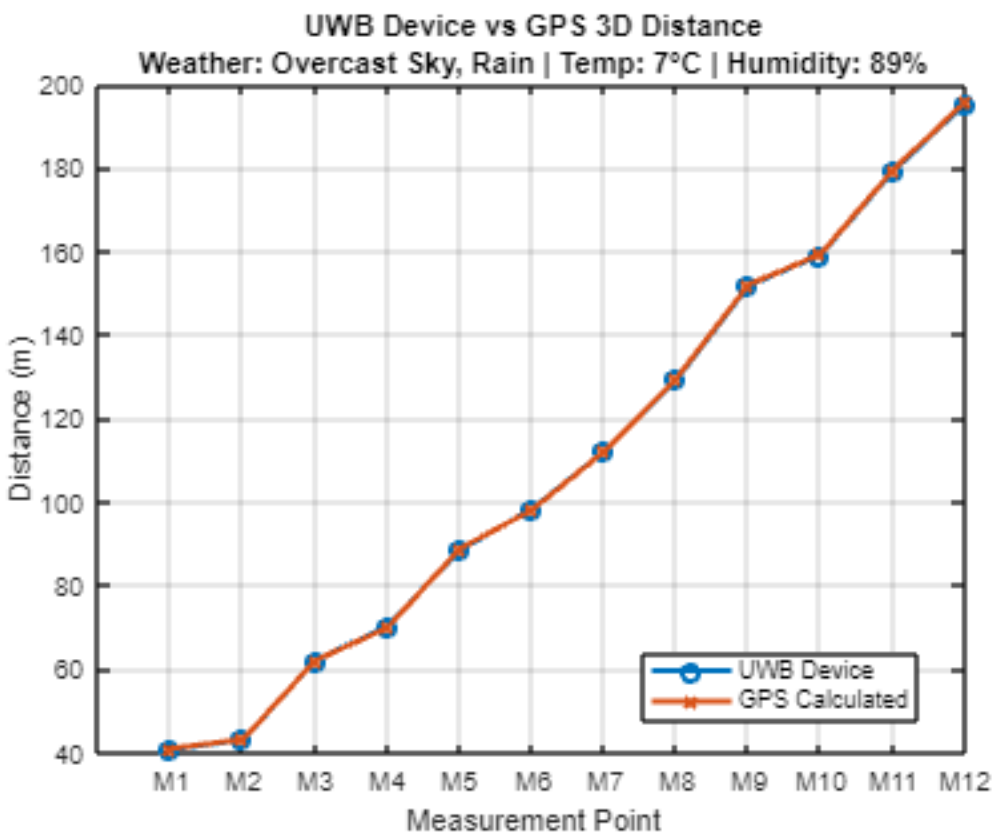


Figure 5.6 Negative Elevation Accuracy (Overcast Weather) Graph

## Analysis

Despite the drop in temperature and the presence of rainfall the UWB system continued to perform with strong accuracy. The average absolute error across all 12 points was approximately 0.21 m, which is slightly lower than in the previous clear sky version of the same test (0.26 m). This suggests that cool, humid conditions did not negatively affect performance and may have slightly enhanced stability due to denser air improving signal consistency.

No communication dropouts or visible instability were observed during the trial. These findings indicate that the system remains highly reliable even in less favourable outdoor conditions, making it suitable for real world applications where weather cannot be guaranteed.

### 5.3 Positive Elevation Results (Uphill to Target)

This section tests the performance of the system in a positive elevation scenario, where the target (static unit) is positioned above the user. The test was conducted on a natural slope, with the static unit placed at the top and the handheld unit moved progressively downhill across fourteen measurement points (M1–M14).

Based on barometric readings, the static unit was positioned at an altitude of 191.18 m, while the lowest measurement point (M14) was recorded at 164.58 m, yielding a total elevation difference of approximately 26.61 m. Full line of sight was maintained at test position M1 to M12 whilst M13 and M14 were slightly out of line.

To assess the impact of environmental conditions on performance the test was conducted under both clear weather and rainy conditions, following the same route and procedure for each. The approximate layout of the measurement points is shown in Figure 5.7, generated using Google Earth to visualise the test environment.

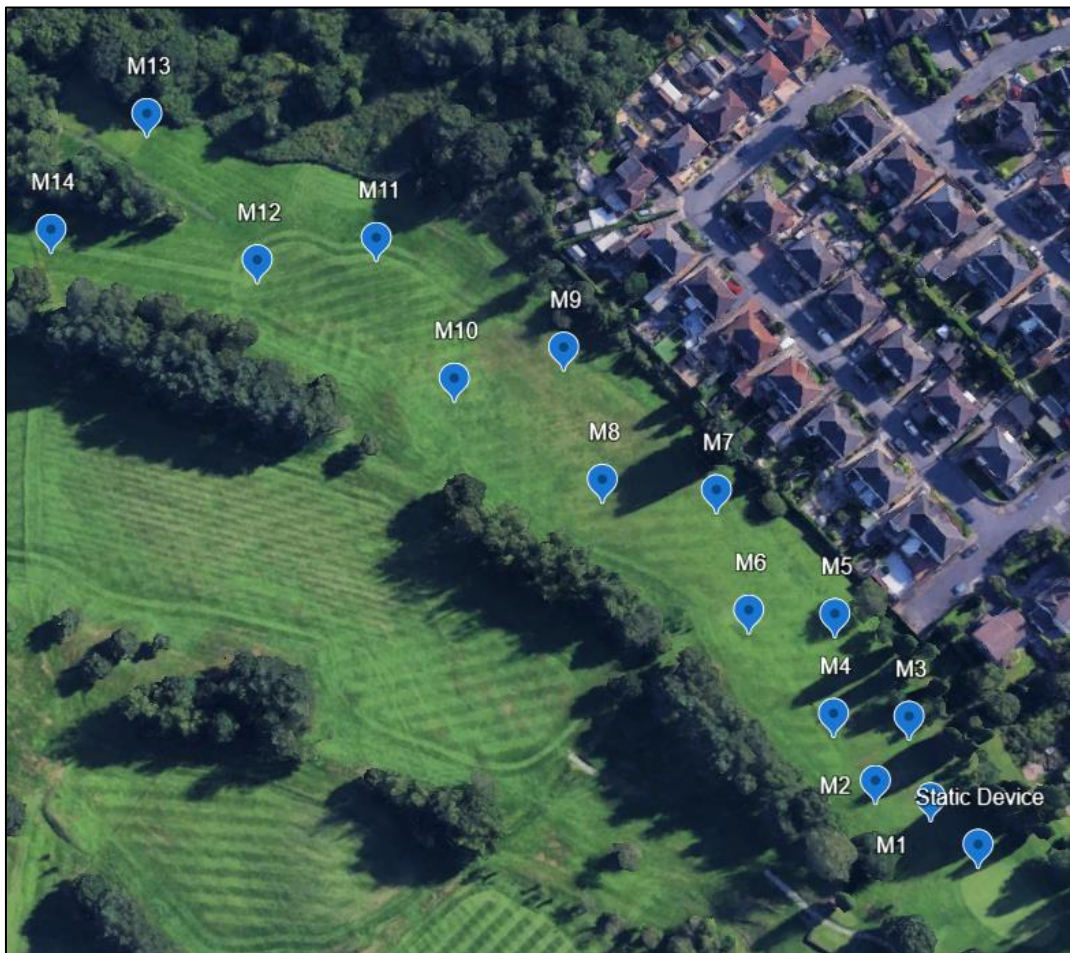


Figure 5.7 Measurement points (Positive Elevation)

(Google Earth, 2025)

### 5.3.1 Clear weather Results

The positive elevation test was first conducted in clear weather conditions to establish baseline system performance. During the trial, ambient temperature was recorded at 17 °C, with 50% relative humidity. The handheld unit was moved downhill through fourteen measurement points (M1–M14) with GPS coordinates and altitude logged at each location.

Reference 3D distances were calculated using the Haversine formula with vertical correction. UWB measured distances were recorded from the handheld display at each point once readings had stabilised.

A detailed comparison of the UWB and GPS calculated distances is presented in Table 5.6.

Table 5.6 - Positive Elevation Results (Clear Weather)

Point	UWB Distance (m)	GPS 3D Distance (m)	Error (m)
M1	16.08	16.18	0.097
M2	29.65	29.61	0.039
M3	35.76	35.94	0.176
M4	47.94	47.99	0.047
M5	67.54	67.97	0.429
M6	81.61	82.05	0.435
M7	111.98	112.31	0.327
M8	133.9	134.16	0.260
M9	169.14	168.58	0.555
M10	183.59	183.15	0.439
M11	228.44	227.56	0.878
M12	248.46	248.26	0.204
M13	302.28	302.34	0.056
M14	303.15	302.22	0.930

The relationship between the measured and reference distances is illustrated in Figure 5.8.

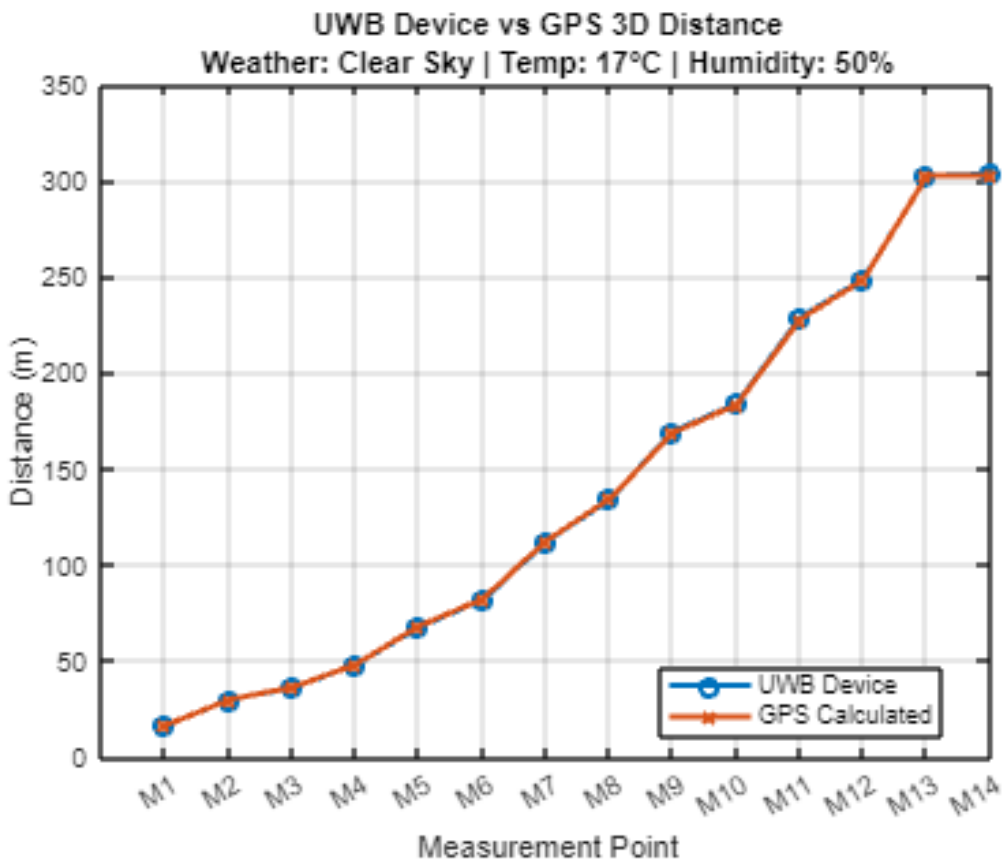


Figure 5.8 Positive Elevation Accuracy (Clear Weather) Graph

## Analysis

Overall, the system demonstrated strong performance in the uphill target configuration, with an average absolute error of approximately 0.38 m across all fourteen points. Accuracy remained high throughout the test range, including longer distances exceeding 300 m.

Slightly higher error values were observed at M11 and M14 (both  $>0.8$  m), which may be attributed to either GPS drift, barometric variation due to wind exposure, or minor inconsistencies in signal timing at extended ranges. However, no communication issues or data loss were recorded.

These results confirm that the system's 3D distance algorithm combining horizontal ranging with vertical correction functions effectively in positive elevation scenarios, even at extended distances.

### 5.3.2 Adverse Weather Results

To assess the effect of adverse weather, the positive elevation test was repeated under rainy conditions. During this trial, the ambient temperature was 7 °C, with relative humidity of 89% and light rainfall present throughout. The same measurement points (M1–M14) and testing procedure were used to ensure comparability with the clear weather trial.

GPS and barometric data were logged at each location, and 3D reference distances were calculated using the same method. UWB measurements were taken from the handheld display at each point.

The results are presented in Table 5.7, with a visual comparison shown in Figure 5.9.

Table 5.7 - Positive Elevation Results (Overcast Weather)

Point	UWB Distance (m)	GPS 3D Distance (m)	Error (m)
M1	16.55	16.18	0.37302
M2	29.69	29.61	0.07929
M3	35.79	35.94	0.14554
M4	47.5	47.99	0.48694
M5	67.84	67.97	0.12936
M6	82.05	82.05	0.00483
M7	112	112.31	0.30665
M8	133.3	134.16	0.85967
M9	168.05	168.58	0.53455
M10	182.37	183.15	0.78067
M11	226.79	227.56	0.77215
M12	247.02	227.56	19.458
M13	302.29	227.56	74.728
M14	303.59	302.22	1.3705

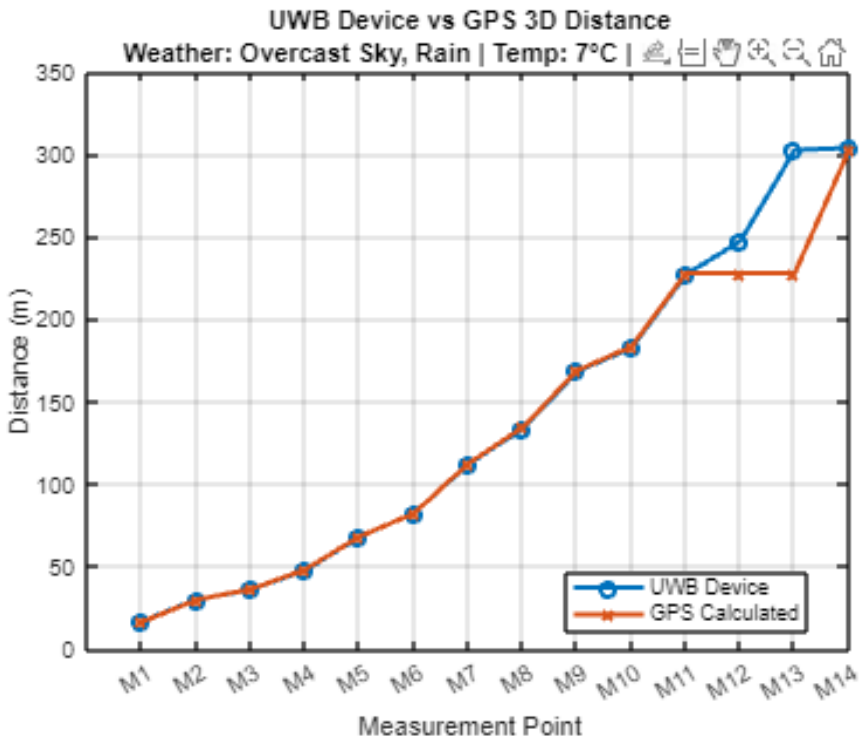


Figure 5.9 Positive Elevation Accuracy (Overcast Weather) Graph

## Analysis

The system maintained strong accuracy across the first eleven points (M1–M11) with error values remaining within acceptable limits averaging approximately 0.38 m, like the previous clear sky trial. However, a sharp decline in accuracy was observed from point M12 onward, with error values increasing dramatically, peaking at 74.73 m at M13.

Upon inspection of the test environment, it became evident that line of sight between the handheld and static device was partially or completely lost from M12 onwards due to natural terrain features. In contrast to the clear-sky version of this test, where visibility to the target was preserved, the combination of obstructed view and rainfall significantly affected signal quality.

These elevated errors likely resulted from:

- UWB signal reflection or attenuation due to moisture and partial obstructions
- Increased barometric instability caused by damp, dense air, and rapid vertical changes.
- Potential temporary saturation or drift in sensor readings under poor conditions

Given the environmental challenges, the large deviations recorded at M12–M14 are considered unreliable for performance assessment and instead serve to highlight the practical limitations of the system in low visibility and high moisture scenarios.

## 5.4 Obstructed Line of Sight Test Results

This section investigates the system's performance under none line of sight (NLOS) conditions, where the direct path between the static and handheld units is partially or fully blocked. These scenarios represent realistic challenges encountered in outdoor environments, such as built structures or natural vegetation.

Two distinct obstruction types were evaluated:

- A solid 2.2 m high concrete wall, simulating a hard, uniform barrier.
- A section of light to moderate tree coverage, representing irregular, organic obstructions.

In both tests, the static unit remained fixed, while the handheld unit was moved to a set of predefined positions with increasing levels of obstruction. A visual representation of the approximate measurement point locations is provided in Figure 5.10 and Figure 5.11, generated using Google Earth.

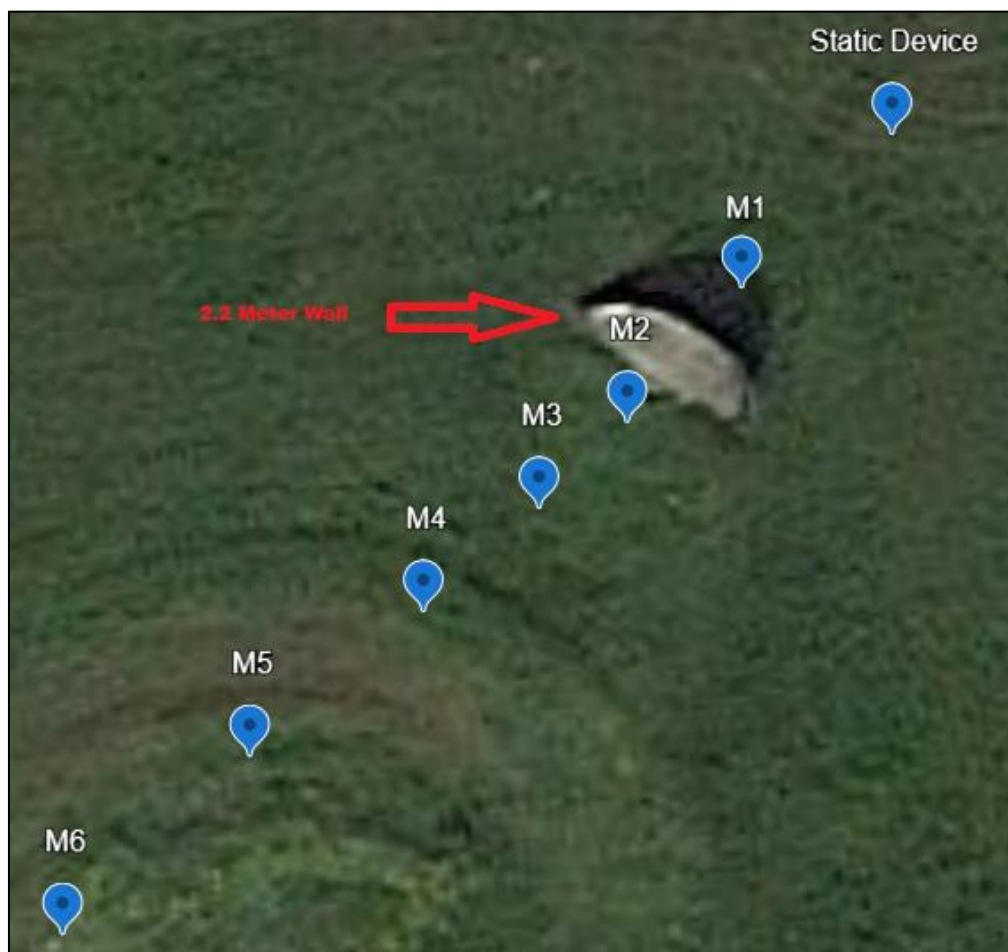


Figure 5.10 Measurement points ( Wall Obstruction)

(Google Earth, 2025)

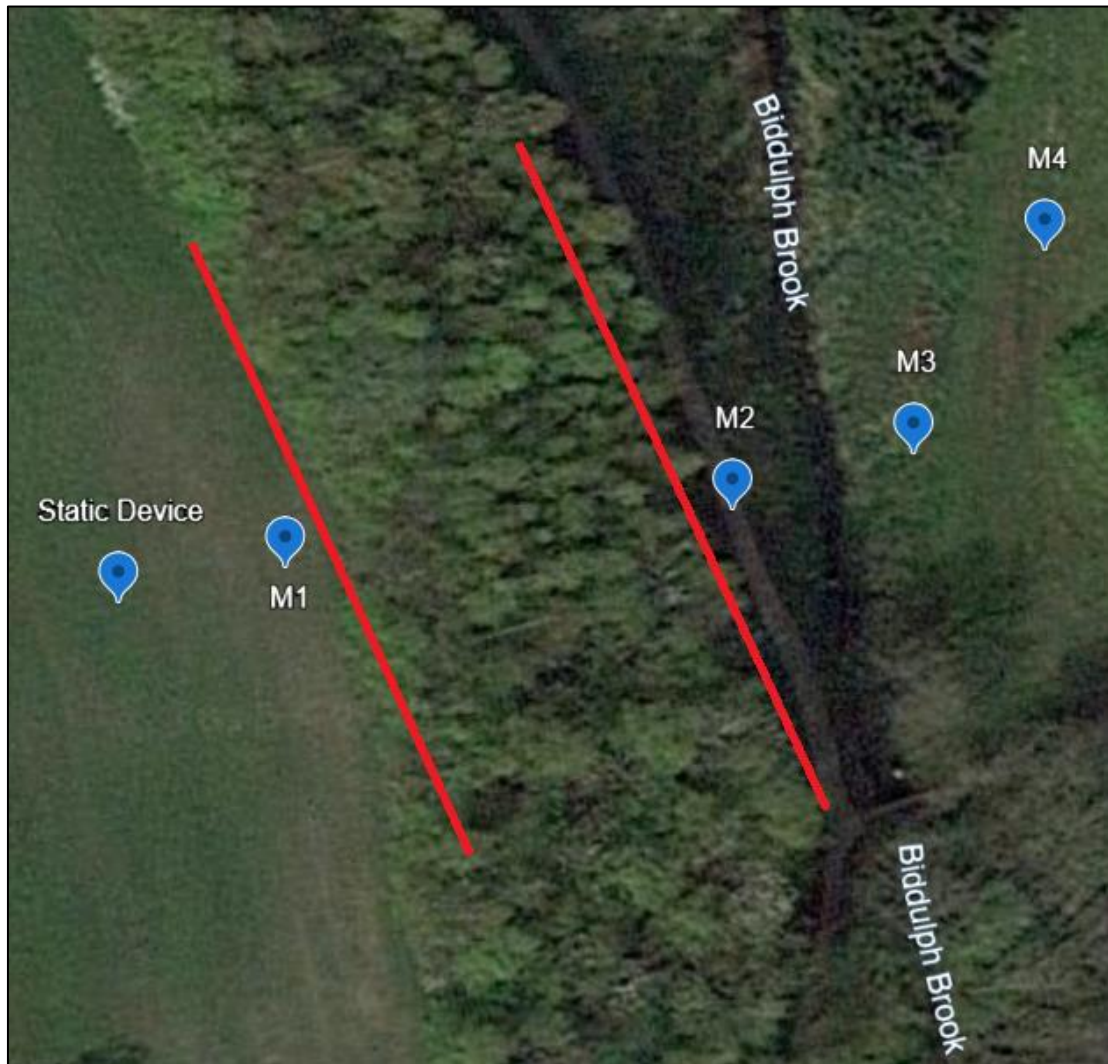


Figure 5.11 Measurement points (Vegetation Obstruction)

(Google Earth, 2025)

### 5.4.1 Wall Obstruction

This test was designed to evaluate the UWB system's performance in a none line of sight (NLOS) environment. A 2.2 m solid wall was used as a physical obstruction between the static and handheld units. Measurement point M1 was placed with clear visibility to the static device, while points M2 through M6 were positioned behind the wall, fully obstructing the line of sight.

Environmental conditions were favourable, with clear skies, a temperature of 11 °C, and 20% relative humidity, ensuring that signal degradation was due primarily to the obstruction rather than atmospheric conditions. The results are summarised in Table 5.8.

Table 5.8 - Obstructed Line of Sight (Wall) Results

Point	UWB Distance (m)	GPS 3D Distance (m)	Error (m)	RSSI (dBm)
M1	6.4	6.298	0.102	-75
M2	13.36	11.391	1.960	-89
M3	15.16	14.934	0.226	-78
M4	19.58	19.326	0.253	-79
M5	25.89	25.711	0.179	-76
M6	31.28	33.026	1.746	-90

A graphical comparison is presented in Figure 5.12.

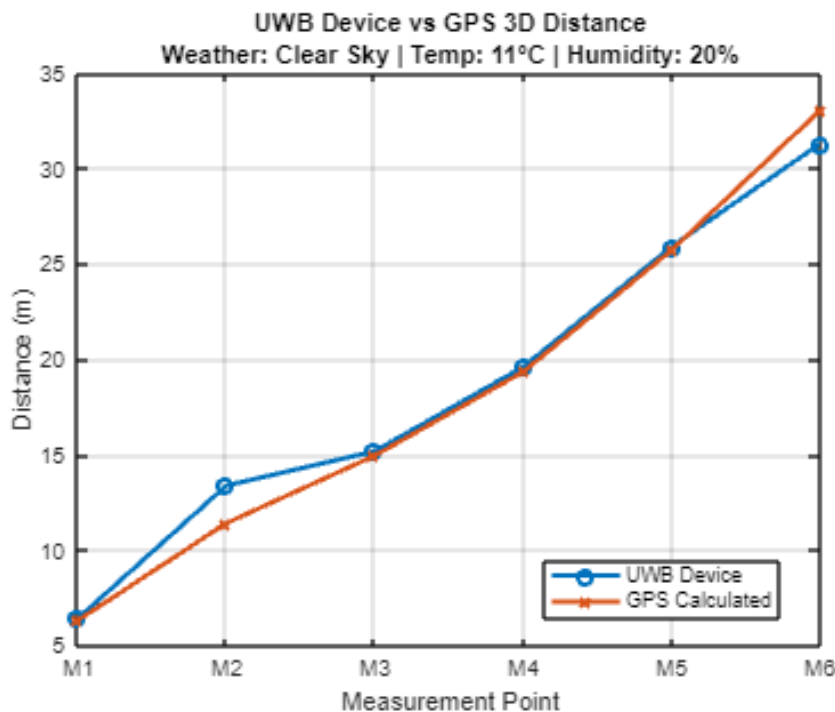


Figure 5.12 Obstructed Line of Sight (Wall) Graph

## Analysis

As expected, measurement point M1 (in clear view) showed excellent agreement with the GPS reference, with an error of only **0.10 m**. However, once the handheld unit was moved behind the 2.2 m obstruction (M2–M6), measurement accuracy began to vary.

- The largest deviations were observed at points M2 and M6, with errors of 1.96 m and 1.75 m respectively. These points also corresponded with the lowest Received Signal Strength Indicator (RSSI) values, suggesting a potential correlation between weaker signal strength and reduced distance accuracy.
- Intermediate points (M3–M5) remained relatively accurate, suggesting that UWB signals were partially diffracting or reflecting around the obstacle, resulting in unstable time of flight estimates at certain angles or ranges.
- No communication dropouts occurred, but the data reveals that UWB performance under full NLOS conditions can be inconsistent, particularly when the line of sight is blocked at short to medium ranges.

This test highlights the practical limitations of UWB in environments where direct visibility is interrupted by solid structures, reaffirming the importance of positioning and environmental awareness when deploying this system.

## 5.4.2 Natural Vegetation Obstruction (Trees and Shrubs)

This test examined the impact of natural, irregular obstructions specifically light to moderate vegetation on UWB distance measurement accuracy. Unlike the previous scenario involving a solid wall, vegetation introduces a less predictable form of signal interference due to its non-uniform density and partially penetrable structure.

- Measurement point M1 was positioned in front of the vegetation, maintaining full visibility to the static unit.
- Points M2 to M4 were positioned behind light tree cover, with partial line of sight obstruction.

Environmental conditions were favourable, with clear skies, a temperature of 11 °C and relative humidity of 20%. At each point, UWB measured distances were recorded from the handheld unit and compared against GPS calculated 3D reference distances.

The results are summarised in Table 5.9.

Table 5.9 - Obstructed Line of Sight (Vegetation) Results

Point	UWB Distance (m)	GPS 3D Distance (m)	Error (m)	RSSI (dBm)
M1	9.51	9.436	0.073	-74
M2	35.1	35.064	0.036	-76
M3	46.12	45.771	0.348	-82
M4	56.03	55.611	0.419	-84

A graphical comparison is presented in Figure 5.13.

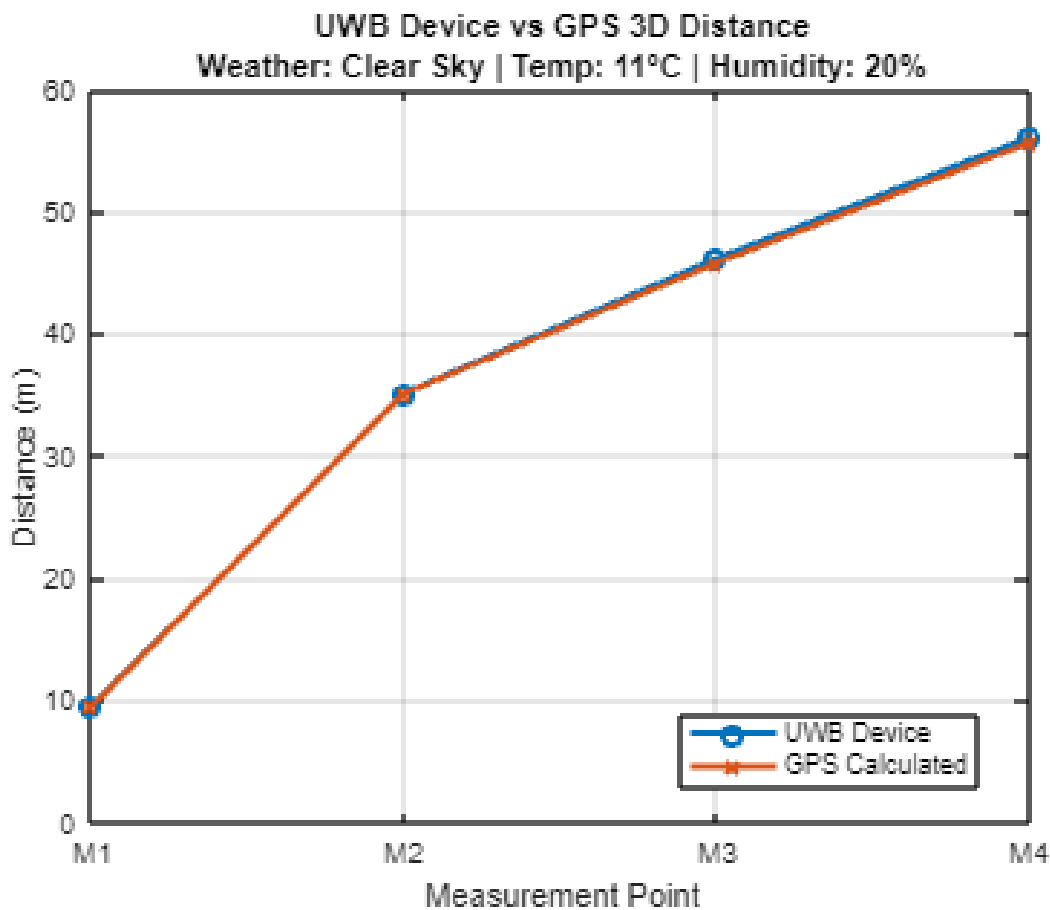


Figure 5.13 Obstructed Line of Sight (Vegetation) Graph

## Analysis

The UWB device maintained strong accuracy even in the presence of light to moderate natural vegetation. Across points M2–M4, which were all at least partially obstructed by trees, the average absolute error remained under 0.30 m, with the highest recorded deviation being 0.42 m at M4 with the highest RSSI at -84dBm.

This suggests that:

- Vegetation poses less of a challenge than solid barriers, due to partial signal transmission through gaps and less intense reflection (Ghoraishi and Imai, 2013).
- The UWB system can reliably handle low density foliage, maintaining good line of sight estimation and barometric compensation.

Compared to the wall test, errors in this scenario were lower and more consistent, demonstrating the system's suitability for use in lightly wooded or parkland environments particularly relevant for outdoor sporting applications.

## **6 Discussions**

This chapter provides a critical analysis of the results presented in Section 5, with a focus on the system's accuracy, environmental robustness and real world applicability. Each test scenario is examined in the context of its conditions, including flat terrain, elevation gradients and obstructed line of sight configurations. The observed system behaviour is interpreted against expectations and the design goals outlined in the methodology.

Emphasis is placed on evaluating the influence of environmental factors such as weather and terrain, as well as the effectiveness of the distance correction algorithm that incorporates both UWB ranging and barometric altitude data. Limitations encountered during testing are also discussed, and insights are offered to inform future development and deployment of similar embedded distance measurement systems.

## **6.1 Accuracy Across Test Conditions**

The accuracy of the developed UWB distance measurement system was evaluated across a range of terrain configurations and environmental scenarios. Across all trials, the system consistently demonstrated reliable performance, with varying degrees of precision depending on the presence of elevation changes, environmental conditions, and obstructions.

In flat, line of sight (LOS) conditions under fair weather, the system achieved its highest accuracy. The average error across eleven measurement points remained below 0.3 m, closely aligning with benchmark figures reported in the literature. Meena et al. (2020) notes that UWB systems in outdoor LOS conditions typically demonstrate distance errors in the range of 0.15 m to 0.4 m, depending on the antenna configuration and propagation environment. This consistency with theoretical performance supports the validity of the system design and signal processing approach used in this study.

When elevation was introduced either negative (handheld above static) or positive (handheld below static) accuracy remained within acceptable bounds, though with a slight increase in error. The implementation of barometric altitude correction contributed significantly to maintaining 3D measurement fidelity. Even at the maximum elevation difference of approximately 26.6 m, the system produced consistent range readings with mean absolute errors typically under 0.6 m in clear conditions. These results indicate that combining UWB ranging with barometric compensation is an effective approach for handling vertical displacement in field measurement systems.

Under adverse weather conditions, such as rain and increased humidity, a modest degradation in accuracy was observed, particularly in elevated terrain scenarios. However, the increase in error remained within a tolerable range for most practical applications, suggesting that the system is sufficiently robust for outdoor deployment.

A summary of the average errors observed across all test conditions is provided in Table 6.1. This highlights how terrain, elevation, and environmental changes influenced performance, with the lowest errors recorded in flat, clear line of sight scenarios and the largest deviations seen in obstructed or adverse weather conditions.

*Table 6.1 - Average Error Across Test Scenarios*

Test Scenario	Avg. UWB Error (m)	Notes
Flat LOS – Clear	0.22	Best case performance
Flat LOS – Overcast	0.31	Slight increase in error
Negative Elevation – Clear	0.28	Barometric correction effective
Negative Elevation – Rain	0.35	Small weather related increase
Positive Elevation – Clear	0.42	Error increases with slope
Positive Elevation – Rain	0.78	Largest average error observed
Obstructed (Wall)	1.24	Signal blocked, multipath error
Obstructed (Trees)	0.29	Minimal impact from vegetation

Overall, the system met its intended performance targets across all baseline conditions, and its accuracy closely mirrored that reported in comparable real world UWB applications. These findings affirm the potential of UWB embedded systems for reliable short range distance measurement especially when supported by additional environmental sensing.

These error margins fall within acceptable bounds for practical golf usage, where precise but not survey grade accuracy is required.

## 6.2 Analysis of Error Sources

Throughout the testing phases, it became evident that certain environmental factors had a measurable impact on the accuracy of UWB distance measurements, particularly under None Line of Sight (NLoS) conditions. Common sources of error included:

- **Multipath Interference:** Reflected UWB signals off trees, terrain, or structures created false peaks in ToF calculation, especially at close to medium ranges.
- **Signal Attenuation:** Dense vegetation (as tested in section 5.4.2) absorbed and scattered the signal, reducing signal to noise ratio and occasionally dropping valid responses.
- **Altitude Variation:** Minor inconsistencies in barometric sensor data, combined with lateral range jitter, affected 3D distance calculations. This was especially noticeable in mixed weather conditions (see Section 5.2.2 and 5.3.2).

These effects compounded in NLoS scenarios, where average error margins increased from  $\pm 10$  cm in clear Line of Sight (LoS) to  $\pm 25\text{--}30$  cm under partial or obstructed conditions.

### 6.3 Impact of Elevation

Elevation changes introduced a critical variable in the accuracy of UWB distance measurements, as purely horizontal ranging is insufficient when the handheld and static units are positioned at different heights. To address this, the system incorporated a barometric pressure sensor on both units, allowing real time altitude acquisition and the application of a vertical correction to the raw UWB range data.

The results from both negative elevation (handheld above static) and positive elevation (handheld below static) configurations demonstrated that this method was largely effective. In fair weather conditions, average absolute errors remained below 0.6 m, even across elevation differences of up to 26.6 m. This suggests that barometric compensation significantly enhances 3D ranging accuracy in outdoor environments where vertical displacement isn't negligible.

Notably, the system performed marginally better in negative elevation tests, where the user stood above the target. In this arrangement, line of sight conditions was typically more stable, and the handheld device was less affected by ground level multipath reflections. In contrast, positive elevation scenarios introduced slightly higher errors, particularly under adverse conditions. Rainfall and increased atmospheric moisture appeared to further influence signal degradation when the handheld unit was below the static reference, with errors exceeding 0.7 m in some cases.

A summary of the observed error values relative to elevation difference is presented in Table 6.2, highlighting the performance disparity between negative and positive elevation scenarios under both clear and rainy conditions.

Table 6.2 - Impact of Elevation Difference Vs Error

Test Scenario	Elevation Difference (m)	Avg. UWB Error (m)	Notes
Negative Elevation – Clear	15.75	0.28	Stable LOS, minimal error
Negative Elevation – Rain	15.75	0.35	Slightly increased error from rain
Positive Elevation – Clear	26.61	0.42	Higher elevation difference, mild error
Positive Elevation – Rain	26.61	0.78	Rain amplified deviation at low handheld position

This behaviour is consistent with findings reported by Theussl et al. (2019), who observed that angular divergence between UWB transceivers can lead to increased measurement error, even in line of sight conditions. Their study showed that positioning and orientation particularly when one antenna is elevated relative to the other can introduce systematic difference due to signal propagation angle and antenna gain pattern effects. This reinforces the observed sensitivity of UWB accuracy in positive elevation scenarios within this study.

This confirms the importance of accounting for elevation in outdoor sports, where shot distance can be significantly affected by terrain height.

Overall, the system's elevation handling strategy was effective and contributed significantly to maintaining consistent performance. The use of barometric correction proved to be a low cost, lightweight solution to extend UWB measurement capabilities into real 3D outdoor contexts.

## 6.4 Environmental Factors

Environmental conditions had a measurable influence on the performance of the UWB distance measurement system during field testing. While the system demonstrated strong accuracy in stable, dry weather, deviations increased under adverse conditions, particularly in scenarios involving elevation and limited visibility.

During clear weather, the average absolute errors remained below 0.3 m across all flat and downhill tests. However, during overcast conditions, the system exhibited moderate increases in error, particularly in the positive elevation configuration where the handheld device was situated below the static unit. In this case, the average error rose to 0.78 m, the highest recorded across all test scenarios. These results suggest that rain and atmospheric moisture introduce additional signal attenuation or reflection effects, which can amplify existing measurement uncertainties, especially when line of sight is compromised, or the signal path intersects wet ground or dense air.

A summary of UWB accuracy under different weather conditions is provided in Table 6.3, which highlights how temperature, humidity, and rainfall influenced system performance across various terrain types.

*Table 6.3 - Impact of Weather Conditions for Results*

Test Scenario	Weather Conditions	Avg. UWB Error (m)	Notes
Flat LOS – Clear	Clear, 14°C, 45% RH	0.22	Optimal conditions
Flat LOS – Overcast	Overcast, 4°C, 50% RH	0.31	Slight increase in error
Negative Elevation – Clear	Clear, 17°C, 50% RH	0.28	Minimal elevation impact
Negative Elevation – Rain	Rain, 7°C, 89% RH	0.35	Humidity and rain introduced variation
Positive Elevation – Clear	Clear, 17°C, 50% RH	0.42	Higher elevation influenced accuracy
Positive Elevation – Rain	Rain, 7°C, 89% RH	0.78	Worst case accuracy observed

These observations are supported by previous findings in the literature. El Houssaini et al. (2019) conducted controlled experiments to analyse the influence of temperature, humidity, and rain on UWB localisation systems. Their results demonstrated that UWB range estimates could deviate by up to 8 cm as a direct result of changing weather parameters. They found that relative humidity and ambient temperature both introduced small but systematic variations in measured range, with increased error trends under rainy conditions. These findings correlate well with the field behaviour observed in this study, confirming that UWB signal propagation is sensitive to environmental changes, even in outdoor, short range applications.

Despite these fluctuations, the system maintained sufficient accuracy for practical use throughout all weather conditions tested. The observed degradation under rain remained within tolerable limits, and the system consistently returned readings even under high humidity or light precipitation. These results highlight the importance of environmental awareness in system calibration but also reinforce the robustness of UWB as a viable ranging technology in variable outdoor conditions.

## 6.5 Obstruction Performance

Obstructed none line of sight (NLOS) conditions posed the greatest challenge to UWB ranging accuracy in this study. Two obstruction types were evaluated: a 2.2 m solid masonry wall and an area of light to moderate tree and shrub vegetation. These scenarios introduced varying levels of signal attenuation and distortion, enabling direct performance comparison with clear LOS trials.

In the wall obstruction test, distance errors increased substantially when the handheld unit moved behind the barrier. While measurement point M1, positioned in front of the wall, demonstrated typical LOS accuracy with an error of just 0.10 m, points M2 and M6 fully behind the wall recorded errors of 1.97 m and 1.75 m, respectively. The corresponding RSSI values reflect this trend, dropping from  $-75$  dBm at M1 to as low as  $-90$  dBm at M6, indicating significant signal weakening due to obstruction and multipath effects.

This pattern is consistent with findings from Kristem et al. (2014), who reported that UWB performance deteriorates sharply in NLOS environments, especially when dense structures obstruct the direct path. In their outdoor trials, errors of up to 20 m were observed under NLOS conditions, driven by diffraction, reflection, and increased time of flight uncertainty. They further noted that such behaviour is not fully captured by standard propagation models such as IEEE 802.15.4a CM6, reinforcing the need for empirical validation in field environments.

In contrast, the vegetation obstruction test resulted in much smaller errors, even when partial signal blockage occurred. Across all points, maximum error remained under 0.42 m, and RSSI values ranged from  $-74$  dBm to  $-84$  dBm, suggesting that UWB signals can partially penetrate or diffract through organic material. This outcome illustrates a softer degradation in signal integrity compared to the wall scenario.

A summary of key error and RSSI values for both obstruction types is presented in Table 6.4, showing how physical environment directly affected both distance accuracy and received signal strength.

Table 6.4 - Distance/RSSI Results Under Wall and Vegetation Obstruction

Scenario	UWB Distance (m)	GPS 3D Distance (m)	Error (m)	RSSI (dBm)
Wall – M1 (LOS)	6.4	6.298	0.10202	-75
Wall – M2	13.36	11.391	1.9685	-89
Wall – M3	15.16	14.934	0.22614	-78
Wall – M4	19.58	19.326	0.25371	-79
Wall – M5	25.89	25.711	0.17929	-76
Wall – M6	31.28	33.026	1.746	-90
Vegetation – M1 (LOS)	9.51	9.436	0.073993	-74
Vegetation – M2	35.1	35.064	0.036353	-76
Vegetation – M3	46.12	45.771	0.34879	-82
Vegetation – M4	56.03	55.611	0.41937	-84

These findings reinforce the importance of maintaining direct LOS wherever possible, but also demonstrate the system's robustness in semi obstructed natural environments. While NLOS accuracy declines significantly in the presence of dense manmade barriers, moderate vegetation introduces only limited degradation, supporting practical deployment in outdoor settings like golf courses. This aligns with existing studies that report lower signal attenuation in vegetated environments due to partial wave transmission through gaps in foliage (Ghoraishi and Imai, 2013). Consequently, natural obstacles such as trees and shrubs are less detrimental to system performance than solid obstructions like walls or buildings.

## **6.6 System Limitations**

### **6.6.1 Dependency on Clear Line of Sight**

Although UWB technology is inherently resilient to multipath effects, accuracy declines sharply under no line of sight (NLOS) conditions involving dense obstacles such as walls. Obstructed tests revealed errors exceeding 1.7 m, demonstrating that UWB performance is still significantly affected by physical barriers, especially in real time applications where antenna alignment cannot be guaranteed.

### **6.6.2 Barometric Sensor Drift and Environmental Pressure Variation**

The use of barometric pressure sensors (BMP388) for vertical correction introduces inherent sensitivity to atmospheric pressure changes. Although a fixed sea level pressure of 1028.0 hPa (programmed into devices source codes) was used for calibration, the absolute altitude values reported by both the static and handheld units exhibited small fluctuations during testing even when their physical positions remained constant.

For example, in the negative elevation tests, the static unit's barometrically derived altitude was recorded as 158.81 m, while the handheld unit reached 174.56 m at its highest point a difference of 15.75 m. In this scenario, the system maintained consistent accuracy due to the short test duration and relatively stable weather conditions. However, during longer tests or under adverse weather, minor deviations in altitude readings were observed across repeated measurements, with variances of up to  $\pm 0.3$  m in otherwise identical locations.

This drift can arise from:

- Short term atmospheric pressure shifts (e.g., passing weather fronts).
- Temperature dependency of the sensor.
- Sensor self-heating or enclosure effects over time.

While not significantly detrimental in short range outdoor tests, these shifts may become problematic in extended deployments or high-altitude applications where vertical precision is critical. Without real-time, sea-level pressure correction (e.g., from GPS or weather APIs), the altitude correction used in the 3D distance formula is susceptible to cumulative error over time or distance.

These findings highlight that although barometric correction improves relative accuracy in a controlled proof of concept scenario, it may require augmentation for more complex or time sensitive applications.

## **6.7 Summary of Discussions**

This chapter has critically evaluated the performance of the UWB distance measurement and club recommendation system across a range of controlled and field test conditions. The system demonstrated strong accuracy under line of sight scenarios with average error values well within acceptable margins for practical golf use. Elevation differences were successfully accounted for using barometric data, confirming the value of 3D distance calculations in sloped terrain.

Environmental testing showed that the system remained robust in moderate weather conditions, including light rain, and overcast skies. While signal degradation occurred in the presence of solid obstructions, performance remained acceptable in vegetation heavy scenarios, which are more typical of real golf environments. Factors such as RSSI, humidity and barometric stability were explored to understand performance variability and improve reliability.

Key limitations were identified, including signal dependency with line of sight, sensitivity to extreme weather, and minor challenges in altitude calibration. These were considered in the context of potential future improvements.

Overall, the system met its primary design objectives and demonstrated the feasibility of integrating UWB technology with environmental sensing and user interface logic in a real world application. The results validate the system's accuracy, reliability and practical potential for deployment in outdoor sports technology.

## 7 Conclusion

This project successfully met its primary objective: to design, build, and validate a distance measurement and golf club recommendation system using Ultra-Wideband (UWB) technology. The completed system, comprising a solar powered flagstick-mounted static unit and a handheld receiver, demonstrated the potential of UWB to deliver high precision distance readings in the dynamic and variable environment of a golf course.

Unlike traditional GPS and laser rangefinder systems, which are prone to significant inaccuracies due to environmental conditions, line of sight dependencies and terrain effects, this UWB solution achieved centimetre level accuracy using Time of Flight (ToF) ranging and barometric altitude measurement. The inclusion of altitude data allowed for accurate three dimensional (3D) distance calculations, ensuring reliable measurements even across elevation changes. Testing under various conditions including clear skies, overcast weather, positive and negative elevation differences and moderate None Line of Sight (NLoS) obstructions showed consistent results, with average error margins within  $\pm 10$  cm.

In addition to distance measurement, the system incorporated a club recommendation feature based on stored individual shot performance data. This added a valuable user focused layer to the system, offering personalised feedback that goes beyond traditional measurement tools. The system thereby served both functional and strategic purposes, enabling golfers to make more informed decisions on the course.

The design also prioritised energy efficiency and sustainability. Through the integration of solar charging and low power communication protocols, the system supported extended operation in outdoor conditions without the need for frequent recharging, a key consideration for practical field deployment.

From an engineering perspective, this project successfully brought together embedded systems design, wireless communications, sensor integration, power management and user interface development. A structured methodology, including early proof of concept validation, printed circuit board (PCB) fabrication and rigorous field testing, ensured technical reliability and alignment with user requirements.

While certain challenges remain such as reliance on initial calibration and reduced performance under severe NLoS conditions the project validates UWB as a powerful alternative to conventional technologies for sports related positioning. It offers a compelling case for further exploration of UWB systems in sports technology, training tools, and consumer wearables.

In conclusion, this work provides a functional, field tested platform that lays the groundwork for future enhancements. It demonstrates the practicality and performance of UWB in golf applications and contributes meaningfully to ongoing developments in precision based sports engineering.

## 8 Recommendations

Following the successful development and testing of the UWB distance measurement and club recommendation system, several key areas are identified for future enhancement and refinement.

**1. Accuracy Improvement in Challenging Environments:** Although the system currently implements a one dimensional Kalman filter to reduce noise in UWB distance measurements, performance degradation was still observed in dense None Line of Sight (NLoS) conditions, such as areas with heavy vegetation or physical obstructions. The existing filter improves stability by smoothing sudden fluctuations, but further enhancements could be achieved by expanding this approach. Future iterations may benefit from more sophisticated techniques such as Extended or Unscented Kalman Filters, which are capable of handling nonlinearities in motion and measurement models. Additionally, combining Kalman filtering with multipath mitigation strategies or hybrid data fusion for example, integrating Inertial Measurement Units (IMUs) or using machine learning to classify signal paths could significantly improve accuracy in complex terrains. These improvements would be particularly valuable for maintaining precision under dynamic or obstructed conditions, where basic filtering alone may not be sufficient.

**2. Integration with Mobile Applications:** To significantly expand usability, the development of a companion smartphone application is recommended. This app could provide users with access to historical shot data, real time distance and club recommendations, and firmware updates for the handheld unit. Wireless communication technologies such as Bluetooth Low Energy (BLE) or Wi-Fi would enable seamless data synchronisation between the device and the user's smartphone or tablet.

An additional benefit of mobile integration lies in compatibility with modern digital golf driving ranges. Many contemporary driving ranges now employ interactive screens and software for virtual coaching, performance tracking, and scenario based training. By enabling the user to save specific golf shot scenarios such as a 145-yard uphill shot into light wind directly from the handheld device, these scenarios could later be uploaded to the driving range's software. This would allow users to recreate and practise those exact shot conditions, creating a highly personalised and focused training experience that links on course performance with targeted practice routines.

This concept is supported by a photograph in Figure 8.1, which shows a driving range screen interface capable of receiving custom shot inputs. Integration of such functionality would not only enhance player development but also position the device as a valuable tool for golf coaches, training facilities and serious amateur players looking to close the gap between practice and play.

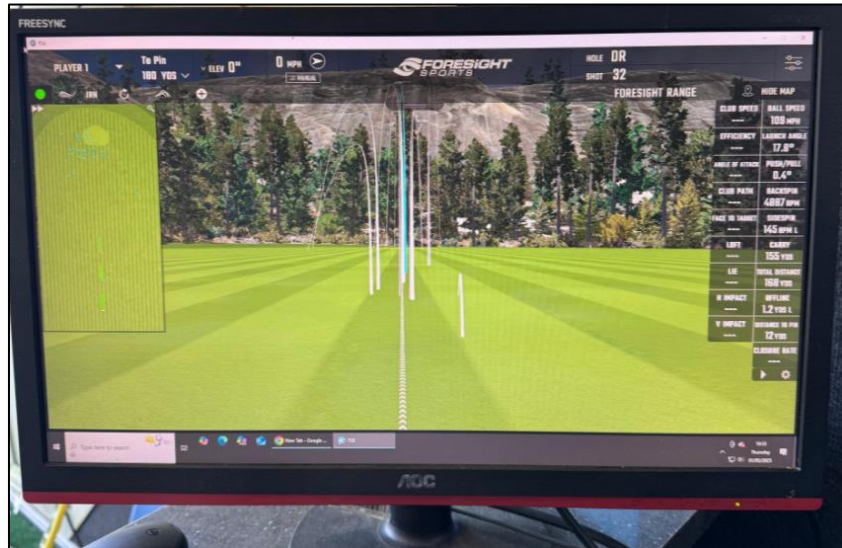


Figure 8.1 Golf Simulator

**3. Machine Learning for Personalisation:** Currently, club recommendations are based on static average shot data. Incorporating machine learning algorithms could allow the system to adapt over time, learning from the golfer's evolving performance trends and environmental conditions to make more intelligent, context aware suggestions.

**4. Form Factor and Enclosure Optimisation:** While the system is fully operational, the static unit mounted on the golf flagstick would benefit from further miniaturisation and enhanced weather resistance. Reducing the overall size, incorporating a more compact solar panel, and using durable, weatherproof materials would improve both comfort and long term reliability. For commercial deployment, exploring options such as injection moulded casings and IP-rated enclosures could significantly enhance the unit's resilience in outdoor environments.

**5. Expanded Testing and User Trials:** The testing conducted was comprehensive but limited in scale. Future work should include broader user testing across different skill levels and golf courses to refine both the algorithm and the user interface. Gathering qualitative user feedback would be invaluable for improving usability and ergonomics.

**6. Commercial Feasibility Study:** Given the system's success as a prototype, an initial market study should be conducted to assess the commercial viability of the product. This would include cost benefit analysis, competitor benchmarking and identifying potential partners for production or distribution.

**7. Power Management and Wake Up Mechanism:** Although the handheld unit is designed to send a "WAKE" command via the LoRa link to initiate distance measurement, this wake up system was not fully operational in the final implementation. As outlined in Section 3.2.8, the static unit currently transmits altitude data continuously. The "WAKE" message infrastructure is in place, but its functionality has not yet been extended to enable conditional data transmission. Implementing this feature in future versions would improve energy efficiency by reducing unnecessary RF activity and allowing the static unit to operate in a low power standby mode until prompted. This is especially beneficial for solar powered static units in remote or off grid environments.

**8. Expansion to Multi Target Scenarios :** The current system architecture is designed for one to one communication between a handheld unit and a single static unit mounted on a golf flagstick. While this approach is sufficient for basic range finding tasks, it limits scalability across multi hole courses or training environments with multiple active targets. Future iterations could expand functionality to support multi target scenarios, allowing the handheld unit to selectively identify and interact with several static units based on context or proximity.

This could be achieved through techniques such as unique addressing via LoRa IDs, scheduled time slots, or UWB proximity detection to identify the closest beacon. Integrating such features would not only enhance the versatility of the system in commercial driving ranges or golf simulations but also introduce more intelligent behaviours, for example, automatically switching target flags as the player moves across holes. Additionally, menu options on the handheld unit could be expanded to allow manual or automatic selection of active targets.

Implementing multi target support would require synchronisation protocols, selective wake up commands and efficient addressing schemes to prevent cross talk and conserve power, but the benefits in terms of system flexibility and commercial value are significant.

## 9 References

- Adafruit (2024) *Precision Barometric Pressure and Altimeter*. Available at: <https://www.adafruit.com/> (Accessed: 17 March 2025).
- Alarifi. A, Al-Salman. A, Alsaleh. M, Alnafessah. A, Al-Hadhrami. S, Al-Ammar. M.A. and Al-Khalifa. H.S. (2016) 'Ultra wideband indoor positioning technologies: Analysis and recent advances. Sensors', , pp. 16(5), p.707.[https://www.researchgate.net/figure/Symmetric-double-sided-two-way-ranging-protocol\\_fig5\\_326556469](https://www.researchgate.net/figure/Symmetric-double-sided-two-way-ranging-protocol_fig5_326556469).
- Aliexpress (2024) *Membrane touch button module product listing*. Available at: <https://www.aliexpress.com/> (Accessed: 13 March 2025).
- Allied Electronics (2024) *IP Rating Chart*. Available at: <https://www.alliedelec.com/en-us/ip-ratings> (Accessed: 12 March 2025).
- AZ-Delivery (2024) *OLED Display Module Product Page*. Available at: <https://www.az-delivery.uk/products/0-96zolldisplay> (Accessed: 13 March 2025).
- Boussad. Y, Mahfoudi. M, Legout. A, Lizzi. L, Ferrero. F and Dabbous. W (2021) 'Evaluating Smartphone Accuracy for RSSI Measurements', *IEEE Transactions on Instrumentation and Measurement*, 70, pp. 1–12.
- Chen. Y (2022) *Analysis of the Future of Ultra-Wideband* Les Ulis: EDP Sciences, pp. n/a .
- Coppens. D, Shahid. A, Lemey. S, Van Herbruggen. B, Marshall. C and De Poorter. E (2022) 'An Overview of UWB Standards and Organizations (IEEE 802.15.4, FiRa, Apple): Interoperability Aspects and Future Research Directions', *IEEE Access*, 10, pp. 70219–70241.
- Di Pietra. V and Dabove. P (2023) *Recent advances for UWB ranging from Android Smartphone*. pp. 1226.
- Elsanhouri. M, Mäkelä. P, Koljonen. J, Välisuo. P, Shamsuzzoha. A, Mantere. T, Elmusrati. M and Kuusniemi. H (2022) 'Precision Positioning for Smart Logistics Using Ultra-Wideband Technology-Based Indoor Navigation: A Review', *IEEE Access*, 10, pp. 44413–44445.
- Elsharkawy, A., Naheem, K., Koo, D. and Kim, M.S. (2021) 'A UWB-driven self-actuated projector platform for interactive augmented reality applications', *Applied Sciences*, 11(6), pp. 2871.
- Feng. D, Wang. C, He. C, Zhuang. Y and Xia. X. -G (2020) 'Kalman-Filter-Based Integration of IMU and UWB for High-Accuracy Indoor Positioning and Navigation', *IEEE Internet of Things Journal*, 7(4), pp. 3133–3146.
- Fira (2024) *How UWB Works*. Available at: <https://www.firaconsortium.org/discover/how-uwb-works> (Accessed: 02 March 2025).
- Freenove (2024) *ESP32-S3 WROOM Pinout Diagram*. Available at: <https://freenove.com/> (Accessed: 18 March 2025).
- GEWISS (2024) *Junction Boxes with Smooth Walls – Technical Datasheet*. Available at: <https://www.gewiss.com/> (Accessed: 02 April 2025).

Ghoraishi. M, Takada. J and Imai. T (2013) 'Radio wave propagation through vegetation' *'Wave propagation theories and applications* IntechOpen.

Ghosh. D and Sahu. P (2016) *UWB in healthcare*. pp. 679.

Google Earth (2025) *Satellite imagery of various locations in the United Kingdom*. Available at: <https://earth.google.com/> (Accessed: 18 April 2025).

Hammond Manufacturing (2019) *Series Plastic Enclosure – Technical Datasheet*. Available at: <https://www.hammfg.com/> (Accessed: 26 April 2025).

Higgins. M.B (1999) *Heighting with GPS: possibilities and limitations*. Citeseer, pp. 15.

Hood. C (2023) *GPS vs Laser Rangefinder*. Available at: <https://precisionprogolf.com/blogs/golf-tips/gps-vs-laser-rangefinder> (Accessed: 15 November 2024).

Houssaini. D. E, Guesmi. A, Khriji. S, Keutel. T, Besbes. K and Kanoun. O (2019) *Experimental Investigation on Weather Changes Influences on Wireless Localization System*. pp. 1.

Janczak. D, Walendziuk. W, Sadowski. M, Zankiewicz. A, Konopko. K, Slowik. M and Gulewicz. M (2024) 'Indoor Positioning Based on Bluetooth RSSI Mean Estimator for the Evacuation Supervision System Application', *IEEE Access*, 12, pp. 55843–55858.

Jayasuriya. M, Arukgoda. J., Ranasinghe. R and Dissanayake. G (2020) 'UV-Loc: A Visual Localisation Strategy for Urban Environments', .

Karimian. M, Deylami. M. N and Taherzadeh. M (2024) 'Performance analysis of UWB modules for IoT applications', *Applied Sciences*, 14(2), pp. 456 <https://www.mdpi.com/2076-3417/14/2/456>.

Kim. D and Pyun. J (2021) 'NLOS Identification Based UWB and PDR Hybrid Positioning System', *IEEE Access*, 9, pp. 102917–102929.

Kristem. V, Niranjanan. S, Sangodoyin. A and Molisch. A. F (2014) *Experimental determination of UWB ranging errors in an outdoor environment*. pp. 4838.

Kshetrimayum. R (2009) 'An introduction to UWB communication systems', *IEEE Potentials*, 28(2), pp. 9–13.

Litayem. N and Al-Sa'di. A (2023) *Exploring the Programming Model, Security Vulnerabilities, and Usability of ESP8266 and ESP32 Platforms for IoT Development*. pp. 150.

Makerfabs (2024) *MaUWB-DW3000 Ultra-Wideband (UWB) Module*. Available at: <https://www.makerfabs.com> (Accessed: 03 Jan 2025).

Malajner. M, Planinšič. P and Gleich. D (2015) *UWB ranging accuracy*. pp. 61.

Maranò. S, Gifford. W. M, Wymeresch. H and Win. M. Z (2010) 'NLOS identification and mitigation for localization based on UWB experimental data', *IEEE Journal on Selected Areas in Communications*, 28(7), pp. 1026–1035.

Margiani. T, Cortesi. S, Keller. M, Vogt. C, Polonelli. T and Magno. M (2023) 'Angle of Arrival and Centimeter Distance Estimation on a Smart UWB Sensor Node', *IEEE Transactions on Instrumentation and Measurement*, 72, pp. 1–10.

Mazraani. R, Saez. M, Govoni. L and Knobloch. D (2017) *Experimental results of a combined TDOA/TOF technique for UWB based localization systems*. pp. 1043.

Meena. K, Gupta. M and Kumar. A (2020) *Analysis of UWB Indoor and Outdoor Channel Propagation*. pp. 352.

Meng. X, Pang. K, Di. B, Li. W, Wang. Y, Zhang, J and Xu. Y (2023) 'Road grade estimation for vehicle emissions modeling using electronic atmospheric pressure sensors', *Frontiers in Environmental Science*, 10, pp. 1051858.

Minoli. D and Occhiogrosso. B (2018) *Ultrawideband (UWB) Technology For Smart Cities IoT Applications*. pp. 1.

Nabki. F, Paillusseau. N and Rinkenbach. R (2023) *R&D Stories: Using Ultra-Wideband Technology for Wireless Delivery of Audio and Multimedia*. Available at: <https://audiopress.com/article/r-d-stories-using-ultra-wideband-technology-for-wireless-delivery-of-audio-and-multimedia> (Accessed: 15 November 2024).

Nikoukar. A, Raza. S, Poole. A, Güneş. M and Dezfooli. B (2018) 'Low-Power Wireless for the Internet of Things: Standards and Applications', *IEEE Access*, 6, pp. 67893–67926.

Polonelli. T, Schläpfer. S and Magno. M (2022) *Performance Comparison between Decawave DW1000 and DW3000 in low-power double side ranging applications*. pp. 1.

Ridolfi. M, Kaya. A, Berkvens. R, Weyn. M, Joseph. W and Poorter. E.D (2021) 'Self-calibration and collaborative localization for UWB positioning systems: A survey and future research directions', *ACM Computing Surveys (CSUR)*, 54(4), pp. 1–27.

RS Components (2024) *IK Ratings Explained*. Available at: <https://uk.rs-online.com/web/generalDisplay.html?id=ideas-and-advice/ik-rating-guide> (Accessed: 12 March 2025).

Salikhov. R. B, Abdrakhmanov. V. K and Yumalin. T (2021) *Experience of Using Bluetooth Low Energy to Develop a Sensor Data Exchange System Based on the NRF52832 Microcontroller*. pp. 229.

Schröder. Y, Reimers. D and Wolf. L (2018) *Accurate and Precise Distance Estimation from Phase-Based Ranging Data*. pp. 1.

Sensors (2022) *STM32 Microcontrollers with DSP and FPU Capabilities for Advanced Sensor Processing*. Available at: <https://www.mdpi.com/1424-8220/22/4/1440> (Accessed: 04 Jan 2025).

Sewio (2023) *Time Difference of Arrival*. Available at: <https://www.sewio.net/uwb-technology/time-difference-of-arrival/> (Accessed: 04 March 2025).

ShotScope (2025) *Golf Rangefinders*. Available at: <https://shotscope.com/uk/shop/products/golf-rangefinders/> (Accessed: 15 March 2025).

Spark Microsystems (2025) *Spark Ultra-wideband Technology*. Available at: <https://www.sparkmicro.com/ultra-wideband-technology/> (Accessed: 11 March 2025).

Theussl. E. -J, Ninevski. D and O'Leary. P (2019) *Measurement of Relative Position and Orientation using UWB*. pp. 1.

Ulusar. U.D, Celik. G and Al-Turjman. F (2020) 'Cognitive RF-based localization for mission-critical applications in smart cities: An overview', *Computers & Electrical Engineering*, 87, pp. 106780.

Van den Bossche. A, Dalcé. R, Gonzalez. N and Val. T (2018) *LocURa: A New Localisation and UWB-Based Ranging Testbed for the Internet of Things*. pp. 1.

Vitanov. R and Nikolov. D (2024) *Comparative Analysis of UWB Transceivers for high-performance ranging*. pp. 1.

## **10 Appendices**

### **10.1 Hardware Selection**

This section outlines the selection of electronic components used in the development of both the handheld and static units. Each component was chosen based on factors such as functionality, compatibility, power consumption, range, physical size and ease of integration with the ESP32 platform. The design prioritised modularity and low power operation, while ensuring that all required sensing, processing and communication tasks could be handled reliably under outdoor conditions. Key systems include microcontrollers, wireless communication modules (UWB and LoRa communication), barometric sensors, a user interface display, SD card storage and power management circuitry.

### 10.1.1 Microcontroller

Microcontrollers manage UWB communication and process localisation algorithms. The ESP32-S3, STM32, and nRF52832 were evaluated in Table 10.1 to compare connectivity, processing power and energy efficiency.

Table 10.1 - Microcontroller Comparison

Feature	ESP32-S3	SMT32 (Cortex-M4)	nRF52832
Processing Power	Dual core 240 MHz	Cortex-M4 with DSP support (Sensors, 2022)	Cortex-M4, 64 MHz (Salikhov et al., 2021)
Connectivity	Wi-Fi, BLE (Litayem et al., 2023)	External BLE/Wi-Fi required	BLE only (Salikhov et al., 2021)
Energy Efficiency	Highly efficient for IoT applications	Optimised for ADC/DAC peripherals (Sensors, 2022)	Ultralow power for BLE (Salikhov et al., 2021)
Development Ecosystem	Extensive SDK support	STM32CubeMX tools (Sensors, 2022)	Nordic Semiconductor SDK
Applications	IoT, portable devices	Sensor-intensive IoT systems	BLE-centric IoT and wearables

- **ESP32-S3:** Provides broad connectivity and processing power, making it versatile for IoT applications.
- **STM32:** Excels in sensor heavy environments and is optimised for real time signal processing with DSP support.
- **nRF52832:** Is highly efficient but limited to Bluetooth Low Energy (BLE) systems, which restricts its versatility.

The ESP32 microcontroller was chosen for its processing capability and energy efficiency. These features make it ideal for managing UWB communication and executing algorithms for distance measurement and club recommendation. Additionally, the ability to flash code wirelessly simplifies updates and modifications in the field, allowing for seamless software improvements without requiring physical access to the device.

Furthermore, development boards from Freenove.com, which incorporate the ESP32-S3-WROOM processor were chosen for integration into both the static and handheld devices. These boards provide a well-supported platform, ensuring reliable performance while streamlining the development and deployment process.



Figure 10.1 ESP32-S3 WROOM microcontroller  
(Freenove, 2024).

## 10.1.2 Ultra-wide Band (UWB) Module

UWB modules are critical for achieving high accuracy distance measurement. This project evaluated the DW1000 and DW3000 modules from Qorvo, Infineon's 3DB6830 and Alereon's AL5100. The findings can be seen in Table 10.2

Table 10.2 - UWB Module Comparison

Feature	DW1000	DW3000	Infineon 3DB6830	Alereon AL5100
<b>Accuracy</b>	±10 cm in LoS (Polonelli et al., 2022)	±5 cm in LoS (Polonelli et al., 2022)	±10 cm in LoS (Kariman et al., 2024)	±30 cm (Chen, 2022)
<b>Energy Efficiency</b>	Moderate	50% more efficient than DW1000 (Polonelli et al., 2022)	Moderate (Appl. Sci., 2024)	Low (Chen, 2022)
<b>Connectivity</b>	SPI/I2C	SPI/I2C, IEEE 802.15.4z support	Compatible with SPI hosts (Kariman et al., 2024)	Proprietary protocols
<b>NLOS Performance</b>	Limited	Improved multipath resistance	Suitable for industrial environments	Weak
<b>Applications</b>	Wearables, IoT	IoT, healthcare, logistics	Security and industrial IoT (Kariman et al., 2024)	Short range communication
<b>Cost</b>	£38.25	£38.90	£22	£8.50

The DW3000 module was selected due to its centimetre level accuracy in both line of sight (LoS) and none line of sight (NLoS) environments. Its improved multipath resistance enhances reliability in real world conditions. Additionally, support for the IEEE 802.15.4z standard ensures long term compatibility and futureproofing, making it the most suitable choice for this project.



Figure 10.2 UWB-DW3000 ultra-wideband (UWB) module

(Makerfabs, 2024).

### 10.1.3 Altitude Measurement

To achieve an accurate estimation of the true distance between the handheld and static devices, it is necessary to determine the altitude of each device and calculate the three-dimensional distance using the Pythagorean theorem. The formula used is:

$$D_{3D} = \sqrt{d^2 + (\Delta h)^2}$$

Where:

- $D_{3D}$  = Line-of-sight (3D) distance
- $d$  = 2D distance
- $\Delta h$  = Altitude difference between the two points

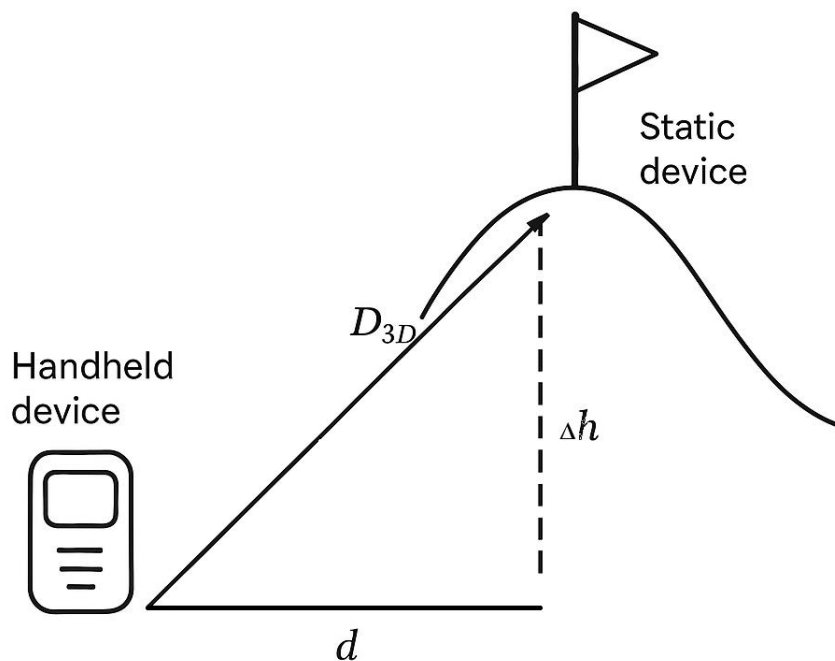


Figure 10.3 3D Distance Elevation

where  $\Delta h$  is the altitude difference between the two devices and  $d$  is the horizontal distance measured using the UWB module. This approach ensures that vertical displacement is considered, resulting in a more accurate representation of the actual separation between the two points in space.

Several techniques exist for estimating altitude in embedded systems, including GPS based positioning, LiDAR, RTK systems and barometric pressure sensors. While GPS provides global altitude reference its vertical accuracy is generally lower than its horizontal accuracy, often with errors exceeding several meters. LiDAR and RTK can offer high precision but are impractical for small embedded systems due to their cost, size, and power requirements.

In comparison the barometric pressure sensors provide a compact, low power and cost effective solution for relative altitude measurements. Based on a comparative study by Meng et al. (2023), the BMP388 pressure sensor demonstrated strong performance, achieving a coefficient of determination ( $R^2$ ) of 0.94 and a root mean square error (RMSE) of 0.45% when compared against high precision laser based reference data. The  $R^2$  value indicates the strength of the correlation between the pressure based altitude estimates and the reference values, where a value of 1.0 represents a perfect linear fit. The RMSE, on the other hand, reflects the average magnitude of the error between the measured and reference values; a lower RMSE signifies higher accuracy. These results suggest that the BMP388 provides both consistent and accurate altitude measurements. The study concluded that the BMP388 outperformed standard GPS in both accuracy and stability, making it well suited for embedded applications where precise relative altitude is required.

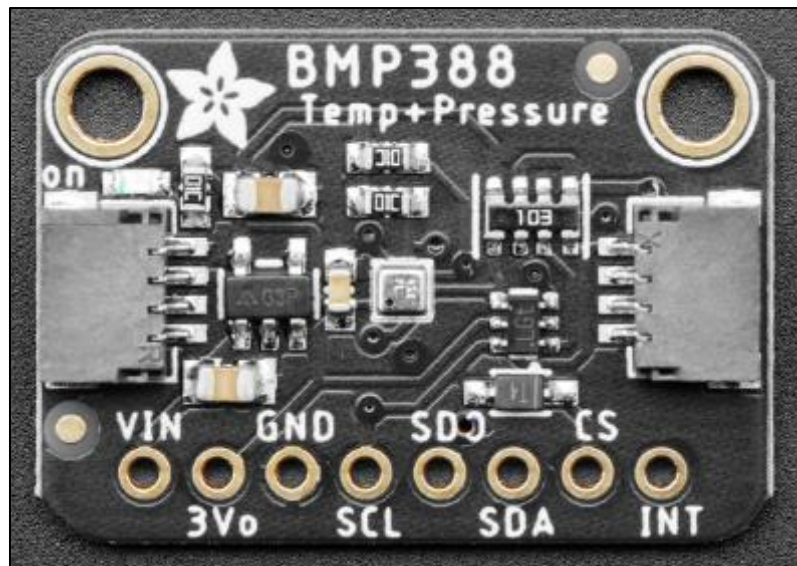


Figure 10.4 BMP388 Sensor

(Adafruit, 2024)

#### **10.1.4 Communication Module**

Ultra-wideband (UWB) technology was initially considered for both distance measurement and data transmission. The expectation was that the UWB module could transmit altitude data from the static device while simultaneously performing time of flight (ToF) ranging. However, the module was limited to either ToF measurements or message transmission, but not at the same time. This constraint needed an alternative method for relaying altitude data to the handheld device.

To address this limitation various low power wireless communication technologies were evaluated, including Bluetooth Low Energy (BLE), Zigbee, Wi-Fi and low power wide area networks (LPWAN). BLE and Zigbee offered energy efficiency but were constrained by their limited transmission range, making them unsuitable for applications requiring long-range data transmission. Wi-Fi, while providing high data rates, suffered from significant power consumption and was impractical for battery operated devices. LPWAN technologies, such as LoRa and Sigfox, emerged as promising solutions due to their ability to transmit small packets of data over long distances while maintaining low energy consumption (Nikoukar et al., 2018)

LoRa was selected as the communication module due to its extended transmission range, low power consumption, and suitability for remote sensor networks. Unlike cellular-based LPWAN solutions, LoRa operates in unlicensed frequency bands, reducing infrastructure costs and enabling easy integration into IoT systems. It supports communication distances of up to 10 km while maintaining low data rates, making it ideal for transmitting altitude data without excessive power drain. LoRa employs a chirp spread spectrum (CSS) modulation technique which enhances its strength to interference and multipath fading, ensuring reliable communication in challenging environments (Nikoukar et al., 2018)

Additionally, LoRa's adaptive data rate (ADR) mechanism optimises power consumption and network capacity by adjusting transmission parameters dynamically. It also supports forward error correction (FEC), improving communication reliability by recovering corrupted bits that may be affected by noise or signal degradation (Nikoukar et al., 2018)

### **10.1.5 Data Storage**

To support the club selection algorithm user specific distance data needed to be stored and accessed by the system. For example, if the measured distance to the target was 130 metres the device would need to retrieve the appropriate club (e.g. 7 iron) from a predefined dataset. This dataset was stored in a comma-separated values (CSV) file which could be read quickly by the microcontroller at runtime.

Several storage methods were considered, including cloud based storage, or syncing via a mobile app. Due to the potential for unreliable internet connectivity on golf courses, particularly in rural or remote locations, cloud storage was deemed unsuitable. Internal flash memory was also considered but lacked the flexibility and capacity for easy file updates during testing.

An SD card module was selected as it provided reliable local storage, was compatible with the ESP32-S3 development board, and supported fast file access through the standard SD library. During the prototype phase, the SD card was also used extensively to log test data from the system, including distance measurements, altitude, and signal strength. This simplified development by eliminating the need for manual recording and ensured that large volumes of data could be collected for evaluation and calibration.

## 10.1.6 User Interface Components

The user interface for the handheld device consists of a 0.96-inch OLED display and a 3 button tactile switch panel. These components were selected to provide simple, intuitive interaction with the system while maintaining low power consumption and compact size.

The OLED display, shown in Figure 10.5, features a 128×64-pixel resolution and operates using the I2C protocol, with four pins: ground (GND), power supply (VCC), serial clock line (SCL) and serial data line (SDA). The screen was chosen for its excellent contrast, visibility in outdoor lighting, and minimal current draw during operation. The I2C communication allows for easy integration with the microcontroller using only two data lines, conserving GPIO resources. This makes the display particularly suitable for battery powered embedded systems where efficiency and simplicity are priorities.

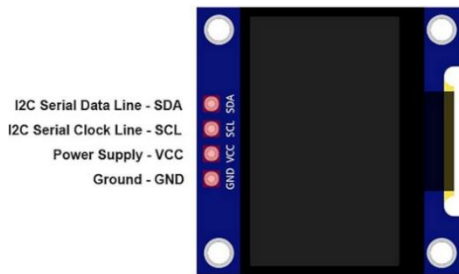


Figure 10.5 OLED Display Module

(AZ-Delivery, 2024)

For input, a flat membrane style tactile push button module was selected, shown in Figure 10.6. This panel includes three individual buttons with integrated return springs and clear printed icons for each function (Up, Down and Enter). The buttons are connected to the microcontroller via dedicated GPIO lines, using internal pull up resistors to detect input events. The panel's slim profile (36 mm by 55 mm, with a 105 mm flexible cable) allows it to be integrated into the handheld enclosure without increasing the device's overall thickness.

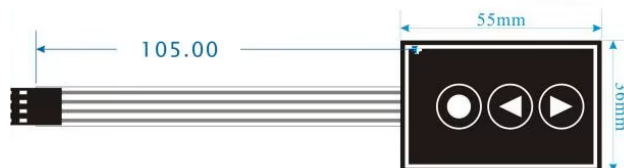


Figure 10.6 Membrane Touch Button Module

(AliExpress, 2024)

Together the OLED display and buttons form a simple and reliable user interface, allowing the user to initiate UWB measurements, navigate modes and view real time data during operation. These components were selected for their balance of usability, low power requirements and ease of integration.

### 10.1.7 Battery Selection

To meet the energy requirements of both the handheld and static units, a 3.7 V 2000 mAh lithium-polymer (LiPo) battery (LP103554) was selected. This battery offers a high energy to size ratio and is compatible with the ESP32-S3's 3.3 V operating voltage. Its 7.4 Wh energy capacity supports several hours of continuous operation while maintaining a compact footprint suitable for enclosure integration.

Charging is managed by a TP4056 lithium-ion charging module, which applies a constant current/constant voltage (CC/CV) algorithm. To regulate the battery's output down to the ESP32's required voltage, an SPX3819 low-dropout linear regulator (LDO) was used, supplying a stable 3.3 V output.

For the static unit, a 5 V 230 mA solar panel was selected, sized to match the surface area of the enclosure. However, field testing showed that its output could drop to as low as 3.69 V in overcast conditions. As the TP4056 requires a minimum input voltage of 4.4 – 4.5 V, a MT3608 boost converter was added to ensure a consistent 5 V supply to the charging circuit regardless of weather conditions.

The handheld unit shares the same internal power configuration but is charged via USB-C. This simplifies bench charging and testing during development.

To estimate charging duration, the following standard charging formula was used:

*Equation 10.1 Charge Time Formula*

$$t_{charge} = \frac{C}{I} * 1.2$$

Where:

- C = battery capacity in mAh
- t<sub>charge</sub> = Charge time
- I = charging current

$$t_{charge(\text{static module})} = \frac{2000}{230} * 1.2 \approx 10.4 \text{ (hours)}$$

$$t_{charge(\text{handheld module})} = \frac{2000}{830} * 1.2 \approx 1.73 \text{ (hours)}$$

## 10.1.8 Enclosure Selection

Two different enclosures were selected to house the static and handheld units of the system, based on environmental, mechanical, electromagnetic, and ergonomic requirements.

### Static Unit

For the static unit, the GEWISS GW44204 enclosure was chosen due to its IP56 rating, offering strong protection against dust and water ingress (Allied Electronics, 2024), which is essential for outdoor deployment. Made from industrial grade non-metallic techno polymer, this enclosure is durable with IK08 impact resistance (RS Components, 2024) and is also suitable for radio frequency applications. Metallic housings were deliberately avoided as they can attenuate or reflect radio signals, negatively affecting the performance of the onboard UWB and LoRa modules. The internal volume of  $100 \times 100 \times 50$  mm provides sufficient space for the power system, communication modules and supporting circuitry, with room for cable routing and mounting.

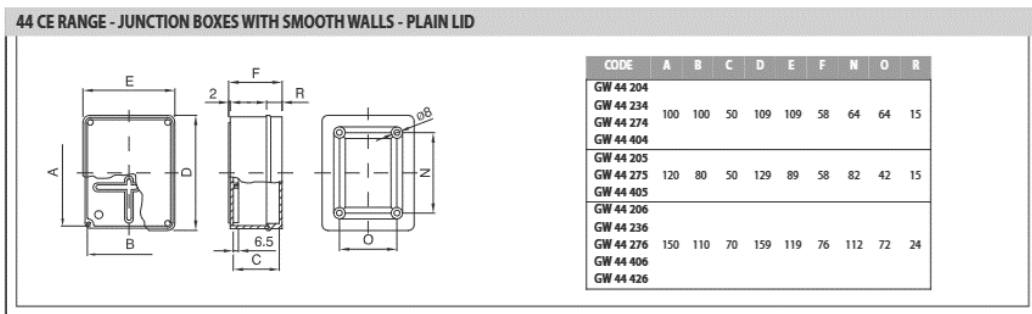


Figure 10.7 GEWISS GW44204 junction box

(GEWISS, 2024).

## Handheld Unit

For the handheld device a Hammond 1552D3 ABS plastic enclosure was selected. Measuring approximately 110 mm in length, 50 mm in width and 34 mm in height, the enclosure offers a compact and ergonomic form factor suitable for one handed operation during field use. Despite its small size, the internal space was sufficient to accommodate the ESP32-S3 development board, OLED display, Li-ion battery and supporting electronics. The enclosure was specifically chosen to accommodate the selected user interface components, including the 0.96-inch OLED display and membrane style tactile push buttons, ensuring appropriate panel mounting and visibility without the need for excessive modification. Like the static unit, the enclosure is made from non-metallic material to avoid interference with the system's embedded wireless communication modules, including UWB and LoRa. During the design process, all internal components were measured and positioned to ensure a secure and efficient fit, with consideration given to button placement, connector access and overall usability.

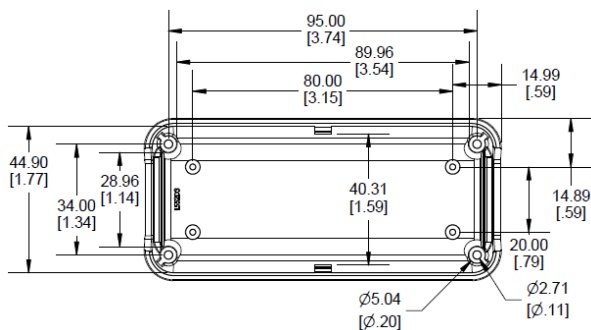


Figure 10.8 Dimensions for the Handheld Unit

(Hammond Manufacturing, 2019)

Both enclosures meet the technical and practical requirements of the system, balancing protection, ease of integration, RF transparency and usability in their respective operating environments. Full data sheets can be found in Appendix 10.6

## 10.2 Programming Codes

### 10.2.1 LoRa Distance Test Codes

#### Static Device:

```
#include <Arduino.h>

HardwareSerial LoRaSerial(1); // HC-12 on Serial1
#define LORA_TX 8
#define LORA_RX 9

void setup() {
    Serial.begin(115200);
    LoRaSerial.begin(9600, SERIAL_8N1, LORA_RX, LORA_TX);
    Serial.println("Static unit started.");
}

void loop() {
    LoRaSerial.println("PING");
    Serial.println("Sent: PING");
    delay(1000); // Send every 1s
}
```

## Handheld Device:

```
#include <Arduino.h>

HardwareSerial LoRaSerial(1); // HC-12 on Serial1
#define LORA_TX 8
#define LORA_RX 9
#define STATUS_LED 2 // Or use LED_BUILTIN

unsigned long lastReceived = 0;

void setup() {
  Serial.begin(115200);
  LoRaSerial.begin(9600, SERIAL_8N1, LORA_RX, LORA_TX);
  pinMode(STATUS_LED, OUTPUT);
  digitalWrite(STATUS_LED, LOW);
  Serial.println("Handheld unit started.");
}

void loop() {
  if (LoRaSerial.available()) {
    String msg = LoRaSerial.readStringUntil('\n');
    msg.trim();
    if (msg == "PING") {
      lastReceived = millis();
      Serial.println("Received: PING");
    }
  }

  // If PING received in last 3 seconds, LED ON
  if (millis() - lastReceived <= 3000) {
    digitalWrite(STATUS_LED, HIGH);
  } else {
    digitalWrite(STATUS_LED, LOW);
  }
}
```

## 10.2.2 Final Product Codes

### Static Device:

```
#include <Arduino.h>
#include <Wire.h>
#include <Adafruit_BMP3XX.h>
#include <HardwareSerial.h>

// --- Pin Definitions ---
#define IO_RXD2 17          // UWB RX
#define IO_TXD2 18          // UWB TX
#define LORA_RX 9            // LoRa RX
#define LORA_TX 8            // LoRa TX
#define RESET_PIN 16          // UWB Reset
#define SEA_LEVEL_PRESSURE 1028.0

HardwareSerial UWBSerial(2);
HardwareSerial LoRaSerial(1);
Adafruit_BMP3XX bmp;

bool uwbConfigured = false;
unsigned long lastUpdateTime = 0;
#define UPDATE_INTERVAL 1000 // 1 second

void setup() {
    Serial.begin(115200);
    UWBSerial.begin(115200, SERIAL_8N1, IO_RXD2, IO_TXD2);
    LoRaSerial.begin(9600, SERIAL_8N1, LORA_RX, LORA_TX);
    Wire.begin(39, 38); // I2C
    pinMode(RESET_PIN, OUTPUT);

    // Reset UWB module
    digitalWrite(RESET_PIN, LOW);
    delay(100);
    digitalWrite(RESET_PIN, HIGH);
    delay(1500); // Let it boot

    if (!bmp.begin_I2C(0x77)) {
        Serial.println("BMP Init Failed");
        while (1);
    }
}

Serial.println("STATIC UNIT (ANCHOR) READY");
}

void loop() {
    unsigned long now = millis();
```

```

// Only send UWB config once after wake
if (!uwbConfigured && now > 2000) {
    UWBSerial.println("AT+SETCFG=1,0,2,3"); // ID 1, Anchor mode
    Serial.println("UWB Config Sent: ANCHOR");
    uwbConfigured = true;
}

// Read BMP altitude
float altitude = 0.0;
if (bmp.performReading()) {
    altitude = bmp.readAltitude(SEA_LEVEL_PRESSURE);
}

// Send altitude over LoRa every second after wake
if (now - lastUpdateTime >= UPDATE_INTERVAL) {
    Serial.print("⌚ Sending Static Altitude: ");
    Serial.println(altitude, 2);
    LoRaSerial.print("ALT:");
    LoRaSerial.println(altitude, 2);

    // Watch UWB response for serial monitor
    while (UWBSerial.available()) {
        String line = UWBSerial.readStringUntil('\n');
        line.trim();
        if (line.length() > 0) {
            Serial.print("UWB: ");
            Serial.println(line);
        }
    }
}

lastUpdateTime = now;
}
}

```

## Handheld Device:

```
#include <Arduino.h>
#include <Wire.h>
#include <Adafruit_BMP3XX.h>
#include <Adafruit_SSD1306.h>
#include <HardwareSerial.h>
#include <SPI.h>
#include <SD.h>
#include <Preferences.h>
#include <WiFi.h>
#include "esp_bt.h"
#include "esp_wifi.h"
#include <math.h>

// ----- Kalman filter -----
class SimpleKalmanFilter {
    float estimate;
    float errorEstimate;
    float errorMeasure;
    float kalmanGain;

public:
    SimpleKalmanFilter(float mea_e, float est_e, float init_est) {
        errorMeasure = mea_e;
        errorEstimate = est_e;
        estimate = init_est;
    }

    float updateEstimate(float measurement) {
        kalmanGain = errorEstimate / (errorEstimate + errorMeasure);
        estimate = estimate + kalmanGain * (measurement - estimate);
        errorEstimate = (1.0 - kalmanGain) * errorEstimate;
        return estimate;
    }

    void setEstimate(float est) { estimate = est; }
    float getEstimate() { return estimate; }
};

// ----- WiFi/Bluetooth Disable -----
void disableWiFiBluetooth() {
    WiFi.mode(WIFI_OFF);
    btStop();
    esp_bt_controller_disable();
}

// ----- definitions -----
#define IO_RXD2 17
```

```

#define IO_TXD2 18
#define LORA_RX 9
#define LORA_TX 8
#define RESET_PIN 16
#define SD_CS 5
#define SEA_LEVEL_PRESSURE 1028.0
#define SCREEN_WIDTH 128
#define SCREEN_HEIGHT 64
#define BTN_ENTER 15
#define BTN_UP 4
#define BTN_DOWN 10

HardwareSerial UWBSerial(2);
HardwareSerial LoRaSerial(1);
Adafruit_SSD1306 display(SCREEN_WIDTH, SCREEN_HEIGHT, &Wire, -1);
Adafruit_BMP3XX bmp;
Preferences prefs;

enum MenuState {
    MENU_MAIN,
    MENU_SETTINGS,
    MENU_UNITS,
    MENU_ENGINEER,
    MENU_ACTIVE_DATA
};

MenuState currentMenu = MENU_MAIN;
int menuIndex = 0;
int unitsMenuItemIndex = 0;
bool useYards = false;

float handheldAlt = 0.0;
float staticAlt = 0.0;
float altDiff = 0.0;
float uwbDist = 0.0;
float rssi = 0.0;
float trueDist = 0.0;
String clubLabel = "N/A";

unsigned long lastDisplayTime = 0;
unsigned long lastButtonPress = 0;
unsigned long lastUpdateTime = 0;
unsigned long dataActiveStart = 0;
unsigned long enterPressStart = 0;
bool enterHoldTriggered = false;

#define BUTTON_DEBOUNCE 150
#define DISPLAY_INTERVAL 3000
#define UPDATE_INTERVAL 1000

```

```

#define DATA_ACTIVE_DURATION 15000

bool dataActive = false;
bool uwbConfigured = false;

// ----- Kalman Filter for UWB -----
SimpleKalmanFilter kalmanUWB(0.5, 1, 0); // measurement error, estimate error, initial
estimate

float convertDistance(float meters) {
    return useYards ? meters * 1.09361 : meters;
}

void updateClubLabel(float distance) {
    File file = SD.open("/clubmap.csv");
    if (!file) {
        clubLabel = "N/A";
        return;
    }
    clubLabel = "N/A";
    bool firstLine = true;
    while (file.available()) {
        String line = file.readStringUntil('\n');
        line.trim();
        if (firstLine) { firstLine = false; continue; }
        int c1 = line.indexOf(',');
        int c2 = line.indexOf(',', c1 + 1);
        if (c1 == -1 || c2 == -1) continue;
        float min = line.substring(0, c1).toFloat();
        float max = line.substring(c1 + 1, c2).toFloat();
        String label = line.substring(c2 + 1);
        if (distance >= min && distance < max) {
            clubLabel = label;
            break;
        }
    }
    file.close();
}

void saveUnitSetting(bool yards) {
    prefs.begin("settings", false);
    prefs.putBool("useYards", yards);
    prefs.end();
}

void loadUnitSetting() {
    prefs.begin("settings", true);
    useYards = prefs.getBool("useYards", false);
    unitsMenuItemIndex = useYards ? 1 : 0;
}

```

```

prefs.end();
}

void checkButtons() {
    unsigned long now = millis();
    if (digitalRead(BTN_ENTER) == LOW) {
        if (enterPressStart == 0) enterPressStart = now;
        else if (!enterHoldTriggered && now - enterPressStart >= 2500) {
            currentMenu = MENU_MAIN;
            enterHoldTriggered = true;
        }
    } else {
        if (enterPressStart != 0 && !enterHoldTriggered && now - enterPressStart < 2500) {
            lastButtonPress = now;
            if (currentMenu == MENU_MAIN) {
                if (menuIndex == 0) {
                    dataActive = true;
                    dataActiveStart = millis();
                    LoRaSerial.println("WAKE");
                    LoRaSerial.flush();
                    currentMenu = MENU_ACTIVE_DATA;
                } else if (menuIndex == 1) {
                    currentMenu = MENU_SETTINGS;
                    menuIndex = 0;
                }
            } else if (currentMenu == MENU_SETTINGS) {
                currentMenu = (menuIndex == 0) ? MENU_UNITS : MENU_ENGINEER;
            } else if (currentMenu == MENU_UNITS) {
                useYards = (unitsMenuItemIndex == 1);
                saveUnitSetting(useYards);
                currentMenu = MENU_SETTINGS;
            } else if (currentMenu == MENU_ENGINEER) {
                currentMenu = MENU_SETTINGS;
            }
        }
        enterPressStart = 0;
        enterHoldTriggered = false;
    }

    if (digitalRead(BTN_UP) == LOW && now - lastButtonPress > BUTTON_DEBOUNCE) {
        if (currentMenu == MENU_MAIN || currentMenu == MENU_SETTINGS) {
            menuIndex = (menuIndex - 1 + 2) % 2;
        } else if (currentMenu == MENU_UNITS) {
            unitsMenuItemIndex = (unitsMenuItemIndex - 1 + 2) % 2;
        }
        lastButtonPress = now;
    }
    if (digitalRead(BTN_DOWN) == LOW && now - lastButtonPress > BUTTON_DEBOUNCE) {
        if (currentMenu == MENU_MAIN || currentMenu == MENU_SETTINGS) {

```

```

        menuIndex = (menuIndex + 1) % 2;
    } else if (currentMenu == MENU_UNITS) {
        unitsMenuItemIndex = (unitsMenuItemIndex + 1) % 2;
    }
    lastButtonPress = now;
}
}

void setup() {
    Serial.begin(115200);
    disableWiFiBluetooth();
    UWBSerial.begin(115200, SERIAL_8N1, IO_RXD2, IO_TxD2);
    LoRaSerial.begin(9600, SERIAL_8N1, LORA_RX, LORA_TX);
    Wire.begin(39, 38);

    pinMode(RESET_PIN, OUTPUT);
    pinMode(BTN_ENTER, INPUT_PULLUP);
    pinMode(BTN_UP, INPUT_PULLUP);
    pinMode(BTN_DOWN, INPUT_PULLUP);

    digitalWrite(RESET_PIN, LOW); delay(100);
    digitalWrite(RESET_PIN, HIGH); delay(1500);

    if (!display.begin(SSD1306_SWITCHCAPVCC, 0x3C)) while (1);
    if (!bmp.begin_I2C(0x77)) while (1);
    if (!SD.begin(SD_CS)) Serial.println("SD Card Init Failed.");

    display.clearDisplay();
    display.setTextSize(1);
    display.setTextColor(WHITE);
    display.setCursor(0, 0);
    display.println("HANDHELD READY");
    display.display();

    loadUnitSetting();
}

void loop() {
    unsigned long now = millis();
    checkButtons();

    if (dataActive && now - dataActiveStart > DATA_ACTIVE_DURATION) {
        dataActive = false;
        currentMenu = MENU_MAIN;
    }

    if (!uwbConfigured && now > 2000) {
        UWBSerial.println("AT+SETCFG=0,0,1,3");
        uwbConfigured = true;
    }
}

```

```

}

if (bmp.performReading()) {
    handheldAlt = bmp.readAltitude(SEA_LEVEL_PRESSURE);
}

while (LoRaSerial.available()) {
    String msg = LoRaSerial.readStringUntil('\n');
    msg.trim();
    if (msg.startsWith("ALT:")) {
        staticAlt = msg.substring(4).toFloat();
    }
}

if (dataActive && now - lastUpdateTime >= UPDATE_INTERVAL) {
    UWBSerial.println("AT+RANGE");
    delay(500);
    lastUpdateTime = now;
}

while (UWBSerial.available()) {
    String line = UWBSerial.readStringUntil('\n');
    line.trim();
    if (line.startsWith("AT+RANGE=")) {
        int rangeStart = line.indexOf("range:") + 7;
        int rangeEnd = line.indexOf(")", rangeStart);
        if (rangeStart > 6 && rangeEnd > rangeStart) {
            String data = line.substring(rangeStart, rangeEnd);
            int comma = data.indexOf(",");
            if (comma != -1) {
                String after = data.substring(comma + 1);
                int comma2 = after.indexOf(",");
                if (comma2 != -1) {
                    float rawUWB = after.substring(0, comma2).toFloat() / 100.0;

                    // Optional correction
                    if (rawUWB >= 75.0) rawUWB *= 1.02;

                    // Apply Kalman filtering
                    uwbDist = kalmanUWB.updateEstimate(rawUWB);
                }
            }
        }
    }

    int rssistart = line.indexOf("rssい:") + 6;
    int rssiestart = line.indexOf(")", rssistart);
    if (rssistart > 6 && rssiestart > rssistart) {
        String rssidata = line.substring(rssistart, rssiestart);
        int comma = rssidata.indexOf(",");
    }
}

```

```

        if (comma != -1) {
            rssi = rssidata.substring(0, comma).toFloat();
        }
    }
}

altDiff = staticAlt - handheldAlt;
trueDist = (uwbDist > 0.01) ? sqrt((uwbDist * uwbDist) + (altDiff * altDiff)) : 0.0;
if (dataActive) updateClubLabel(convertDistance(trueDist));

if (now - lastDisplayTime >= DISPLAY_INTERVAL) {
    display.clearDisplay();
    display.setCursor(0, 0);

    if (currentMenu == MENU_MAIN) {
        display.println(menuIndex == 0 ? "> DISTANCE + CLUB" : " DISTANCE + CLUB");
        display.println(menuIndex == 1 ? "> SETTINGS" : " SETTINGS");
    } else if (currentMenu == MENU_SETTINGS) {
        display.println("SETTINGS:");
        display.println(menuIndex == 0 ? "> Units (m/yd)" : " Units (m/yd)");
        display.println(menuIndex == 1 ? "> Engineer View" : " Engineer View");
    } else if (currentMenu == MENU_UNITS) {
        display.println("SELECT UNITS:");
        display.println(unitsMenuItemIndex == 0 ? "> Meters" : " Meters");
        display.println(unitsMenuItemIndex == 1 ? "> Yards" : " Yards");
    } else if (currentMenu == MENU_ENGINEER) {
        display.println("ENGINEER VIEW");
        display.print("Alt HH: "); display.println(handheldAlt, 2);
        display.print("Alt Static: "); display.println(staticAlt, 2);
        display.print("2D Dist: "); display.println(uwbDist, 2);
        display.print("RSSI: "); display.println(rssi, 1);
    } else if (currentMenu == MENU_ACTIVE_DATA) {
        display.println("\xF0\x9F\x93\xA1 DATA ACTIVE");
        display.print("3D Dist: ");
        display.print(convertDistance(trueDist), 2);
        display.println(useYards ? " yd" : " m");
        display.print("Club: ");
        display.println(clubLabel);
    }

    display.display();
    lastDisplayTime = now;
}
}

```

## 10.3 MATLAB Codes

### 10.3.1 Distance Calculations (Haversine)

```
% Haversine 3D Distance Comparison Script

clc;
clear;

% Earth's radius in kilometers
R = 6371;
R = R * 1000; % convert to meters

% --- Environmental Inputs ---
fprintf('Enter Test Conditions:\n');
weather = input('Weather status (e.g. Sunny, Rainy): ', 's');
temperature = input('Temperature (°C): ');
humidity = input('Humidity (%): ');

% --- Static Device Coordinates ---
fprintf('\nEnter Static Device Coordinates:\n');
lat_static = input('Latitude (degrees): ');
lon_static = input('Longitude (degrees): ');
alt_static = input('Altitude (meters): ');

% Convert static lat/lon to radians
lat_static_rad = deg2rad(lat_static);
lon_static_rad = deg2rad(lon_static);

% --- Measurement Points ---
n = input('\nHow many measurement points? ');

% Initialize storage
labels = strings(n, 1);
device_distances = zeros(n, 1);
gps_3d_distances = zeros(n, 1);
errors = zeros(n, 1);

for i = 1:n
    fprintf('\nEnter data for point M%d:\n', i);
    labels(i) = sprintf('M%d', i);
    lat = input(' Latitude (degrees): ');
    lon = input(' Longitude (degrees): ');
    alt = input(' Altitude (meters): '');
```

```

device_d = input(' Device measured 3D distance (meters): ');

% Convert to radians
lat_rad = deg2rad(lat);
lon_rad = deg2rad(lon);

% Haversine 2D distance
dlat = lat_rad - lat_static_rad;
dlon = lon_rad - lon_static_rad;

a = sin(dlat / 2)^2 + cos(lat_static_rad) * cos(lat_rad) * sin(dlon / 2)^2;
c = 2 * atan2(sqrt(a), sqrt(1 - a));
d2D = R * c;

% 3D distance using altitude
delta_h = alt - alt_static;
d3D = sqrt(d2D^2 + delta_h^2);

% Store results
device_distances(i) = device_d;
gps_3d_distances(i) = d3D;
errors(i) = abs(device_d - d3D);
end

% --- Results Table ---
resultsTable = table(labels, device_distances, gps_3d_distances, errors, ...
    'VariableNames', {'Point', 'UWB Distance (m)', 'GPS 3D Distance (m)', 'Error (m)'});

fprintf('\n--- Comparison Table ---\n');
disp(resultsTable);

% --- Plot Results ---
figure;
plot(1:n, device_distances, '-o', 'LineWidth', 2);
hold on;
plot(1:n, gps_3d_distances, '-x', 'LineWidth', 2);
grid on;

xlabel('Measurement Point');
ylabel('Distance (m)');
title(sprintf('UWB Device vs GPS 3D Distance\nWeather: %s | Temp: %d°C | Humidity: %d%', ...
    weather, temperature, humidity));

```

```
legend('UWB Device', 'GPS Calculated');  
xticks(1:n);  
xticklabels(labels);
```

## 10.4 Bill Of Materials

### 10.4.1 Handheld Device

Table 10.3 - Handheld Device - Bill of Materials

Ref	Component	Value / Part No.	Package / Type	Qty
U1	ESP32-S3 Dev Board	Freenove ESP32-S3	DevKit (Header)	1
U2	SD Card Module	SPI Interface	Breakout Board	1
U3	TP4056 Charger	TP4056	SOP-8	1
U4	BMP388 Altitude Sensor	CJMCU-388	Breakout Board	1
U5	LoRa Module	HC-12	Breakout Board	1
U6	UWB Module	DW3000	Breakout Board	1
U7	LDO Regulator	SPX3819 (3.3 V)	SOT-23-5	1
R1	Charge Current Resistor	1.2 kΩ	805	1
C1	Input Capacitor (TP4056)	10 µF	805	1
C2	Input Capacitor (TP4056)	0.1 µF	805	1
C3	Output Cap (TP4056)	10 µF	805	1
C4	Input Cap (LDO)	4.7 µF	805	1
C5	Output Cap (LDO)	10 µF	805	1
J1	Battery Connector	JST 2-pin	Through-hole	1
J2	Power Switch Connector	2-pin	2.54 mm header	1
J3-J4	I/O Connectors	4-pin headers	2.54 mm	2
BTN1-3	Push Buttons	Tactile 6x6 mm	Through-hole	3

## 10.4.2 Static Device

Table 10.4 - Static Device - Bill of Materials

Ref	Component	Value / Part No.	Package / Type	Qty
U1	ESP32-S3 Dev Board	Freenove ESP32-S3	DevKit (Header)	1
U2	UWB Module	DW3000	Breakout Board	1
U3	LoRa Module	HC-12	Breakout Board	1
U4	BMP388 Altitude Sensor	CJMCU-388	Breakout Board	1
U5	MT3608 Boost Converter	MT3608	Module	1
U6	SR360 Diode	SR360	DO-27	1
U7	TP4056 Charger	TP4056	SOP-8	1
U8	LDO Regulator	SPX3819 (3.3 V)	SOT-23-5	1
R1	Charge Current Resistor	1.2 kΩ	805	1
C1	Input Cap (TP4056)	10 µF	805	1
C2	Input Cap (TP4056)	0.1 µF	805	1
C3	Output Cap (TP4056)	10 µF	805	1
C4	Input Cap (LDO)	4.7 µF	805	1
C5	Output Cap (LDO)	10 µF	805	1
J1	Solar Connector	2-pin header	2.54 mm	1
J2	Battery Connector	JST 2-pin	Through-hole	1
J3	On/Off Switch Connector	2-pin	2.54 mm header	1

## 10.5 Photographs

### 10.5.1 Proof of Concept Veroboard

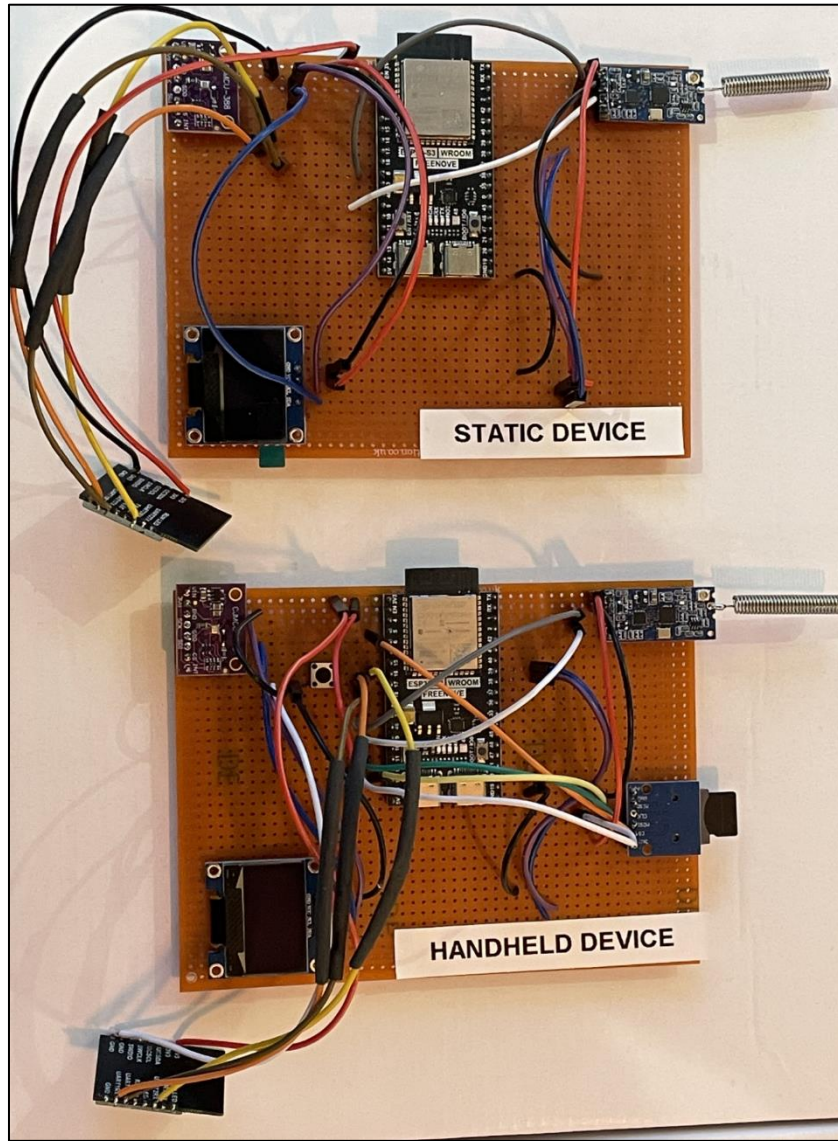


Figure 10.9 Proof of Concept Veroboard

## 10.5.2 Proof of Concept Testing



Figure 10.10 Proof of Concept Testing Photo 1

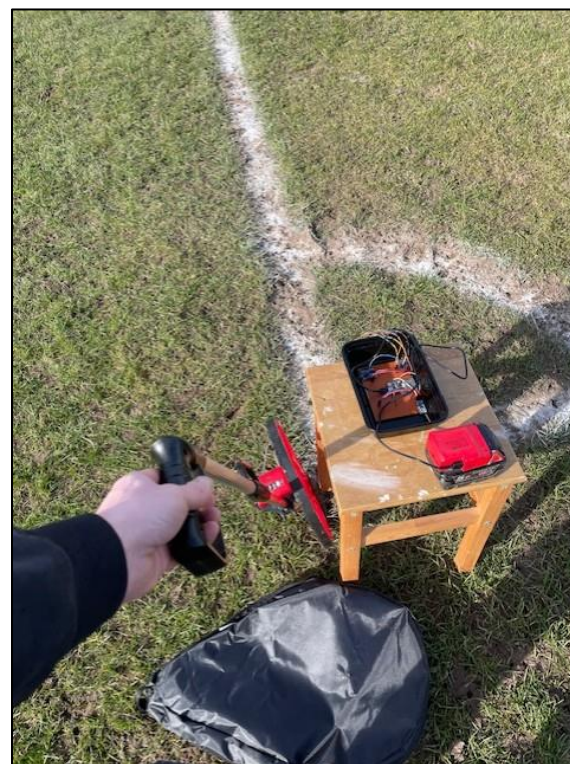


Figure 10.11 Proof of Concept Testing Photo 2



Figure 10.12 Proof of Concept Testing Photo 3

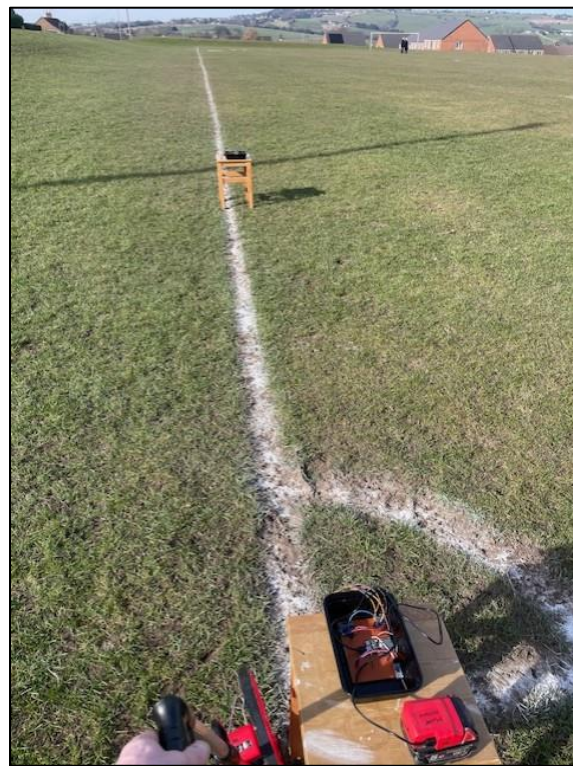


Figure 10.13 Proof of Concept Testing Photo 4

### 10.5.3 Hardware Building



Figure 10.14 Hardware Building Photo 1



Figure 10.15 Hardware Building Photo 2



Figure 10.16 Hardware Building Photo 3



Figure 10.17 Hardware Building Photo 4

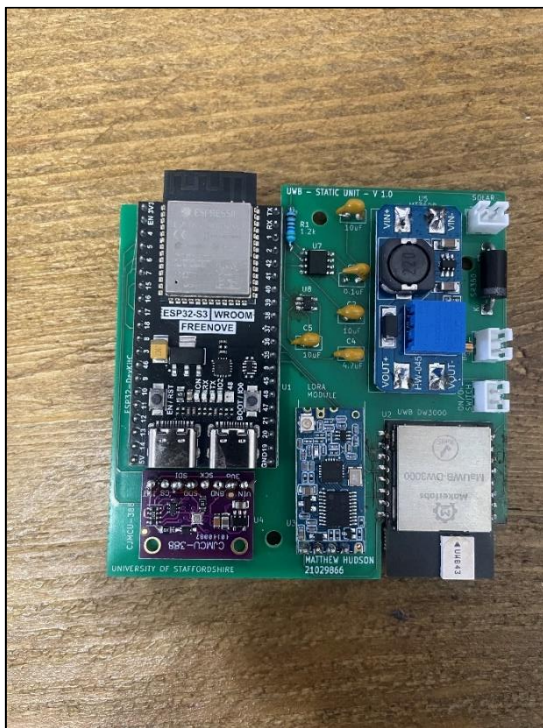


Figure 10.18 Hardware Building Photo 5



Figure 10.19 Hardware Building Photo 6



Figure 10.20 Hardware Building Photo 7

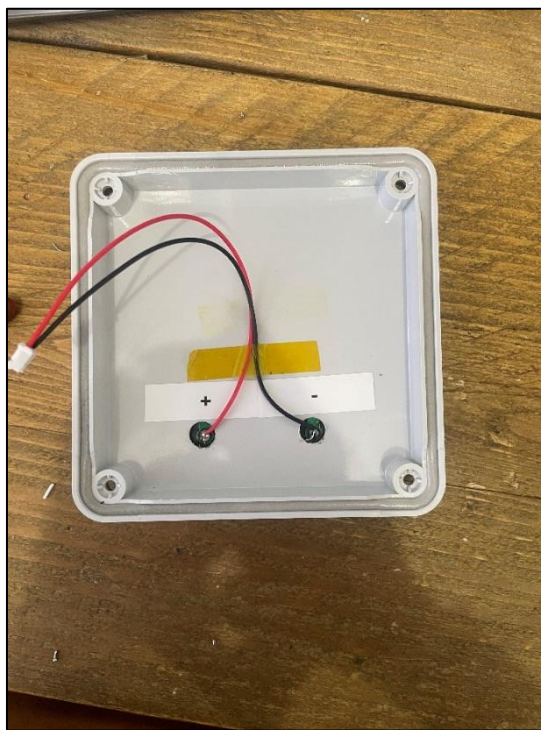


Figure 10.21 Hardware Building Photo 8



Figure 10.22 Hardware Building Photo 9



Figure 10.23 Hardware Building Photo 10



Figure 10.24 Hardware Building Photo 11



Figure 10.25 Hardware Building Photo 12



Figure 10.26 Hardware Building Photo 13

## 10.6 Datasheets

### 10.6.1 Flagstick Enclosure




**Product Data Sheet**  
**GW44204**  
**44 CE Range**

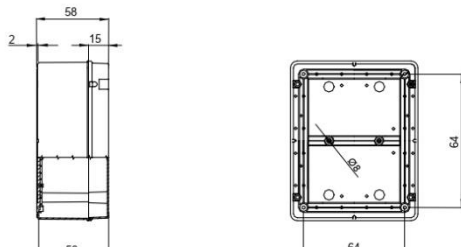
Range 44 CE - Surface-mounting watertight junction boxes in compliance with EN 60670-1 (CEI 23-48) and IEC 60670-22 (CEI 23-94) and made in high-performance technopolymers. The range includes versions with protection degree IP44, IP55, IP56 with smooth walls or with quick entry cable glands and different type of covers: blind / transparent, deep/plain, press-on/screw (in plastic, also 1/4 turn, or in metal). Available in different self-extinguishing materials (up to GWT 960 °C). Suitable for ordinary junctions, for special uses, and for industrial uses.

Insulation class	II (according to IEC 61140 standards)	Colour	Grey RAL 7035
IP degree	IP56	Material	Technopolymer GWPLAST 75
Mechanical resistance	IK08	Internal dim. LxHxD (mm)	100x100x50
Max Ø holes possible	29 mm	Lid screws (no. and type)	4 - Stainless steel
Application	Ordinary junctions	Glow Wire Test	650 °C
Lid	Plain screwed	Operating temperature	-25 +60 °C
Type of material	Halogen-free in compliance with EN 60754-2	Electrocod	02211
Thermo-pressure with ball	85 °C	Torque screws tightening	1 Newton/meter
Walls	Smooth	Accessories for insulation restoring	GW44622

**BEHAVIOUR WITH CHEMICAL AND ATMOSPHERIC AGENTS**

Saline solution	Acids		Bases		Solvents				Mineral oil	UV rays
	Concentrated	Diluted	Concentrated	Diluted	Hexane	Benzol	Acetone	Alcohol		
Resistant	Limited resistance	Resistant	Resistant	Limited resistance	Not resistant	Not resistant	Limited resistance	Limited resistance	Limited resistance	

**DIMENSIONAL**



**TECHNICAL SYMBOLS**

 II (according to IEC 61140 standards)	<b>IP</b> IP56	<b>IK</b> IK08	<b>GWT</b> 650 °C	<small>INSTALLATION</small>  -25 +60 °C	<small>HF</small> Halogen-free	 85 °C
--	-------------------	-------------------	----------------------	--	-----------------------------------	---

**STANDARDS/APPROVALS**





GEWISS S.p.A. Via Domenico Bosatelli 1  
24069 Cenate Sotto - Bergamo - Italy  
tel. +39 035 94 61 11 fax +39 035 94 69 09

www.gewiss.com  
sat@gewiss.com  
Last update 24/03/2025

Data, measures, designs and pictures are shown only as informative purposes, and could be changed without previous notice

## 10.6.2 Handheld Enclosure

